1-1-2013

Biochemical, Structural, And Drug Design Studies Of Multi-Drug Resistant Hiv-1 Therapeutic Targets

Tamaria Grace Dewdney
Wayne State University,

BIOCHEMICAL, STRUCTURAL, AND DRUG DESIGN STUDIES OF MULTI-DRUG RESISTANT HIV-1 THERAPEUTIC TARGETS

by

TAMARIA GRACE DEWDNEY

DISSERTATION

Submitted to the Graduate School

of Wayne State University,

Detroit, Michigan

in partial fulfillment of the requirements

for the degree of

DOCTOR OF PHILOSOPHY

2013

MAJOR: **BIOCHEMISTRY AND MOLECULAR BIOLOGY**

Approved by:

_____
Advisor   Date

_____

_____

_____

_____

DEDICATION

This dissertation is dedicated to my sister, Iman Dewdney.

ACKNOWLEDGEMENTS

I thank my parents for all they have done, particularly, my mother and bestest friend, Jillian Sutherland. She has truly been my source of encouragement, strength and motivation over the past 27 years. Many thanks to the Dewdney's: Iman, Wendell, Nadine, Kurt, and Kylen.

I would like to thank my doctoral advisor and mentor, Dr. Ladislau C. Kovari for giving of his time, energy and guidance over the past four years. I would like to especially thank him for his patience, for challenging me intellectually, being an amazing supporter from the very beginning, and for giving me the opportunity to work in his lab. My experience here has provided the space to grow into who I am today as a scholar, a scientist, a teacher, and a mentor.

I would like to thank Drs. Sharon H. Ackerman, Zhe Yang, and Steven Firestine for serving on my dissertation committee and providing their invaluable support and insights throughout this journey.

I would especially like to thank Dr. Sharon H. Ackerman for being my undergraduate research advisor. She gave me the opportunity to work in her lab as a sophomore in college. I was 19, hadn't even taken biology yet, and while I thought I knew everything, I knew nothing at all. She took the time to personally teach me how to pipette! I certainly attribute my love for research to my experience as an undergraduate in her lab and her support every step of the way.

I would like to thank Drs. Rasheeda Zafar and Joseph Dunbar for their mentorship and support through the IMSD and AGEP programs. As a freshman nearly a decade ago, they saw something in me that I had no idea even existed. I am eternally grateful for their foresight, support, encouragement, and motivation.

I'd like to thank Dr. Iulia Kovari for her friendship, support, amazing personality, her joy,

TABLE OF CONTENTS

vii

LIST OF TABLES

LIST OF FIGURES

Chapter 1: Introduction

1.1 HIV-1 Epidemiology

Human immunodeficiency virus (HIV) was first discovered in 1983 as the causative agent of Acquired Immune Deficiency Syndrome (AIDS) [1-8]. Significant advances in treatment options have been made, resulting in a 24% reduction in AIDS-related deaths since 2005. However HIV/AIDS remains a global epidemic as approximately 34 million people worldwide are living with HIV, with 2.5 million infected individuals as of the end of 2011[9].

Table 1.1 Global summary of the AIDS epidemic as of 2011. Biannually, the World Health Organization, the UNAIDS and Unicef provide a detailed epidemiological report on the global AIDS epidemic [9].

Number of people living with HIV		
Total	34.0 million	[31.4–35.9 million]
Adults	30.7 million	[28.2–32.3 million]
Women	16.7 million	[15.4–17.6 million]
Children (<15 years)	3.3 million	[3.1–3.8 million]

People newly infected with HIV in 2011		
Total	2.5 million	[2.2–2.8 million]
Adults	2.2 million	[1.9–2.4 million]
Children (<15 years)	330 000	[280 000–390 000]

AIDS deaths in 2011		
Total	1.7 million	[1.5–1.9 million]
Adults	1.5 million	[1.3–1.7 million]
Children (<15 years)	230 000	[200 000–270 000]

1.2 HIV life cycle

HIV-1 and HIV-2 are lentiviruses belonging to the *Retroviridae* family associated with a long incubation period which causes immune deficiencies of the hematopoietic system. The HIV viral life cycle begins with attachment of viral particles to host immune cells (Figure 1.1). The primary cell target is T4-lymphocytes which express the CD4 receptor on its cell surface. The interaction between the viral envelope glycoproteins, gp120 and gp41; with CD4 and its co-receptors, CxCR4 and CCR5 facilitate binding and entry into host cells.
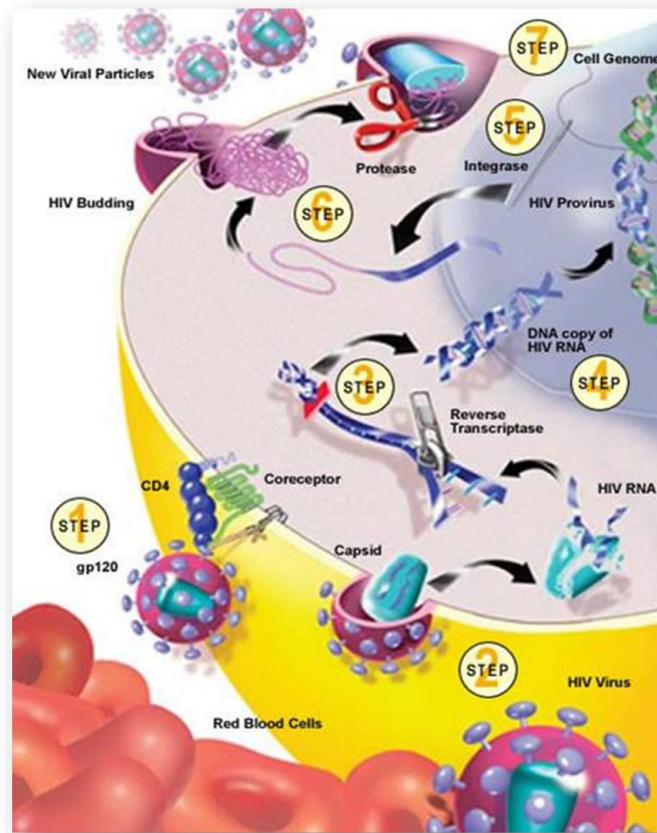
Figure 1.1. The HIV life cycle. This figure was adapted from an original illustration by Dominic Doyle at Vanderbilt University.

Following membrane fusion, the viral capsid containing two copies of the viral RNA genome, reverse transcriptase, and integrase; is released into the cell. After uncoating of the capsid, reverse transcriptase reverse transcribes the RNA to DNA and subsequently synthesizes a second DNA strand to form a double stranded DNA molecule. Integrase then cleaves a dinucleotide sequence from the 3' ends to generate reactive hydroxyl groups primed for integration. The pre-integration complex containing HIV integrase, reverse transcriptase and a series of host proteins then shuttles the DNA duplex to the nucleus where integrase, with magnesium ions as a cofactor, performs the strand transfer reaction in which the reactive hydroxyl groups hydrolyze a phosphodiester bond in actively transcribed regions of the host genome. Host cell DNA machinery then repair the single stranded breaks to seal the viral genome into the host cell DNA. Next, the inserted viral genome is transcribed into messenger RNA and translated into a

polyprotein which is then proteolytically processed by the HIV protease. Mature virus particles are assembled followed by budding from the host cells into the plasma to start a new infectious cycle.

1.3 The HIV-1 genome

The HIV-1 genome consists of a long single stranded RNA molecule that is 9.18 kb in length containing nine genes, gag-pol, gag, vif, vpr, tat, rev, vpu, env, and nef (Figure 1.2) [10, 11]. The Gag-Pol polyprotein is proteolytically cleaved by the protease enzyme to release mature protease, integrase and reverse transcriptase; three enzymes required for HIV reproduction. Once processed, cleavage of Gag generates the matrix protein (MA, p17), capsid protein (CA, p24), nucleocapsid protein (NC, p7), spacer peptide 1 (SP1, p2) spacer peptide 2 (SP2, p1) and p6. The env gene is processed by host proteases to generate the external glycoprotein gp120 and the transmembrane glycoprotein gp41 which interact noncovalently with each other on the surface of HIV-1 virions [12]. The regulatory proteins Tat and regulator of virion (Rev) function primarily in the cell nucleus by stimulating transcription and regulating viral RNA production, respectively [13]. The negative regulator protein (Nef) is an accessory protein having multiple roles including increasing or decreasing virus replication, reducing expression of MHC class I and the CD4 receptor; T-cell activation; and enhancing virion infectivity [14]. Another accessory protein, virion infectivity factor (vif) increases virus infectivity by affecting virion assembly during viral replication as it induces degradation of the antiretroviral cytidine deaminase, APOBEC3G [15]. The viral protein r (vpr) causes G_2 arrest and facilitates nuclear entry of the preintegration complex and viral protein u (vpu) affects virus release by disrupting the Env-CD4 complexes on the cell surface[16]. An important feature of the HIV-1 viral genome is the presence of the long terminal repeat sequences (LTR) on the viral ends which provide recognition sites for the HIV-1 integrase to bind and perform the 3'processing reaction to be discussed later in section 1.5.
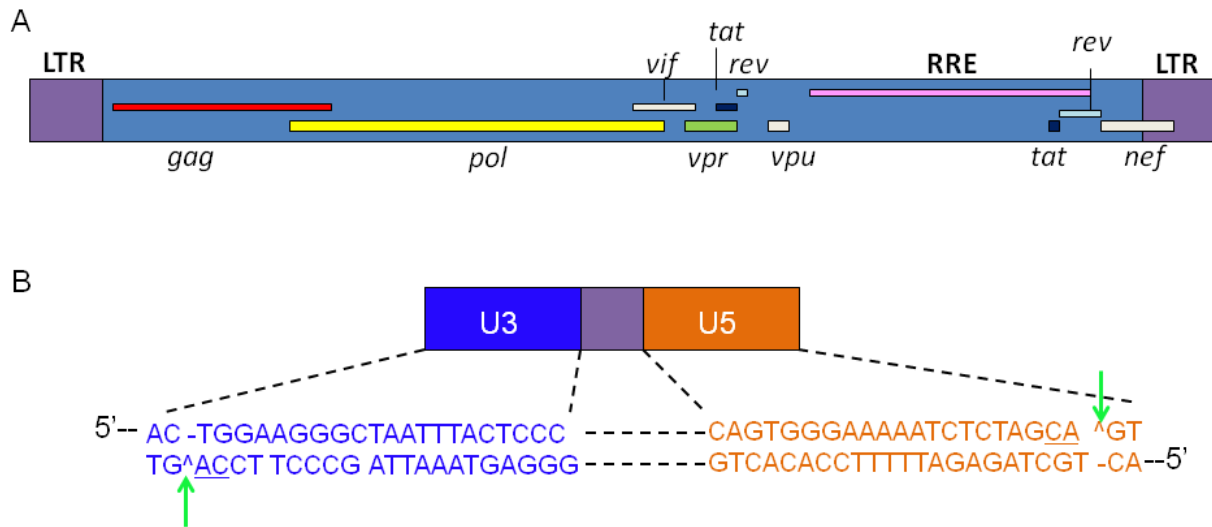
Figure 1.2 The HIV-1 genome. A. The elements of the HIV-1 viral genome are expressed in three different open reading frames as indicated by the vertical spacing. B. The long terminal repeat regions are shown to illustrate the di-nucleotide cleavage site indicated by the green arrow.

1.4 Treatment of HIV-1 infection with Highly Active Antiretroviral Therapy (HAART)

Treatment options for both treatment naïve and treatment experienced HIV patients span five different drug classes including nucleoside/nucleotide reverse transcriptase inhibitors, protease inhibitors, fusion and entry inhibitors, non-nucleoside reverse transcriptase inhibitors, and integrase inhibitors. Various combinations of these drug classes comprise Highly Active Antiretroviral Therapy (HAART) which has emerged as the current standard of care.

1.5 HIV-1 protease

HIV-1 protease (PR) functions as a homodimer containing 99 residues per monomer. It is an aspartic protease required for the maturation of HIV viral proteins and thus the reproduction of infectious virions [17]. As a member of the aspartic protease family of protease enzymes, HIV-1 PR uses two aspartic acid residues; one from each monomer (Asp25 and Asp25'); to make up the active site for catalysis of peptide substrates, Gag and Gag-Pol polyprotein precursor [18] . For this reaction to proceed,

one aspartic acid is protonated to serve as a general acid to polarize the scissile carbonyl oxygen of the substrate while the ionized form of the opposing aspartic acid is the nucleophile which deprotonates the required lytic water molecule (Figure 1.3) [19-24]. During substrate cleavage, the protonated aspartate the oxyanion intermediate then hydrolysis the peptide bond thus cleaving the substrate into two peptides. In addition to the two aspartic acid residues HIV-1 PR also contains a highly conserved Asp-Ser/Thy-Gly sequence motif at the active site which may also play a critical role in substrate binding [25, 26]. The PR active site is covered by two flexible β-hairpin loops which open and close to allow substrate binding and release [27].
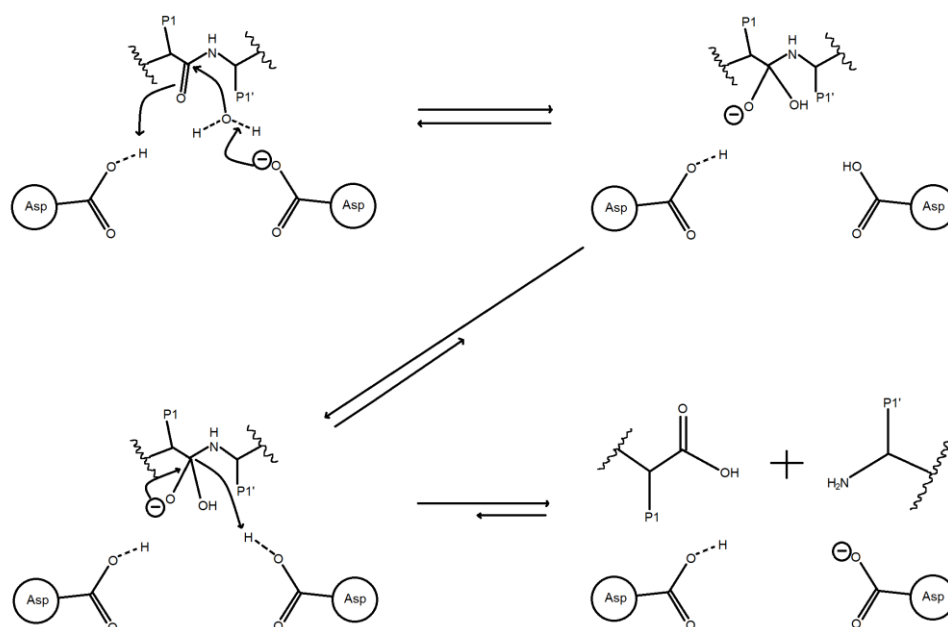
Figure 1.3 Mechanism of HIV-1 substrate cleavage by the protease enzyme.

1.5.1 Protease inhibitors

A major breakthrough in the treatment of HIV/AIDS came with the development of HIV-1 PR inhibitors which are currently being used extensively in HAART therapy. The United States Food and Drug Administration has approved 9 protease inhibitors; tipranavir, darunavir, amprenavir, lopinavir, atazanavir, saquinavir, indinavir, ritonavir, and nelfinavir. With the exception of darunavir, PR inhibitors were designed as peptidomimetic compounds to resemble the transitions state between the endogenous

substrates and PR based on a series of X-ray crystal structures of the HIV-1 PR bound to several inhibitors. These structures revealed key features that became instrumental in the subsequent design and development of these inhibitors; (1) HIV-1 PR is a homodimer with C_2 symmetry, (2) the catalytic aspartic acid residues lie at the bottom of the active site (3) a tetrahedrally coordinated water molecule between the HIV-1 PR flaps and the bound ligand may play a role in stabilizing the drug in the active site [28, 29].
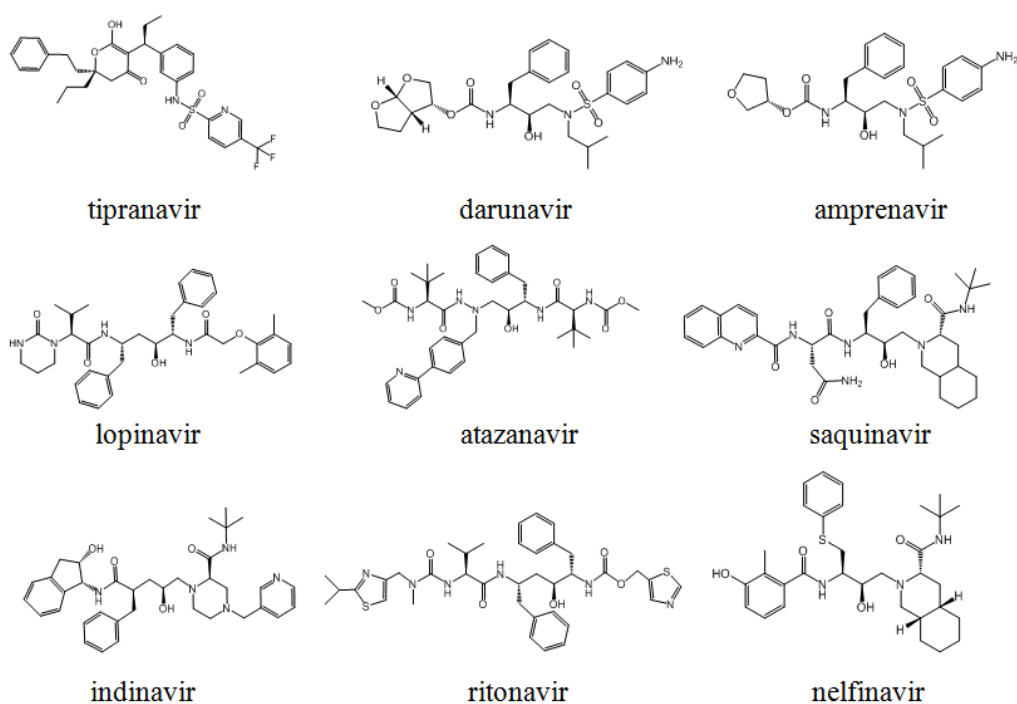
Figure 1.4. Chemical structure of the FDA approved HIV-1 protease inhibitors

1.5.2 Protease inhibitor mechanism of inhibition

Each of the HIV-1 PR inhibitors (PIs) currently on the market contains a hydroxyl group required to mimic the transition state of proteolytic cleavage. This reaction proceeds through a gem-diol reaction intermediate as observed using [18]O isotope exchange experiments [30]. This hydroxyl group interacts with the D25 and D25' to inhibit the HIV-1 PR. In addition to this feature, the PIs also bind the PR in a

similar fashion in which the P1 and P1' groups of the inhibitor bind to the S1 and S1' pockets of the HIV-1 PR similar to the binding mode seen in substrate binding (Figure 1.5) [31-33]. The inhibitors consistently make contacts with Gly, 27, Asp 29, Asp 30 and Gly 48.
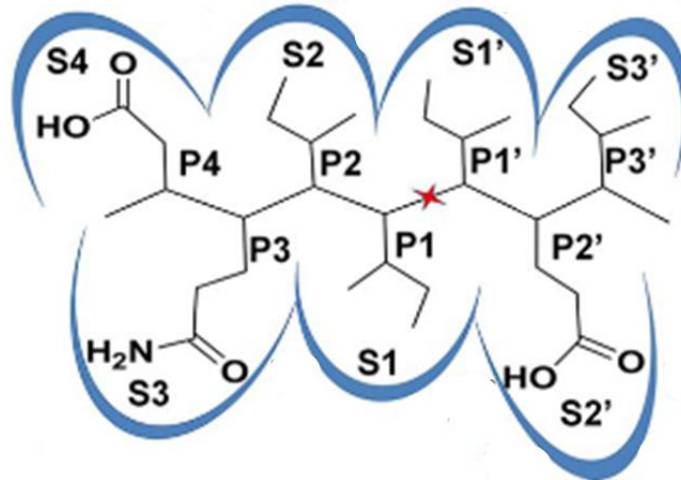
Figure 1.5 Binding mode of the substrate in the HIV-1 protease active site. P4-P3' indicate the position of the substrate peptide while S4-S3' indicate the binding pockets of the HIV-1 protease. The red star represents the substrate cleavage site.

1.6 HIV-1 integrase

Viral DNA integration mediated by HIV integrase is a key process required for viral replication [34]. While in the cytoplasm, integrase assembles into a dynamic complex termed the pre-integration complex (PIC), known to consist of the viral proteins; Vpr, matrix, integrase, and reverse transcriptase. Vpr has been shown to be involved in modulating the viral reverse transcription, nuclear import of the HIV-1 pre-integration complex, and transactivation of the HIV-1 LTR promoter. The HIV integrase enzyme catalyzes 3' processing (3'p); a dinucleotide sequence is cleaved from the 3' end of the viral genome at the long terminal repeat sequences generating reactive hydroxyl ends primed for integration [35]. Integrase interacts with cellular proteins importin α and transportin 3 to assist with effective import through the host nuclear pore complex [36]. After translocation to the host cell nucleus, HIV integrase then facilitates the strand transfer transesterification reaction where the viral DNA is inserted into the host chromosome. Concerted integration of the viral DNA is performed by the synaptic complex in which

integrase functions as a tetramer, however the monomer has been shown to interact specifically with the viral LTR. [37] Insertion of the viral genome is also mediated by the PWWP domain of the cellular chromatin interacting protein LEDGF/p75 by tethering and targeting the HIV-1 integrase to regions with specific post translational modifications [38]. Upon insertion, host DNA repair pathways are induced increasing expression of Rad51, a protein involved in the homologous recombination-directed DNA repair (HHR) pathway as well as various other cellular proteins [39].

1.6.1 Integrase inhibitors

In 2007, raltegravir (RAL) was the first HIV integrase inhibitor to be approved by the US Food and Drug Administration (FDA) Two additional integrase inhibitors, elvitegravir (EVG), and dolutegravir (DTG, S/GSK1349572), are currently in clinical trials while other compounds are in development.

Raltegravir

Raltegravir was the first strand transfer inhibitor (STI) to be approved by the FDA for the treatment of HIV-1 infection. 400 mg twice-daily dosing of RAL with once-daily tenofovir-emtricatabine; a reverse transcriptase inhibitor, is one of the preferred treatment options for treatment-naïve HIV-1 infected patients, while once daily dosing of RAL was not recommended for increased risk of the development of drug resistance resulting in treatment failure [40].

RAL was optimized from two scaffolds; dihydroxyperimidine and N-methyl pyrimindinone carboxamides, both of which had been shown to inhibit strand transfer [41]. RAL is metabolized by UGT1A1. While the increase in plasma concentration of RAL caused by co administration with a UGT1A1 inhibitor was not found to be clinically meaningful, the decrease caused by a UGT1A1 inducer is being investigated in clinical studies [42]. The site of RAL action is intracellular, however studies showed that RAL penetration into cells is approximately 5% of plasma levels with high variability between patients [43].
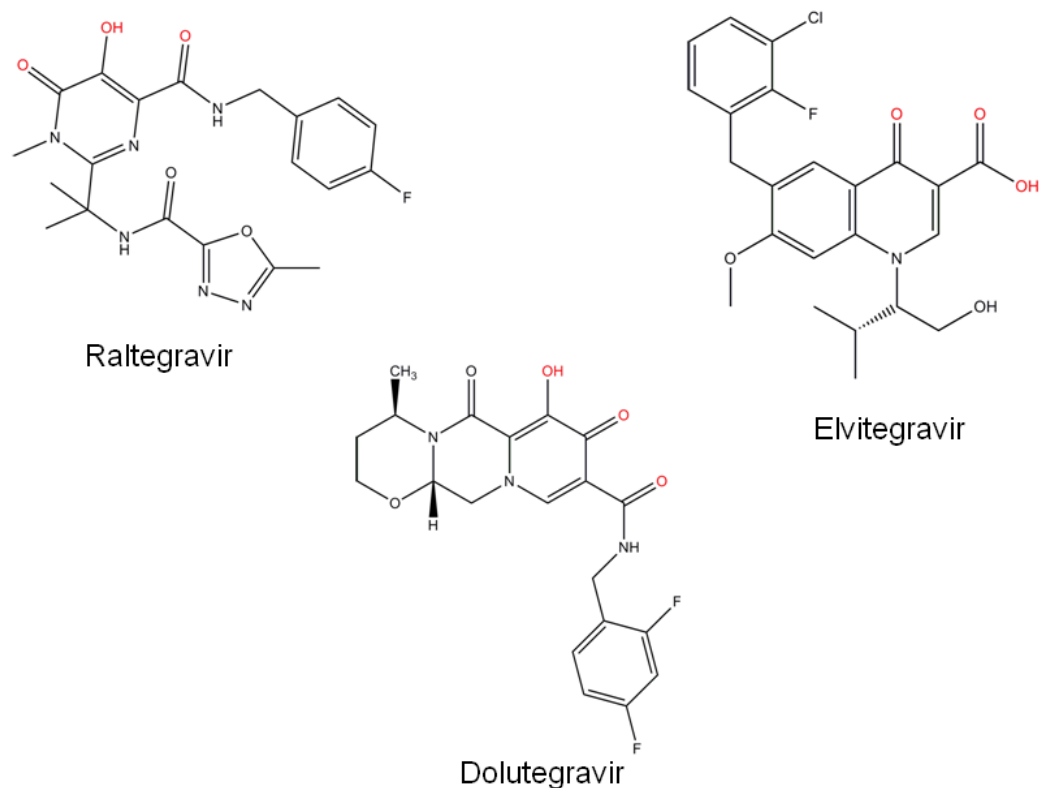
Figure 1.6 Chemical structure of FDA approved HIV-1 integrase strand transfer inhibitors. Oxygen atoms involved in metal chelation are shown in red.

Elvitegravir

Elvitegravir (GS9137) is an integrase inhibitor approved as part of a "Quad" formulation pill containing EVG, emtracitabine, tenofovir disoproxil fumerate and cobicistat (GS0350) which has the advantage of once daily dosing [44, 45]. The structure was derived from chemical modification of quinolone antibiotics containing a monoketo acid motif capable of integrase inhibitory efficacy comparable to the diketo acid structural motif [46]. EVG has been observed to possess post antiviral effects in cultured CD4-positive cells suggesting a possible role as a potential prophylaxis application [47]. EVG was shown to inhibit the ABC transporter, ABCB1 in P388/dx and L-MDR1 cells suggesting that EVG may play an important role in resistance and drug-drug interactions [48].

Dolutegravir

Dolutegravir (S/GSK1349572) is a potent second generation STI currently in phase III clinical trials with a cell-based therapeutic index of 9,400 showing efficacy against NNRTI, NRTI, and PI-resistant viruses with activity equivalent to that against the wild-type virus [49]. Its pharmacokinetic profile, short-term tolerability and potent antiviral activity support once-daily dosing as demonstrated in treatment –naïve HIV patients [50]. According to crystal structures with the prototype foamy virus (PFV), DTG binds the active site of the retroviral intasome with its three coplanar oxygen atoms coordinated to the active site Mg^{2+} cations and the halogenated phenyl group displaces the 3' terminal viral DNA [51]. DTG has a 5 to 40 times slower dissociation constant than RAL and EVG in the integrase-DNA complex [52].

1.6.2 Integrase inhibitor mechanisms of inhibition

HIV-1 integrase inhibitors currently on the market work by competing with viral DNA for active site binding to inhibit the strand transfer step of the HIV life cycle. Alternatively, allosteric inhibitors are being developed which modulate integrase activity by affecting assembly, or interfering with binding to host cell factors.
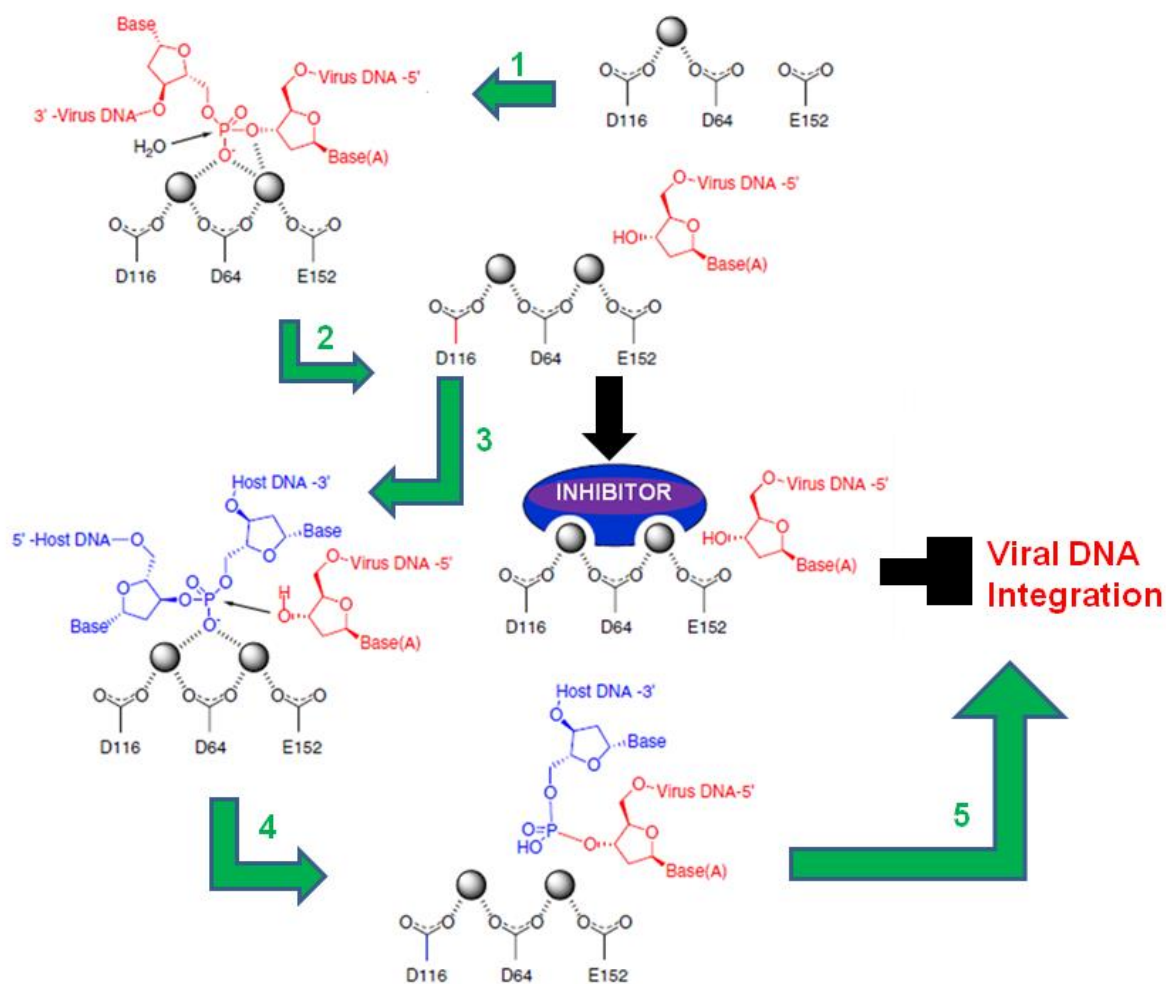
Figure 1.7 Mechanism of action of HIV-1 integrase strand transfer inhibitors

1.6.2.1 Strand transfer inhibitors

Integrase strand transfer inhibitors (STIs) bind to the HIV-1 integrase enzyme in complex with its viral DNA and two divalent metal ions (Figure 1.7) [53]. The ability of an STI to physically trap the synaptic complex and therefore inhibit concerted integration correlates with its inhibitory efficacy, IC_{50} [54]. The metal chelating functionality of integrase STIs may be involved in multiple processes such as the exchange of metals in the active site and the coordination of a second metal; suggesting a mechanistic explanation of some molecules' ability to inhibit 3' processing in addition to strand transfer. The halogenated phenyl group plays a vital role in displacing the viral terminal DNA residue from the active

site [55, 56]. Before the structure of the PFV intasome had been published a number of molecular modeling studies provided insights on possible binding modes and mechanisms of action. Induced fit docking experiments with the integrase inhibitors L-708,906, L-731,988, S-1360, L-870,810, raltegravir, and EVG showed consistent support of the proposed metal chelating mechanism. [57] Inhibition kinetics studies of these inhibitors as well as GSK364735 indicate time-dependent inhibition consistent with a two step binding mechanism [58].

1.6.2.2 Allosteric inhibitors

Allosteric integrase inhibitors are designed to either disrupt subunit assembly, indirectly disrupt DNA-binding site conformation or disrupt obligatory protein-protein interactions [59]. The N-terminal domain of integrase contains a highly conserved HHCC zinc binding motif that enhances multimerization and is also involved in DNA binding [60, 61]. Disruption of the HHCC domain renders intergrase incapable of catalytic activity and of initiating reverse transcription making the virus non-infectious [62-64]. Crystal structures of cyclic peptides bound to the HIV-1 integrase catalytic core domain identified residues 170, 171, and 174 as potential targets to inhibit the LEDGF/p75 interaction [65]. Molecules such as PLP targeting the C-terminal domain have revealed its importance in DNA binding as viruses carrying the K244E substitution are deficient in 3'processing and strand transfer activity [66]. A number of compounds have been identified to reveal allosteric binding sites on the dimeric interface disrupting oligomerization [59].

1.7 Antiretroviral resistance

While there are many different types of antiretrovirals (ARV) used in the treatment of HIV, the development of drug resistance resulting in treatment failure remains a major challenge. To combat the resistance problem, the development of molecules with a new mode of action or active substituent and improved potency are needed.

1.7.1 Protease inhibitor resistance

Multi-drug resistance mutations in the HIV-1 PR selected under PI treatment occur which reduce the effectiveness of the PI. Common mutations conferring cross resistance to the PI class of inhibitors include V32I, L33F, M46IL, I47VA, G48VM, I50LV, I54VTALM, L76V, V82ATFS, I84V, N88S, and L90M (Figure 1.8) [67, 68]. While most of the PIs have a similar resistance profile, darunavir and tipranavir seem to have a higher barrier to resistance with increased resilience against these common mutations [69].
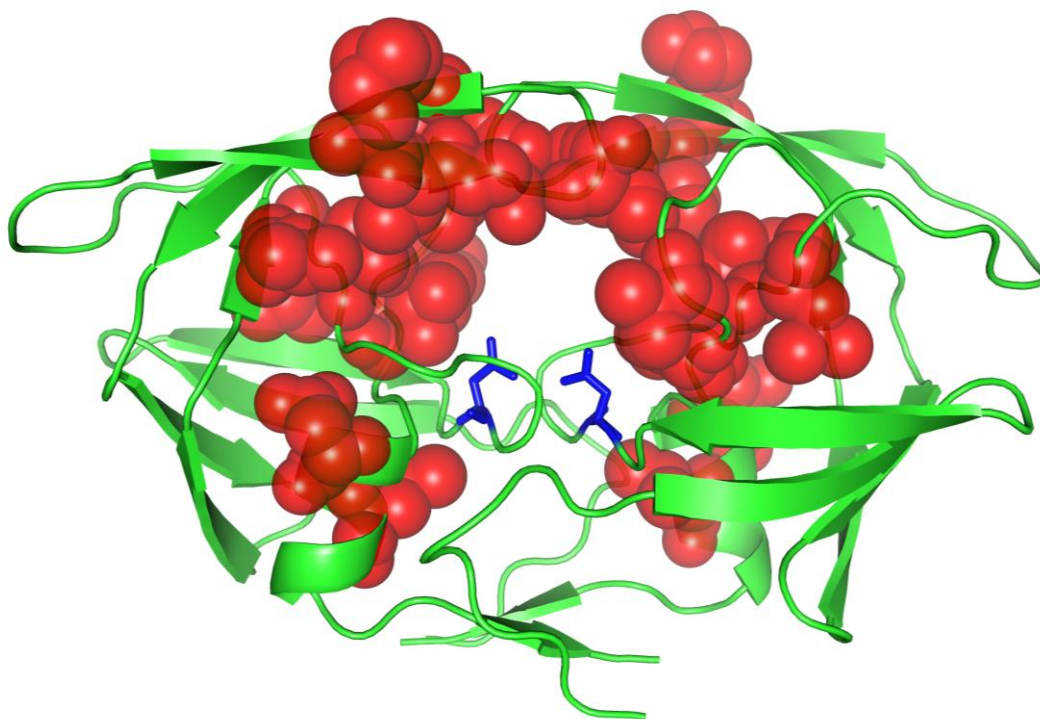
Figure 1.8 Major drug resistant mutations cluster around the active site of HIV-1 protease. The major drug resistant mutations are shown in red sphere representation. The catalytic residues D25 and D25' are shown in blue stick model.

Atazanavir resistance

Ritonavir boosted atazanavir in combination with tenofovir and emitricitabine, two nucleoside reverse transcriptase inhibitors, is currently one of the first line treatment options for initial treatment of HIV/AIDS patients [70]. The following mutations have been observed in patients and contribute to

reduced susceptibility in combination with other PI resistance mutations; V32I, L33F, M46IL, I47V, I54VTALM, and V82ATFS [71, 72]. G48VM and L90M mutations reduce susceptibility and virological response while I50L, I84V, and N88S are associated with the highest levels of reduced susceptibility to atazanavir [73-75].

Darunavir resistance

Ritonavir boosted darunavir containing regimens are also included in the preferred treatment guidelines[70]. Darunavir has the most favorable drug resistance profile in that mutations I47VA, I50V, I54LM and L76V are associated with reduced susceptibility as opposed to virological failure as seen with the other protease inhibitors [76, 77].

Fosamprenavir resistance

Fosamprenavir is the only pro-drug HIV-1 protease inhibitor with efficacy comparable to lopinavir [78]. As a pro-drug its long acting nature allows for less frequent dosing making it an attractive option for patients with compliance issues. Resistance to fosamprenavir occurs with mutations V32I, I47VA, I50V, I54VTALM, L76V, V82ATSF, I84V, and L90M resulting in significantly reduced susceptibility and virological response. Despite the cross resistance profile of fosamprenavir, dual boosted protease inhibitor-based regimens containing atazanavir and fosamprenavir may be effective against treatment experienced pediatric patients [79].

Indinavir resistance

Resistance mutations resulting in the highest levels of virological failure under indinavir selection pressure include I54VTALM, L76V, V82AFTS, and I84V. While not in the first line treatment options; indinavir remains susceptible to protease populations containing the common I50LV mutation which are resistant to atazanavir, darunavir and lopinavir [76, 80]. Indinavir is quickly metabolized by liver enzymes and has been shown to result in kidney failure due to its hepatotoxicity [81]. Both the side effect

profile and the dosing schedule play a major role in the development of drug resistance due to patient compliance.

Lopinavir resistance

Lopinavir is the first line treatment option for pregnant women and children due to its safety and efficacy in pediatric HIV-1 treatment [70]. A long-term clinical study performed in the UK showed that 27% of patients on lopinavir containing regimens experienced virological failure after one year in which I54V, M46I, V82A and L76V were the most frequently occurring mutations [82].

Nelfinavir resistance

Nelfinavir resistance is seen with mutations similar to the other PIs. However, nelfinavir is the only protease inhibitor which results in reduced virological response as a result of the D30N mutation. The precise structural mechanism resulting in failure with nelfinavir is not well understood, however molecular dynamics simulations with HIV-1 protease enzymes of different subtypes suggest that D30N may be responsible for conformational changes associated with the loss of secondary structure in the HIV PR [83]. The accessory mutation K20I has been shown to contribute to reduced susceptibility in B-subtypes [84].

Saquinavir resistance

Saquinavir resistance is acquired with the major mutations G48VM, I54VTALM, V82AT, I84V, N88S and L90M. While many accessory mutations contribute to reduced susceptibility against other PIs, the I47A mutation actually increases susceptibility to saquinavir [85]. Interestingly this mutation reduces susceptibility to lopinavir. The structural mechanisms underlying these differences in PI efficacy have yet to be explored.

Tipranavir resistance

Like darunavir, tipranavir has a high barrier to resistance with a similar resistance profile. Complications with tipranavir however are due in part to the high risk of intracranial hemorrhage and

liver-associated deaths [86-88]. Tipranavir has demonstrated reduced susceptibility against drug resistant proteases harboring V30I, L33F, M46IL, I47VA, I54VAM, V82TL, and I84V. Interestingly, tipranavir remains effective against the common multidrug resistant mutations G48VM, I50LV, L76V, N88DS, and l90M.

1.7.2 Integrase inhibitor resistance

Raltegravir resistance

Patients failing on RAL containing regimens frequently carry viruses harboring primary mutations at codons 148, 155 and 143 [89]. The G140S mutation has been shown to increase viral fitness while the Q148H mutation is likely responsible for resistance to RAL as the double mutation displays replication capacity near wild-type levels [90]. The Q148H, G140S double mutation also confers cross resistance to EVG and G-quadruplex inhibitors [91]. Cocrystal structures of S217Q, S217H and N224H mutant PFV intasomes corresponding to HIV-1 integrase RAL resistance mutations Q148H and N155H in complex with the second generation STI MK2048, showed that these substitutions interfere with metal coordination [92]. Based on the mechanism of STI action, any loss in metal coordination would subsequently decrease the chelating power of the inhibitor. RAL resistance may also occur through transmission of multi drug resistant variants highlighting the importance of genotyping even in treatment naïve patients [93].

Viral strains harboring the 148H/140S mutations have a ten-fold reduction in susceptibility to MK-2048 and the S153F/Y mutations confer resistance to MK-2048 as well as GSK-1349572 suggesting a common mechanism between these two molecules [94]. The secondary mutation T97A rescues the catalytic defect caused by the RAL primary resistance mutation, Y143R/C, and reduces in vitro susceptibility to RAL [95]. The second generation STI MK-0536 binds to HIV-1 IN CCD with nanomolar inhibitory efficacy and increased potency against classical RAL resistance mutations [96].
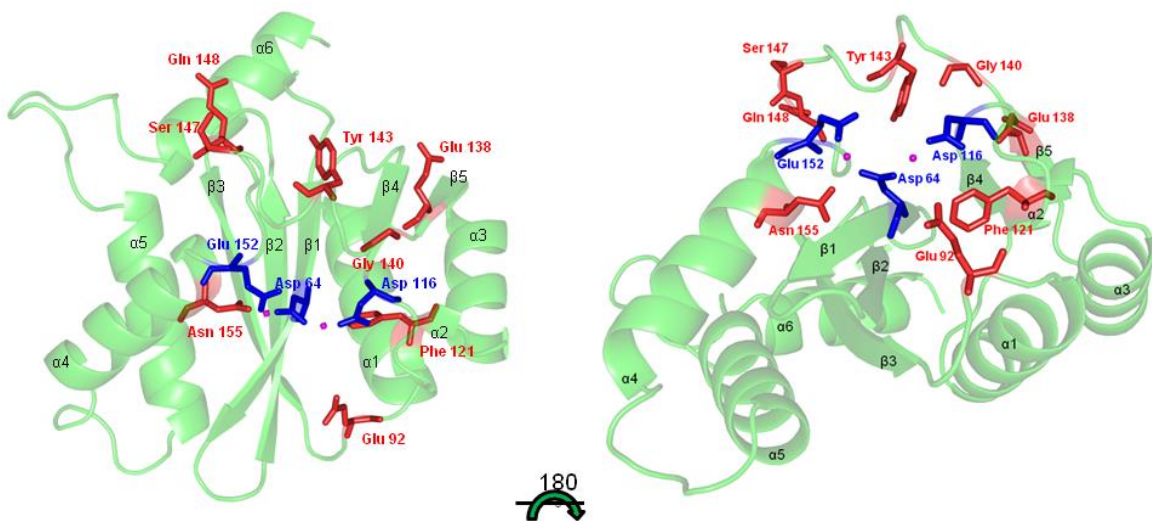
Figure 1.9. Resistance mutations in HIV integrase. HIV-1 IN CCD (50-212) raltegravir resistance mutations associated with 5-10 fold decreased susceptibility are shown in red, Mg^{2+} in magenta, and catalytic residues in blue.

Elvitegravir resistance

EVG is a potent STI, however resistance mutations have been observed with primary mutations at T66I, E92E/Q, Q146P, and S147G and secondary mutations H51Y, Q95K, E138K, and E157E/Q [97].The T66I/A mutation was observed most frequently among patients experiencing virologic failure on EVG containing regimens during phase 3 clinical trials [98]. Additional EVG resistance mutations F121Y and S153F/Y have also been observed to cause cross resistance to other STIs [99-101]. While EVG overcomes resistance to the RAL mutation Y123C/R, the 148 and 155 pathway of RAL resistance confers cross resistance to RAL [102].

Dolutegravir resistance

No treatment-naïve patient has developed resistance to DGV, however the mutations involving T134A, S153F/Y, and L101I mutations have been observed *in vitro*[49, 52]. In vitro DTG selection experiments revealed the R263K mutation that causes low-level resistance to DTG as well as reduced viral fitness due to the specific reduction DNA binding [103]. DTG has been shown to be effective

against first generation STIs RAL and EVG mutations at Y143 and N155H however the Q148H/R in combination with G140S/A pathway confers reduced susceptibility to DTG as well and early discontinuation of RAL is necessary for treatment with DTG as a rescue therapy for patients who have experienced virological failure [104, 105].
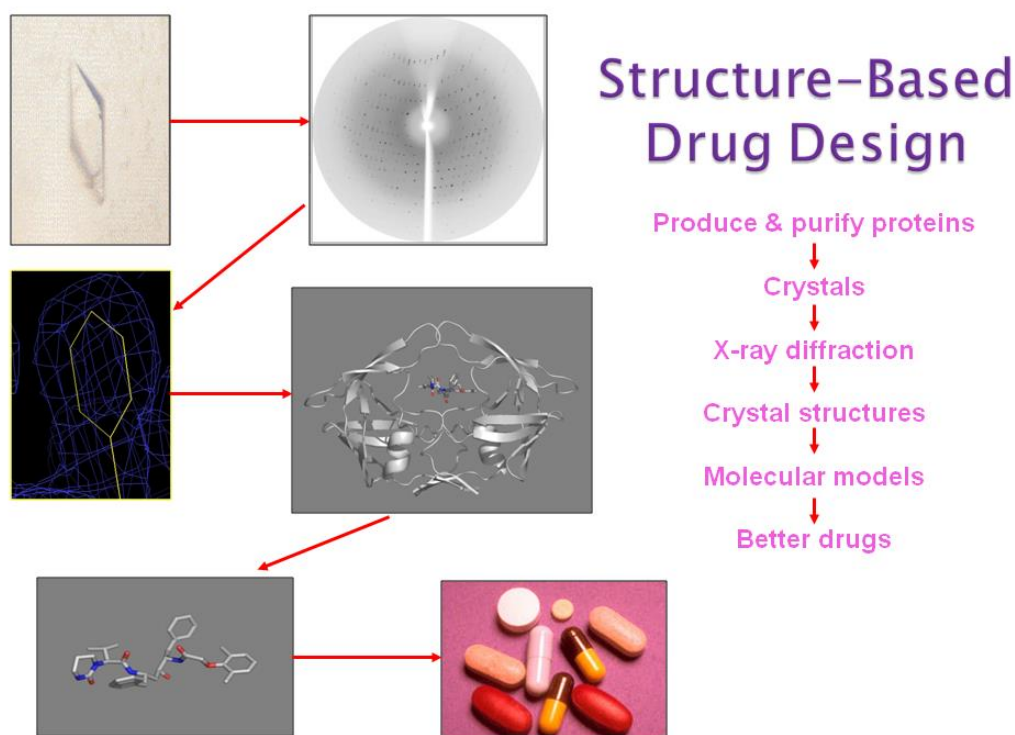
Figure 1.10 Structure-based drug design. The goal of this work is to use structural information to design better inhibitors for the treatment of multi-drug resistant HIV-1 infection.

1.8 Structure-based drug design

Historically, drugs were discovered by identifying active components of traditional remedies; however more recently drugs have been discovered or optimized using a structure-based approach (Figure 1.9). Quantitative drug design is a method which relates the biological properties of a compound as a function of its physiochemical parameters such as solubility, lipophilicity, electronic effects, ionization, and stereochemistry [106]. The original Hansch equation of the form:

$$\log (1/C) = k_1 \log P - k_2(\log P)^2 + k_3\sigma + k_4$$

Where C is the concentration of the compound required to produce a standard response in a given time, log P is the logarithm of the partition coefficient of the compound between 1-octanol and water (which was chosen as a suitable measure of relative hydrophobicity), σ is the Hammett substituent parameter and k_1- k_4 are constants; relating a molecule's electronic characteristics to hydrophobicity was used to define these parameters [29, 107-109]. This concept of quantitative structure activity relationships (QSAR) has since been adapted to reflect a number of different relationships. Of particular interest to the design of protease inhibitors, the use of relative shape of the substrate envelope has proven to be effective [28, 31, 110]. Using structural information from x-ray crystallography, NMR and molecular modeling, the 3D-QSAR methodology makes it possible to identify specific interactions between the ligand and the enzyme. Therefore, optimizing these interactions to increase binding affinity can potentially increase the potency of an inhibitor.

Chapter 2: Materials and Methods

2.1 HIV-1 protease expression and purification

Active and inactive MDR HIV-1 protease genes were codon optimized for *E. coli* expression with the software DNA 2.0 [111], synthesized by GENEART, Inc. (Regensburg, Germany), and inserted into the pET21b plasmid. The inactive MDR 769 82T protease carries an active site mutation, D25N, to eliminate catalytic activity. To prevent auto-proteolyses, the Q7K mutation was introduced into the active MDR HIV-1 protease gene. All MDR HIV-1 proteases were expressed in the *E. coli* strain BL21 (DE3) pLysE and the cells were lysed by sonication. The HIV-1 protease expressed in inclusion bodies was separated by centrifugation and dissolved in a buffer of 50 mM Tris, 25 mM sodium chloride, 0.2% β-mercaptoethanol, and 6 M urea. The dissolved HIV-1 protease variants were purified using a Q-Sepharose ion exchange column (Amersham Biosciences, Piscataway, NJ) pre-equilibrated with the buffer containing 6 M urea. The optimal buffer pH varied from 7.8-8.6 for the active and inactive protease variants. The flow-through containing the pure HIV-1 protease was refolded in the dialysis buffer (20 mM sodium phosphate, 0.2% β-mercaptoethanol, and 10% glycerol) with step-wise decreases in urea concentration. The final protein buffer was 20 mM sodium acetate, pH 5.0, 1 mM dithiothreitol (DTT), and 10% (v/v) glycerol. The proteases prepared for crystallization were concentrated to 1.5 mg/ml using Amicon concentrators with a 5-kDa molecular mass cut-off (Millipore Corporate, Billerica, MA).

2.2 Protease inhibition assays

HIV protease Forster Resonance Energy Transfer (FRET) substrate I, purchased from AnaSpec, Inc. (Fremont, CA, USA), was used in the half-maximal inhibitory concentration (IC_{50}) determination experiments. The FDA-approved HIV-1 protease inhibitors were kindly provided by the NIH AIDS Research and Reference Reagent Program (www.aidsreagent.org). The CA/p2 pseudopeptide with a reduced scissile peptide bond [-ψ(CH2NH)-] was synthesized in the laboratory of Patrick Woster in the Department of Chemistry, Wayne State University. The fluorescence emitted by substrate cleavage was

monitored by a microplate reader (SpectraMax M5, Molecular Devices, Sunnyvale, CA) at a 340 nm excitation wavelength with an emission wavelength of 490 nm. The HIV-1 protease reaction buffer was adjusted to pH 4.7 [0.1 M sodium acetate, 1.0 M sodium chloride, 1.0 mM ethylenediaminetetraacetic acid (EDTA), 1.0 mM DTT, 10% dimethylsulfoxide (DMSO), and 1mg/ml bovine serum albumin (BSA)]. In the reaction buffer containing 5 μM FRET substrates, the concentration of all the HIV-1 proteases used in the enzyme assays was adjusted to a substrate cleavage velocity of 0.08 Relative Fluorescence Units (RFU)/sec. The final HIV-1 protease concentration was approximately 7 nM. The protease inhibitor was serially diluted in DMSO from 10 μM to 0.013 nM. The protease and inhibitors were pre-incubated at 37°C for 20 min prior to signal monitoring. An enzyme-free control was tested as the background substrate fluorescent signal. The progress of the reaction was monitored over 20 min sampling fluorescence at 1 min intervals. The FRET data were plotted with the software SoftMax Pro V5.2 (Molecular Devices, Sunnyvale, CA) using a 4 parameter fit to determine the IC_{50} values.

2.3 Crystallization and diffraction data collection

Reduced substrates (F-r-L and F-r-F) were co-crystallized with the MDR769 82T inactive protease using the hanging drop vapor diffusion method. The protease and ligand were pre-mixed at a molar ratio of 1:20 before crystallization set-up. The protease-ligand solution was then mixed at 2:1 v/v ratio with the precipitant solution. The optimal crystallization condition was obtained from for the MDR 769 82T-/F-r-L complex from 0.1 M citric acid and 2.4 M ammonium sulfate at pH 5.2 while the MDR 769 82T-/F-r-F complex crystallized with 0.1M MES, 2.4 M $(NH_4)_2SO_4$, pH 6.2. The reservoir volume was 750 μl. Needle shape crystals grew to a suitable size for diffraction within a week. The crystals were placed in a 30% w/v glucose cryoprotectant solution before the crystals were frozen in liquid nitrogen. The diffraction data were collected at the Life Sciences Collaborative Access Team (LS-CAT) at the Advanced Photon Source (APS) Sector 21, Argonne National Laboratory (Argonne, IL, USA) and the diffraction data were processed with the HKL2000 program suite [112].

2.4 Structure refinement and analysis

Molecular replacement was performed with the CCP4 program Molrep-autoMR [113]. A previously solved HIV-1 protease structure was used as a searching model for molecular replacement. The models of the reduced substrate peptides were built with the program COOT [114] using a ligand finding algorithm where the molecular formulas of the inhibitors were provided in SMILES representation. The protease-ligand model was further refined using the program Refmac5. The structure was validated using Procheck V3.4.4 [115]. The co-crystal structures were deposited in the Protein Data Bank (http://www.pdb.org/). The accession codes for the L-r-F-MDR 769 82T complex and the F-r-F-MDR 769 82T complex are 4GZF and 4GYE, respectively.

2.5 Molecular dynamics

Molecular dynamics (MD) is a computational method to calculate the time dependent behavior of a molecular system by numerically solving Newton's equations of motion using a molecular mechanics force field which defines the forces between charges as well as the potential energy function. Internal motions of proteins cause conformational changes that play an essential role in protein function [116]. These simulations provide detailed structural information regarding local motions such as atomic fluctuations, side chain motion and loop motions. MD simulations on the scale of nano seconds to seconds may demonstrate larger protein dynamics such as helix, domain and subunit motions. Large-scale motions greater than 5 Å, including helix coil transitions, dissociation/association and folding and unfolding behaviors may take minutes to be observed in an MD simulation [117-120].

2.5.1 The CHARMM force field

All computational work presented here has been performed using the CHARMM (Chemistry at HARvard Macromolecular Mechanics) force field originally developed at Harvard in the laboratory of Martin Karplus and continues to be updated regularly [121, 122]. The components of the potential account for bond stretching, bond angle bending, torsion (dihedral angle), and nonbonded interaction.

The nonbonded interactions include van der Waals (vdW) energy and electrostatic (Coulomb) energy. The potential energy and its derivatives are calculated from the coordinates corresponding to the structure or conformation based on fixed point charges as shown in Equation 1 below [122].

$$U(\vec{R})= \sum_{bonds} K_b(b-b_0)^2 + \sum_{angles} K_\theta(\theta-\theta_0)^2 + \sum_{Urey-Bradley} K_{UB}(S-S_0)^2 +$$
$$\sum_{dihedrals} K_\phi(1+\cos(n\phi-\delta)) + \sum_{impropers} K_\omega(\omega-\omega_0)^2 +$$
$$\sum_{\substack{non-bonded \\ pairs}} \left\{ \varepsilon_{ij}^{min} \left[\left(\frac{R_{ij}^{min}}{r_{ij}}\right)^{12} - 2\left(\frac{R_{ij}^{min}}{r_{ij}}\right)^6 \right] + \frac{q_i q_j}{4\pi\varepsilon_0 \varepsilon r_{ij}} \right\} + \sum_{residues} U_{CMAP}(\phi,\psi)$$

(Eq 1.)

The potential energy, ($U(\vec{R})$), is a sum over individual terms representing the internal and non-bonded contributions as a function of the atomic coordinates. Internal terms include bond (b), valence angle (θ), Urey-Bradley (UB, S), dihedral angle (φ), improper angle (ω), and backbone torsional correction (CMAP, φ,ψ) contributions. The parameters Kb, $K\varphi$, KUB, $K\theta$ and $K\omega$ are the respective force constants and the variables with the subscript 0 are the respective equilibrium values; here n is the multiplicity or periodicity of the dihedral angle and δ is the phase shift.

2.5.2 Scalable molecular dynamics with NAMD

The MD simulations were performed using the parallel computing program Scaling NAno Molecular Dynamics (NAMD) V. 2.7b [123]. The protease complex models were solvated in a water box using TIP3P models for water molecules. To prevent translational and rotational displacement and to prevent the simulation of the catalytic reaction, positional restraints were applied for the carbonyl protease. The cutoff of non-bonded interactions was 10 Å. Particle Mesh Ewald was implemented to calculate long-range electrostatic interactions [124]. The systems were energy minimized using a conjugate gradient method and gradually heated from liquid nitrogen temperature of 70K to 310K in 200 ps. Simulations were conducted in the isobaric-isothermal ensemble at 310K and 1.0 atm (NPT ensemble)

for 10-40 ns using the CHARMM force field 27 or the CHARMM force field 36 and a timestep of 2 fs to ensure all the all conformers are sampled during the simulation.

All simulations were performed in the NPT ensemble. Langevin dynamics was used to keep the system at a constant temperature of T = 310K. The Langevin damping coefficient was set to 5 ps^{-1}. Constant pressure was maintained using the Nose-Hoover Langevin piston method at 1 atm. [125, 126] MD simulations were performed in parallel on multiple processors using the Wayne State University high performance scientific computing Grid (www.grid.wayne.edu). The WSU Grid has the combined processing power of 1558 cores: 898 Intel cores, 660 AMD Opteron cores, with over 2TB of RAM and over half a petabyte of disk space.

An example of NAMD configuration commands with annotations is listed as follows.

Adjustable Parameters

structure   *input.psf* ; # Specify a protein structure file that contains molecular characteristics required by a particular force field.

coordinates   *input.pdb* ; # Specify an atomic coordinate file

set temperature 310 ; # The simulation was conducted at 310 K.

set outputname   *output* ; # Name the output files

firsttimestep   *0* ; # Start the simulation from step 0.

Simulation Parameters

paraTypeCharmm   *on* ; # Turn on CHARMM force field.

parameters   *Par_all27_prot_na.prm* ; # Specify the CHARMM27 parameter file which define forces and energies for protein, lipid, DNA, and RNA.

parameters   *par_all36_cgenff.prm* ; # Specify the CHARMM General Force Field parameter file for compounds.

temperature   *$temperature* ; # Read temperature from "temperature" variable.

reassignFreq   *2000* ; # Reassign temperature every 2000 steps.

reassignTemp   70 ; # Increase temperature from 70 K (the liquid nitrogen temperature).

reassignIncr   5 ; # The temperature increment is 5 K.

reassignHold   310 ; # Hold the temperature at 310 K.

 # Force-Field Parameters

exclude scaled1-4 ; # Four adjacent covalently bonded atoms are excluded from non-bonded

calculations.

1-4scaling   1.0 ; # The constant factor of electrostatic interactions for 1-4 atom pairs.

cutoff   12. ; # The cutoff distance for non-bonded interaction is 12 Å.

switching   on ; # Smoothing functions are applied to both the electrostatics and van der

Waals forces.

switchdist   10. ; # The smoothing function takes effect when atom distance is between 10

and 12 Å.

pairlistdist   13.5 ; # When distance between atoms is less than 13.5 Å in each cycle, the

atom pair is included in pair list for electrostatics and van der Waals interaction

calculation.

margin   2.5 ; # Add 2.5 Å length in patch dimension.

 # Integrator Parameters

timestep   2.0 ; # The length of each step is 2fs.

rigidBonds   all ; # The bond between hydrogen and its bonded atoms is constrained.

nonbondedFreq 1 ; # Non-bonded interactions are calculated in every time step.

fullElectFrequency   2 ; # Full electrostatic interactions are calculated in every 2 time step.

stepspercycle   10 ; # The interacting particle lists are updated every 10 time step.

 # Constant Temperature Control

langevin   on ; # Perform Langevin dynamics to introduce additional damping and random

forces to the system.

langevinDamping   *5* ; # Langevin damping coefficient is 5/ps

langevinTemp   *$temperature* ; # Langevin dynamics adjust the effect on atoms based on the

temperature variable.

langevinHydrogen   *off* ; # Turn off Langevin dynamics for hydrogen atoms.

Constant Pressure Control

useGroupPressure   *yes* ; # Pressure is calculated using hydrogen-group based pseudo-

molecular virial and kinetic energy which results in smaller fluctuations.

useFlexibleCell   *no* ; # Do not allow three orthogonal dimensions of the periodic cell to f

luctuate independently.

useConstantRatio   *no* ; # Do not maintain a constant ratio of the unit cell in the x-y plane.

langevinPiston   *on* ; # Turn on Langevin piston pressure control.

langevinPistonTarget   *1.01325* ; # The target pressure is 1.01325 bar.

langevinPistonPeriod   *100* ; # The barostat oscillation time scale is 100 fs.

langevinPistonDecay   *50* ; # The barostat damping time scale is 50 fs.

langevinPistonTemp   *$temperature* ; # The barostat noise temperature is the same as the

temperature specified in temperature control.

Output

outputName   *$outputname* ; Specify the output name for output files.

restartfreq   *1000* ; # Prepare the restart files every 1000 steps (2 ps).

dcdfreq   *1000* ; # The trajectory file is updated every 1000 steps.

outputEnergies *1000* ; # Output energy to log file every 1000 steps.

outputPressure *1000* ; # Output pressure to log file every 1000 steps.

#Harmonic constraints

constraints   *on* ; # Turn on positional restraints.

Consex p   *2* ; # Use 2 as an exponent for constraint energy function

conskcol   *B* ; # Specify the B factor column of the PDB file to use for the harmonic

constraint force constant.

consref constraint.pdb ; # Input the PDB file indicating constraint atoms.

conskfile   *constraint.pdb* ; # Input the PDB file to use for force constants for harmonic

constraints.

Extra Parameters

Periodic Boundary Conditions

cellBasisVector1   *80.16 0.0 0.0* ; # Specify the x-dimension of the periodic cell size in Å.

cellBasisVector2   *0.0 63.51 0.0* ; # Specify the y-dimension of the periodic cell size in Å.

cellBasisVector3   *0.0 0.0 64.93* ; # Specify the z-dimension of the periodic cell size in Å.

cellOrigin   *5.26 1.74 16.96* ; # Specify the position of the periodic cell center.

wrapWater   *on* ; # When water molecules cross a periodic boundary, they are not

translated to the other side of the periodic cell.

wrapAll   *on* ; # When a molecule cross a periodic boundary, it is not translated to

the other side of the periodic cell.

PME Particle Mesh Ewald

PME   yes ; # Turn on Particle Mesh Ewald method, an efficient full electrostatics method in

periodic boundary conditions.

PMEGridSizeX 90 ; # Number of grid points in X dimension.

PMEGridSizeY 72 ; # Number of grid points in Y dimension.

PMEGridSizeZ 72 ; # Number of grid points in Z dimension.

Execution Script

Minimization

minimize   *10000* ; # Run 10,000 step conjugate gradient energy minimization.

reinitvels   *$temperature* ; # Reset the temperature according to the temperature variable

after minimization

 # Molecular Dynamics

run   *7500000* ; #Run molecular dynamics for 7500000 steps, equal to 15000 ps (15 ns)

2.5.3 Initial model preparation for molecular simulation

The X-ray structures of the protease-substrate complex (MDR 769-CA/p2 co-crystal structure) is

solved and used as an initial structure for homology modeling using SWISS-MODEL [127]. Based on the

catalytic mechanism of HIV-1 protease, Asp 25 was assigned as a protonated state while Asp 25' was

assigned as a deprotonated state. All histidine residues were assigned a neutral charge. Protonation states

of other amino acid residues were assumed based on the buffer pH in the HIV-1 protease enzymatic

assays (pH 4.7). To avoid simulating catalytic interactions, positional restraint was applied to the scissile

peptide bond of the substrate and β-carboxyl group of catalytic residue Asp 25 and Asp 25'.

The catalytic core domain structure of HIV-1 integrase was obtained from the Protein Data

Bank[128] with PDB entry 1BL3[129]. While this structure contains chains A, B and C, chain A was

used as a template to generate a homology model for each mutant using The Swiss-Model Workspace

[127]. Crystallographic waters were added to the system by merging the coordinates from the original

PDB into the new model. Magnesium ions were inserted into the active site as described previously [130].

The inhibitor RAL was uploaded to ParamChem (www.paramchem.org) to generate parameter files for

the inhibitor. RAL was then manually docked into the active site of the IN core in PyMol [131] based on

the bis-chelation motif of RAL and previously reported modeling structure of the HIV-1 intasome. [132]

(Fig. 2). The complex was placed into a 62 x 68 x 69 $Å^3$ TIP3P water box and magnesium chloride atoms

were added to neutralize the system. The magnesium ions in the active site and the two coplanar oxygen

atoms of RAL were given positional restraints while to reduce bias over the metal coordination scheme

throughout the simulation. The system was prepared in VMD [133].

Crystallographic water molecules were retained in each simulation.

2.5.4 Analysis of molecular dynamics ensembles

Trajectories of MD simulation were visualized and analyzed using the Visual Molecular Dynamics (VMD) program V. 1.91. The superposition of molecular structures was carried out using Pymol. The root-mean-square deviation (RMSD) values were calculated using the VMD RMSD trajectory plug-in with the post equilibration frame used as a reference. The molecular mechanics energy was calculated using the NAMD energy plug-in in VMD. The final molecular mechanics energy is the average of molecular mechanics energy of the last 100 frames (the last 200 ps simulation). Previous studies demonstrated that HIV-1 protease ligands show single-maxima probability density function of energy [134]. Therefore, the last 200 ps simulation represents a relatively stable protease-ligand complex conformation. Hydrophobic solvation energy and electrostatic solvation energy were calculated and averaged based on the 10 snapshot coordinates of the last 200 ps simulation.

The trajectory from NAMD was loaded into VMD. The averages of two independent 10ns MD trajectories were used for the RMSD analysis. The RMSD trajectory tool was used to generate RMSD data for backbone atoms in the protein of each complex. φ,ψ angles and Ramachandran plots were calculated using the Ramachandran analysis tool in VMD independently for each simulation. The figures shown here are representative of both simulations. Structure figures were prepared in PyMol.

2.6 In silico ligand docking and scoring with SwissDock

Using computational techniques combined with knowledge-based design approaches can be used to do a virtual screen to predict binding properties to a receptor for lead optimization [135]. Drug design studies performed here were analyzed using automated docking with the SwissDock Online Server to predict binding properties of the inhibitors.

SwissDock is a protein-small molecule docking web service based on EADock DSS with a user friendly interface that allows for rapid and accurate prediction of binding modes[136]. In a test set of 251 complexes, 57% of the top-scoring binding modes were within 2 Å RMSD to the crystal structure and 70% when considering the top five scoring predictions [137]. The MDR 769 HIV-1 protease crystal

structure in complex with darunavir (PDB 3SO9), tipranavir (3SPK), and the wild-type HIV-1 protease in complex with darunavir (PDB) were used as the target input. The server prepares the input PDB file by converting it to CHARMM format, adding hydrogen atoms in accordance with physiological pH, and performs 100 steps of energy minimization using the steepest decent method. Modified lopinavir analogs were drawn in ChemDraw and converted to a three dimensional structure .mol2 file format in ChemBioDraw3D and uploaded to the SwissDock to perform energy minimization of the ligand using the Merck Molecular Force Field (MMFF) [138-143]. SwissDock server performs the docking in four steps; first, many binding modes are generated while their CHARMM energies are simultaneously estimated on a grid. Next the binding modes with the most favorable energies are evaluated with FACTS (Fast Analytical Continuum Treatment of Solvation) and clustered [144]. Lastly, the most favorable clusters can be visualized online and downloaded as a Dock4 file. The SwissDock server provides an output of ranked poses which were visualized in UCSF Chimera and rescored based on their predicted ΔG values as well as visual inspection of the ligand [145]. Molecular graphics and analyses were performed with the UCSF Chimera package, developed by the Resource for Biocomputing, Visualization, and Informatics at the University of California, San Francisco (supported by NIGMS P41-GM103311).

Chapter 3: Ligand modifications to reduce the relative resistance of multi-drug resistant HIV-1 protease

3.1. Introduction

HIV-1 protease (PR) is a 99 amino acid residue aspartic protease responsible for processing the HIV-1 viral polyprotein, thus providing the structural proteins, capsid, matrix and nucleocapsid as well as the essential viral enzymes PR, reverse transcriptase, and integrase [146]. Since its discovery, PR has become an interesting target for the development of antiretroviral drugs. There are currently 9 compounds approved by the Food and Drug Administration (FDA) as protease inhibitors (PIs) for the treatment of HIV/AIDS. Most PIs are asymmetric substrates which essentially disrupt the symmetric structure of the HIV protease (PR), during the blockage of the protease active site. Two of these inhibitors; lopinavir (LPV) and ritonavir (RTV); however are identical about the P1/P1' positions. The molecular mechanism for the disruption of PR symmetry and the mechanism by which drug resistant variants are able to combat these inhibitors however remains unclear [147]. Co-crystal structures of the MDR HIV protease with the endogenous substrate cleavage site peptides reveal an expanded substrate envelope in the MDR PR compared to the wild type with significant deviation of the N-terminus from the WT envelope [31]. The asymmetric expansion of the MDR PR active site cavity is likely to play a role in the reduced efficacy of PIs against these variants [148].

Developing novel HIV-1 protease inhibitors that overcome drug-resistance is still a challenging task. In drug development, it is difficult to keep pace with the emergence of drug resistance. Compared to *de novo* drug design, drug modification and optimization could lower the risk of failure in clinical trials. The modification of available protease inhibitors according to the MDR HIV-1 protease isolate may provide a solution to overcome drug resistance. LPV is a second-generation protease inhibitor, derived from ritonavir. The smaller P2 and P2' groups of LPV decrease the contact with highly variable residues at the 82 site of HIV-1 protease and improve the inhibitory efficacy against drug-resistant mutants of

HIV-1 protease [149]. The P1 and P1' groups of LPV also involved in the interactions with the protease 82 site. Therefore, non-identical P1/P1' modified LPV could be more tolerant to the 82 site variants.

The MDR HIV-1 protease isolate 769, exhibits cross resistance to HIV-1 protease inhibitors [150]. The presence of the I10V mutation in the MDR 769 variant induces alternative conformations of the 80's loop, playing a unique role in disrupting the S1/S1' binding pockets Though LPV inhibits MDR 769 with low relative resistance, further modification of LPV may improve its efficacy against drug resistance mutations in the HIV protease. The P1 and P1' groups of the HIV-1 protease substrate CA/p2 possessing a reduced scissile peptide bond have been mutated and tested for HIV-1 protease inhibition. The current first line protease inhibitor, darunavir, also contains the non-identical combination of leucine side chain and phenylalanine side chain at the P1' and P1 sites [151]. However, LPV carries the symmetric P1 and P1' groups mimicking the phenylalanine side chain. The P1/P1' ligands, LPV, Leu-LPV, CA/p2 F-r-F, and CA/p2 L-r-F are shown in figure 3.1. Therefore, by changing the P1 site of LPV from a phenylalanine side chain to a leucine side chain (isobutyl group), the inhibitory potency of the modified LPV may increase and the relative resistance against MDR protease may decrease.
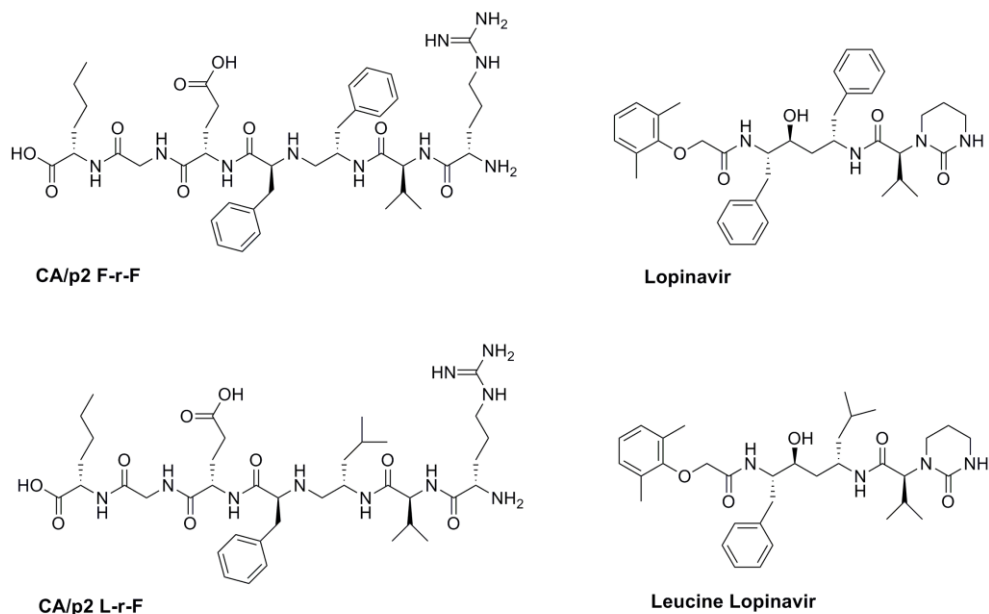
Figure 3.1 Chemical structures of CA/p2 F-r-F, Lopinavir, CA/p2 L-r-F, Leucine lopinavir

Compared to a phenylalanine-phenylalanine combination at P1 and P1' sites, the combination of leucine at the P1 site and phenylalanine at the P1' site exhibits relatively high inhibitory efficacy and reduced relative resistance against MDR769 [152]. We have designed and synthesized a LPV analog (Leu-LPV), containing a leucine-phenylalanine type substitution at the P1' site. Our results suggest that both wild-type PR and the multidrug resistant (MDR) 769 protease variant are preferentially inhibited by the non identical ligands, and particularly by those ligands containing an isobutyl group in the P1 site and a phenylalanine group in the P1' position inducing asymmetry in the MDR HIV-1 PR resulting in reduced relative resistance.

3.2. Results

3.2.1 Leucine lopinavir reduces the relative resistance against the MDR HIV-1 Protease 769

The half maximal inhibitory concentration (IC_{50}) of Leu-LPV with an isobutyl P1 group was determined and listed in Table 3.1. The IC_{50} values of the synthesized original LPV control the CA/p2 F-r-L and the CA/p2 F-r-F were also measured. Leu-LPV achieved 50% inhibition of the WT HIV-1 protease and MDR 769 at the concentration of 2.1±0.1 nM and 6.8±0.4 nM, respectively. The inhibition efficacy of Leu-LPV was higher than the LPV control synthesized in parallel which exhibited the IC_{50} values of 2.5±0.5 nM and 16±0.6 nM for the WT HIV-1 protease and MDR 769, respectively. Furthermore, Leu-LPV decreased the relative drug resistance from 6.4 to 3.2. The CA/p2 F-r-L still showed the lowest IC_{50} value (4.4±0.2 nM) inhibiting the MDR HIV-1 protease as well as having the lowest relative resistance (1.7 fold).

Table 3.1. Half-maximal inhibitory concentration (IC_{50})

Compounds (nM)	HIV-1 protease		Relative
	NL4-3	MDR 769	resistance
leucine lopinavir	2.1±0.1	6.8±0.4	3.2
lopinavir control*	2.5±0.5	16±0.6	6.4
CA/p2 L-r-F	2.6±0.4	4.4±0.2	1.7
CA/p2 F-r-F	30.7	142	4.6

*The lopinavir control was synthesized in parallel using the same procedures and equipments. The only different reagent is benzyl chloride instead of 1-chloro-2-methyl propane.

3.2.2 Non-identical P1 and P1' groups induce asymmetric 80's loop conformations of the MDR HIV-1 protease 769

The combination of isobutyl and benzyl group as P1 and P1' sites could induce an asymmetric movement of the mobile 80's loops of the HIV-1 protease. In Figure 4A and 4B, the MDR 769 82T-(F-r-L) complex crystal structure was superimposed to the WT HIV-1 protease-LPV complex crystal structure (PDB 2Q5K) [153].

Compared to the protease 80's loops interacting with the identical P1 and P1' benzyl groups of LPV, the P1 leucine of CA/p2 F-r-L peptide brought the protease 80s loop closer to the P1 group (Figure A) while the phenylalanine P1' group of the CA/p2 F-r-L peptide induced a similar loop conformation as that of the LPV complex (Figure 4B) despite the similar binding mode of the reduced peptides (Figure 3.3). The non-identical conformations of protease 80s loops have also been observed in the MDR 769 82T-darunavir complex due to the non-identical P1 (benzyl) and P1' (isobutyl) groups of darunavir [69]. The identical CA/p2 F-r-F binds to the MDR HIV PR in a similar manner as LPV with the WT HIV-1 protease and no such 80's loop movement is observed.
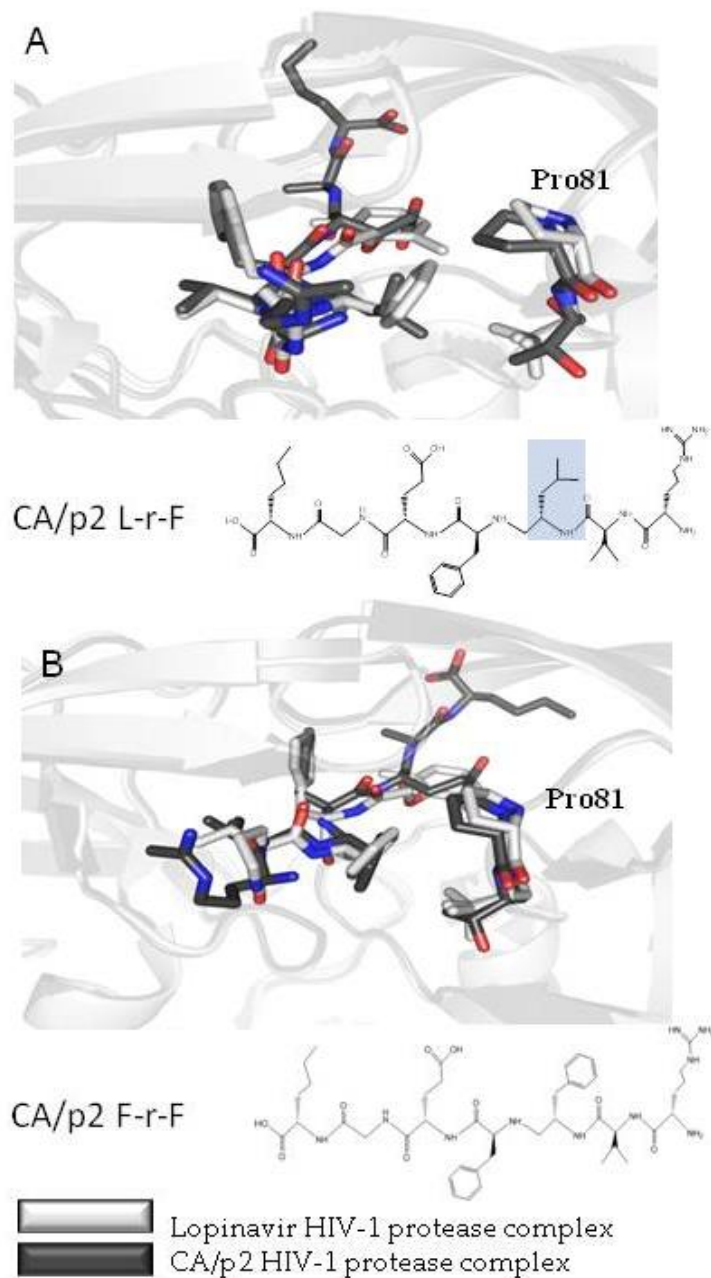
Figure 3.2. 80's loop analysis of crystal structures. The lopinavir-WT complex is shown in light gray with lopinavir and proline 81 in stick model. The MDR complex structures with CA/p2 L-r-F (A) and CA/p2 F-r-F (B) shown in dark gray. These structures were superimposed based on the Cα positions of the HIV-1 protease.

Table 3.2. Crystallographic statistics of CA/p2-MDR 769 complexes.

Dataset	The MDR 769 82T in complex with CA/p2 L-r-F	The MDR 769 82T in complex with CA/p2 F-r-F
Data collection		
Space group	P6$_1$	P6$_1$
Wavelength (Å)	0.979	0.979
Cell constants (Å)	a=62.29 b=62.29 c=84.05	a=62.26 b=62.26 c=83.92
Resolution range (Å)	42.02-2.05 (2.16-2.05)	33.11-2.11 (2.19-2.11)
Number of unique reflections	11642	10619
Completeness (%)	100.0 (99.0)	99.2 (99.0)
Redundancy	8.2 (7.6)	7.8 (7.3)
Mean I/σ (I)	16.2 (4.1)	18.9 (4.1)
R_{merge} [a]	0.092 (0.438)	0.106 (0.576)
Refinement		
R_{work} (%) [b]	19.59	19.29
R_{free} (%) [b]	26.32	26.41
Number of atoms		
Ligand	59	62
Protease	1514	1514
Solvent	159	131
Average isotropic B factor (Å^2)		
Ligand	20.28	36.06
Protease	19.17	27.06
Solvent	39.45	43.82
RMSD bond length (Å)	0.022	0.021
RMSD bond angle (°)	2.04	2.17
Ramachandran plot		
Allowed/generous/disallowed (%)	99.5/0.5/0	99.5/0/0.5
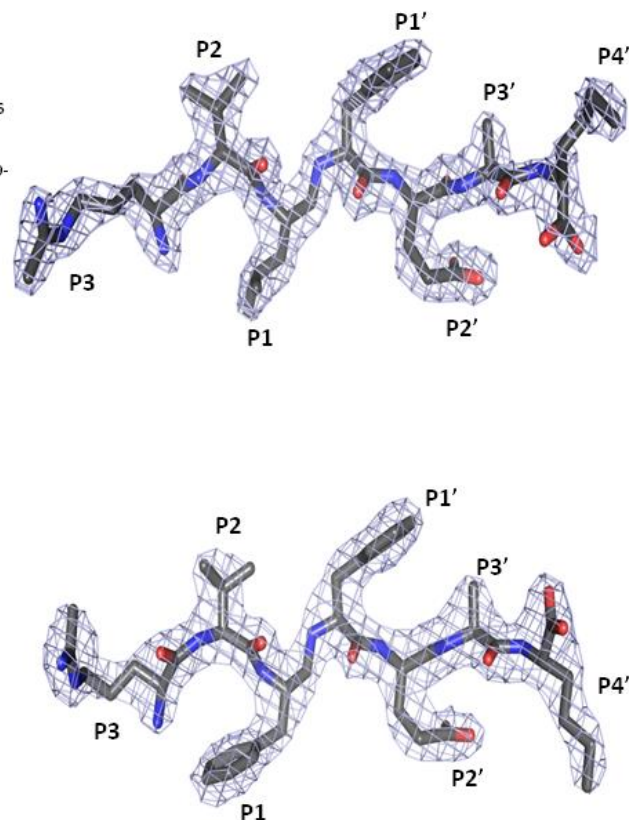
Figure 3.3. Electron density 2|Fo|-|Fc| omit map of reduced peptide ligands; the asymmetric CA/p2 L-r-F (A) and the symmetric CA/p2 F-r-F (B) are shown in stick model with their corresponding electron density maps at a sigma level of 1.0. The peptide residues are labeled as P3 through P4'.
[a]Rmerge= Σhkl Σi |Ii (hkl) - <I(hkl)>| / Σhkl Σi Ii(hkl), where Ii (hkl) is the intensity of an observation and I(hkl) is the mean value for its unique reflection.
[b]Rwork =Σhkl ||Fo|−|Fc|| / Σhkl |Fo|, where Fo and Fc are the observed and calculated structure factor amplitudes. Rfree is calculated exactly as Rwork using a random 5% of the reflections omitted from refinement.

3.2.3. Simulation analysis of leucine lopinavir binding to the MDR HIV-1 protease revealed movement of the 80's loop towards the active site

The LPV and isobutyl P1 Leu-LPV in complex with MDR 769 were modeled and simulated for 10

ns. The average conformations of the last 200 ps simulation were analyzed for both the LPV and Leu-

LPV complexes. In the average conformation of the MDR 769-LeuLPV complex simulation, the

asymmetric conformation of protease 80's loops was observed as well. One 80's loop of the MDR HIV-1 protease 769 moved closer to the isobutyl P1 group of the Leu-LPV (Figure 3.4). The interaction energy calculated between the inhibitor and protease is listed in table 3.3. The calculated interaction energy suggested that the Leu-LPV interacted with MDR 769 stronger (-99.47 kcal/mol) than LPV did (-92.39 kcal/mol). The interaction energy was increased in both electrostatic interactions and van der Waals interactions.
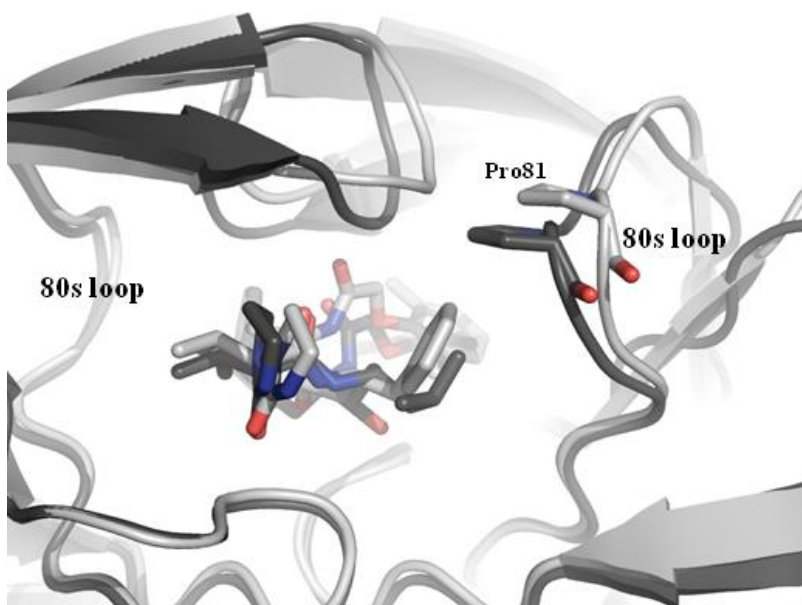
Figure 3.4. MD simulation of lopinavir and leucine lopinavir complex. The average coordinates of the last 200 ps of MD simulation of the MDR 769 in complex with lopinavir (light gray) and leucine lopinavir (dark gray) were superimposed based on the Cα positions of the HIV-1 protease.

Table 3.3. Interaction energy of lopinavir and leucine lopinavir in MDR 769 HIV-1 protease. The interaction energies from the 10ns simulation of LPV and Leu-LPV with MDR protease are given in kcal/mol.

Compounds	Interaction energy (kcal/mol)		
	Electrostatic	Van der Waals	Nonbonded (total)
lopinavir analog	-37.39±6.55	-62.08±3.57	-99.47±7.45
lopinavir	-32.27±8.57	-60.12±3.76	-92.39±9.34

3.3. Discussion

The drug-resistant mutations may increase the flexibility of HIV-1 protease and therefore alter the active site conformation to be unfavorable for drug binding. The 80's loop is a mutation hot spot of HIV-1 protease; as it directly interacts with the P1 and P1' group of substrates or drugs. The V82A/C/F/I/L/M/S/T mutations on the loop have been identified [67, 154]. Both structural analyses and enzymatic results indicate that a smaller P1 or P1' group, such as leucine, brings the 80s loop closer to the ligand and increases binding affinity. An isobutyl group at the P1 or P1' position suggests a promising role to aid in overcoming drug-resistance in the expanded active site cavity.

The lopinavir analog, LeuLPV does not reach the inhibitory potency of CA/p2 F-r-L against the MDR 769 protease. The potency of CA/p2 F-r-L may be influenced by the glutamic acid at P2'. Studies have shown that the binding efficacy of reduced peptides with a glutamic acid in the P2' position are pH-sensitive [155]. The electrostatic interactions of the CA/p2 F-r-L reduced peptide are superior to the hydrophobic Leu-LPV, which explains the relatively lower potency of Leu-LPV compared to the CA/p2 F-r-L reduced peptide.

LeuLPV with an isobutyl group at the P1 position may serve as an HIV-1 protease inhibitor against MDR proteases, especially MDR HIV-1 proteases containing mutations on the 80s loops. Currently, genotypic assays are recommended to assess resistance in the adult and adolescent guidelines of antiretroviral treatment [151]. Benefiting from protease gene sequences of patience isolates, the choice of optimal regimen could be decided based on the types of drug-resistance mutations. Therefore, there is a demand for developing modified protease inhibitors against various groups of HIV-1 protease variants.

3.4. Author's Contribution

The author conducted the protein expression of MDR 769 HIV-1 protease D25N A82T, the crystallization screening, setup, solved the crystal structures, data analysis and interpreted the data. The diffraction data collection and initial data processing were conducted by Dr. Joseph S. Brunzelle

from the Department of Molecular Pharmacology and Biological Chemistry, Feinberg School of Medicine, Northwestern University, Chicago, IL.

Chapter 4: Structure based design of modified lopinavir analogs targeting the multi-drug resistant HIV-1 protease

4.1. Introduction

One of the main challenges in treating and curing HIV is dealing with the development of drug resistance. HIV-1 protease is an aspartyl protease responsible for cleaving the gag/pol polyprotein resulting in mature virus particles. Inhibiting the protease leads to viral suppression as indicated by a reduced viral load. Previous work in our lab has shown that drug resistance mutations lead to 1) an expanded active site cavity, 2) an enlarged substrate envelope, 3) alternative 80's loop conformations and 4) altered binding modes of approved protease inhibitors compared to the WT [31-33, 69]. These factors contribute to reduced binding affinity and reduced inhibitory efficacy of the FDA approved inhibitors. Therefore designing inhibitors to combat the drug resistance problem is essential to next generation therapies.
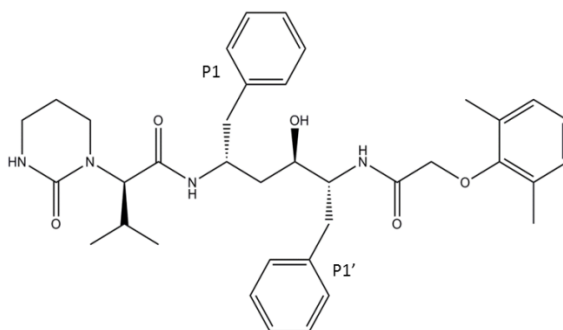
Figure 4.1. Chemical structure of the FDA approved protease inhibitor lopinavir.

This chapter further explores modifications to the FDA approved HIV-1 protease inhibitor lopinavir (Figure 4.1) to enhance efficacy against two drug resistant variants, the clinical isolate MDR 769 and the darunavir resistant I54V mutation. To test the non-identical P1/P1' hypothesis (Chapter 3), we designed additional modifications to the P1 and P1' positions *in silico*. These modifications were designed to explore the role of size diversity and identity of P1 and P1' in binding to drug resistant

protease variants. Compounds 1-18 contain modifications at only P1, while compounds 19-36 contain modifications at both P1 and P1' resulting in an identical and non-identical series (Table 4.1).

Table 4.1. Modifications made to the P1 or P1' positions of lopinavir

Position		Modification
P1	P1/P1'	
1	19	p-methyl benzyl
2	20	p-flourobenzyl
3	21	isobutyl
4	22	m-dimethyl benzyl
5	23	m-diethyl benzyl
6	24	o-methyl benzyl
7	25	m-isopropyl benzyl
8	26	o-isopropyl benzyl
9	27	m-ethyl benzyl
10	28	o-dimethyl benzyl
11	29	m-di-isopropyl benzyl
12	30	p-ethyl benzyl
13	31	m-methyl benzyl
14	32	o-ethyl benzyl
15	33	napthalene
16	34	tryptophan
17	35	cyclohexyl (chair)
18	36	p-methylflourine benzyl

The modified lopinavir analogs were submitted for automated docking with the online software SwissDock. Docking with SwissDock is a computer based method to predict binding affinity and binding modes using the CHARMM forcefield (Chapter 2.6) [136, 137]. This program has been proven to be 70% accurate within 2Å of the crystal structure. Using the SwissDock output we performed additional analysis in UCSF Chimera, a molecular graphics program, to visually inspect and identify the top 7 compounds in our series[145]. Three criteria were used to make these selections. We choose the compounds that had 1) the highest predicted binding affinity in kcal/mol, 2) maintained key contacts such as coordination of the hydroxyl group to the aspartic acid residues in the active site, D25 and D25', 3) were consistent in criteria 1 and 2 across three different protease targets; WT, MDR 769, and darunavir resistant I54V. The

SwissDock output for the lopinavir control was validated using the crystal structures 3D20, 3SPK, and 2O4S.

Further analysis the top three scoring analogs and the lopinavir control, using 10 ns all-atom molecular dynamics simulations with scalable molecular dynamics with NAMD, confirmed p-fluorobenzyl lopinavir (compound 20) as the lead compound. Structure-activity relationships of these analogs suggest two important strategies for rational drug design of protease inhibitors: (1) the presence of fluorinated P1 or P1' groups enhance the binding affinities in both wild-type and MDR PR variants and (2) fluorinated compounds contribute to stabilizing the protein backbone by increasing hydrophobic contacts between the protease and the inhibitor. These factors may increase overall efficacy against MDR protease variants.

4.2. Results

4.2.1. Fluorinated lopinavir has the highest predicted binding affinity against drug resistant HIV-1 protease.

Compound 20 has the highest average binding affinity with the lowest standard deviation across the three different isolates. The predicted binding affinities of the top scoring compounds are shown in Figure 4.2 in order of their docking score. The top 3 compounds have similar binding affinities in the WT protease and in the single mutant containing the I54V mutation. In addition these compounds display comparable binding affinities as lopinavir. In MDR 769 however the performance of the compounds is reduced where the top four compounds have a higher binding affinity than LPV.

LPV Variant	204S (WT)	3D20 (I54V)	3SPK (MDR 769)	Binding Affinity (kcal/mol)
(0) Control	-10.45	-10.69	-9.64	-10.3 ± 0.6
(20) P-flourobenzyl (P1/P1')	-10.3	-10.75	-10.09	-10.4 ± 0.3
(2) P-flourobenzyl (P1)	-10.52	-10.45	-10	-10.3 ± 0.3
(3) isobutyl (P1)	-10.3	-10.62	-9.75	-10.2 ± 0.4
(18) P-methylflourine benzyl (P1)	-10.19	-9.7	-10.38	-10.1 ±0.4
(35) cyclohexyl (chair) (P1/P1')	-9.19	-10.51	-9.38	-9.7 ± 0.7
(31) M-methyl benzyl (P1/P1')	-9.46	-10.08	-9.47	-9.7 ± 0.4
(9) M-ethyl benzyl (P1)	-8.92	-10.18	-9.71	-9.6 ± 0.6

Figure 4.2 SwissDock binding affinities of the lopinavir analogs

4.2.2. P1/P1' fluorinated lopinavir stabilizes the HIV-1 protease

The RMSD over the 10 ns trajectory (figure 4.3 A) is used as a measure of flexibility and protein stability during an MD simulation. Lower RMSD corresponds to increased rigidity and therefore stabilization of the protease. Therefore inhibitors that lower the RMSD and have an enhanced binding affinity are more favorable. The average RMSD of the top 3 modifications as well as the lopinavir control in complex with the WT, MDR 769, and I54V protease variants is shown in figure 4.3, B. The compound that performs similarly in WT and the drug resistant variants would then have a higher barrier of resistance. This means that if a patient were to be taking compound 20 for example and managed to develop the mutations present in MDR 769, they would not have to change their treatment regimen.
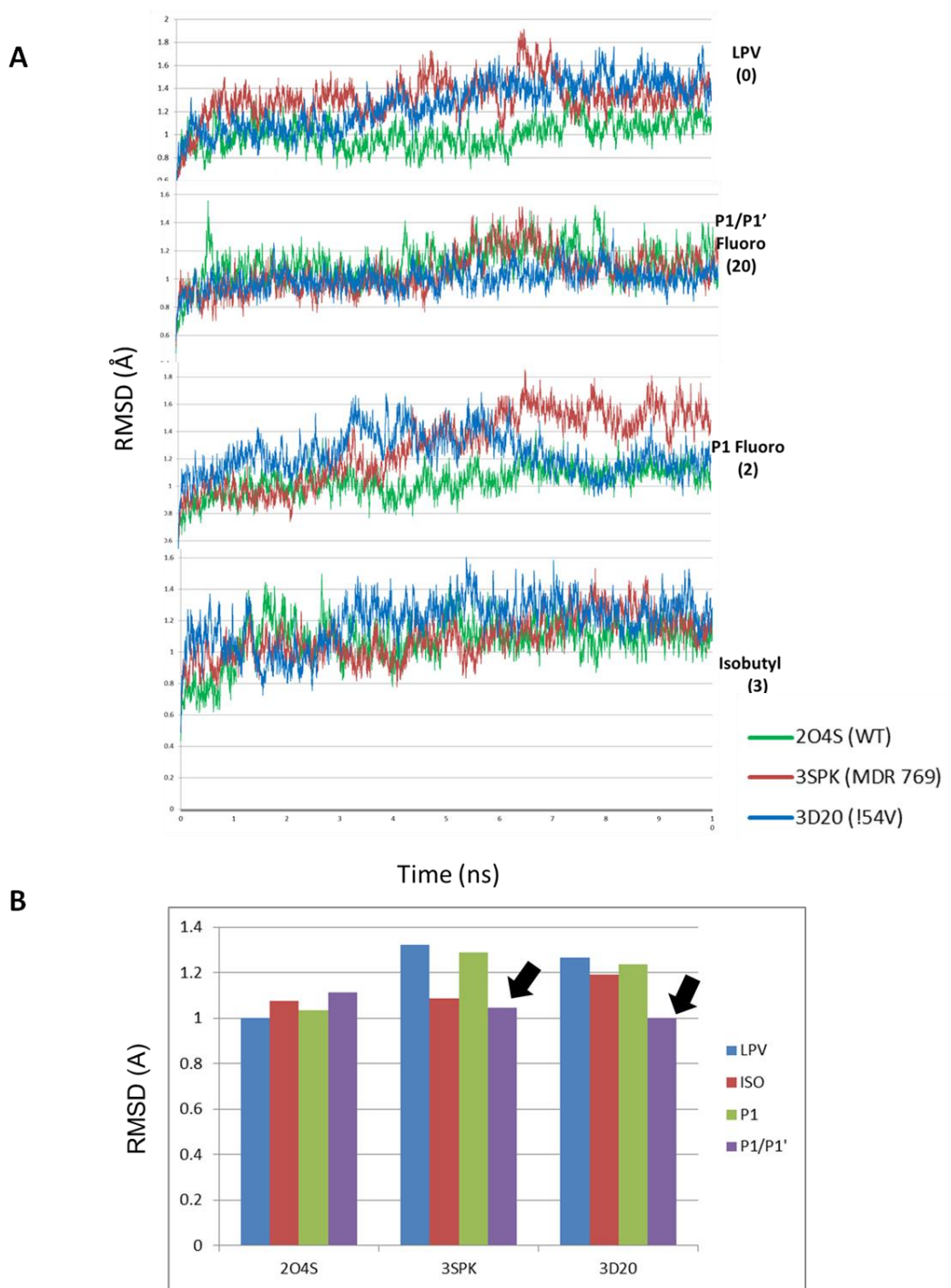
Figure 4.3 Root mean square deviation (RMSD) of Cα backbone atoms for the HIV-1 Protease-ligand complexes. A. Average RMSD of all backbone atoms over the 10 ns trajectory. The PDB codes of the protease targets are shown in the figure legend. B Average RMSD for of each HIV-1 protease isolate. The arrows indicate the p-fluoro

4.2.3. P1/P1' fluorinated lopinavir increases non bonded interactions with HIV-1 protease.

The final frame of the molecular dynamics simulations was submitted to LigPlot+ to identify non bonded interactions between the ligand and the target protein. The final frame of the MD was used because in this method the conformational sampling later in the trajectory is likely to be more energetically favorable. Interestingly, the p-fluorinated lopinavir complexes not only increase the number of contacts but also the changes the residues involved in these contacts as seen in the LigPlot+ diagram (Figure 4.4).
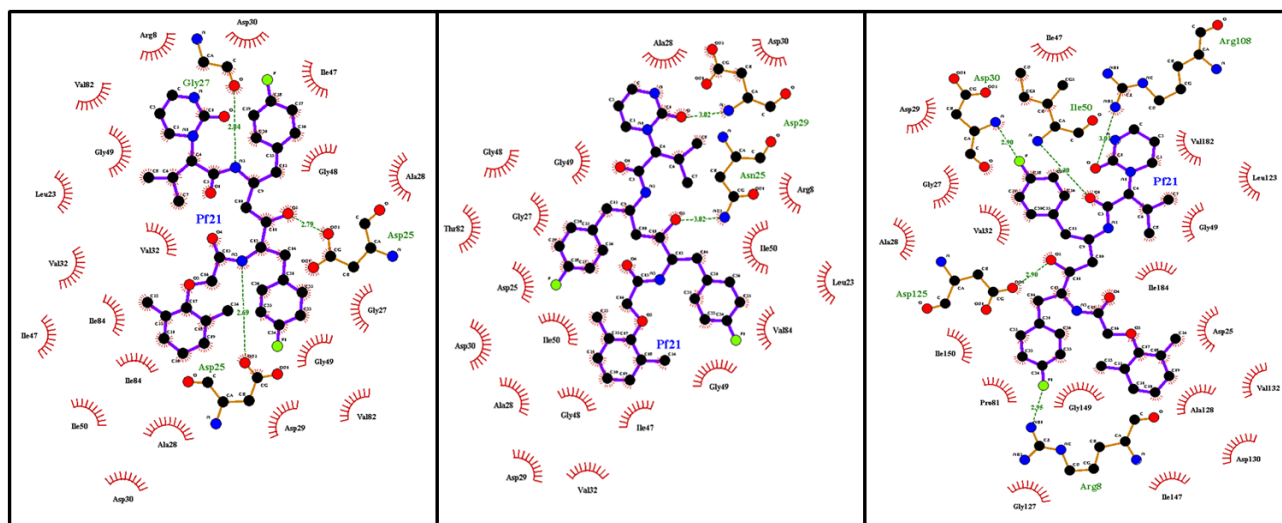
Figure 4.4. p-fluorinated-LPV interacts with alternative HIV-1 protease residues. Left WT (2O4S), middle MDR 769 (3SPK) and right I54V (3D20).

Compared to LPV, compound 20 has increased contacts with all 3 protease variants. The specific interactions that are gained and lost as compared to the LPV complexes are shown in Table 4.2. The different protease variants cause an alteration in the binding mode of compound 20 and those binding modes are shown here. An important feature of compound 20 is that it is flexible enough to accommodate the altered binding pockets of the protease variants and the fluorine groups' increase and alter the hydrophobic contacts with the protease regardless of the differences in the binding pockets caused by the drug resistant mutations.

Table 4.2 Non bonded interactions identified by LigPlot+ analysis

	LPV		P1/P1' Fluoro	
	Hydrophobic Contacts	Hydrogen Bonds	Hydrophobic Contacts	Hydrogen Bonds
2O4S (22:23)	A28 A28' G27 G48 G48' G49 G49' I47 I47' I50 I50' I84 P29 P30 P81 V32 V32' V82	D25 D25' D29 G27	A28 A28' D29 D30 D30' G27 G48 G49 G49' I47 I47' I50 I84 I84' L23 R8 V32 V32' V82 V82'	D25 D25' G27
3SPK (16:21)	A28 D29 D30 G27 G48 G49 I50 I50' L23 P81 R8 V32 V84	G49 N25 P25	A28 A28' D25 D29 D30 D30' G27 G48 G48' G49 G49' I47 I50 I50' L23 R8 T82 V32 V84	D29 N25
3D20 (21:23)	A28 A28' D25 D29 D29' D30 V32 V32' G27 G27' G48 G48' G49 I50 I84 L23 L23' R8 R8'	D25' I50'	A28 A28' D25 D29 D30' G27 G27' G49 G49' I47 I47' I50 I84 L23 P81 V32 V32' V82	D25' D30 I50 R8 R8'

Table 4.3 Non bonded interactions gained and lost in the HIV-1 protease-(20) complexes as compared to the HIV-1 protease-lopinavir complexes.

	Contacts Gained	Contacts Lost		Contacts Gained	Contacts Lost		Contacts Gained	Contacts Lost
2O4S	D29	*D29	3SPK	A28'	*G49	3D20	D30'	D29'
	D30	G48'		D25			G49'	D30
	D30'	I50'		D30'			I47	G48
	I84'	P29		G48'			I47'	G48'
	L23	P30		G49'			P81	R8
	R8	P81		I47			V82	R8'
	V82'			T82			*D30	L23'
	*D29			*D29			*I50	
							*R8	
							*R8'	

*denotes hydrogen bonds

4.3. Discussion

Treating patients who have acquired drug resistance remains a major challenge in HIV-1 therapy and represents a major barrier towards viral eradication. While eradication is a lofty goal we can certainly begin with developing inhibitors to combat resistance using structural approaches. In this chapter, we have designed a series of lopinavir analogs with modifications at either P1 or both P1 and P1' positions to explore the role of size diversity in at these loci.

Our results suggest that the presence of fluorinated P1 or P1' groups, particularly p-fluorobenzyl at P1 and P1', produces greater binding affinity to multi-drug resistant HIV-1 protease variants. Substitution of the benzene ring hydrogen at the para position facilitates an increase in the number of contacts between the ligand and the protease target. In addition to increasing the total number of contacts an alternative binding pocket is formed in each of the protease targets (Figure 4.5). This suggests that the ability of the ligand to adapt to the conformation of the active site while maintaining or increasing contacts with the protease is a major contributor in reducing fluctuations in binding affinity across multiple protease variants.

Analysis of MD simulation data further suggests that these groups play a role in stabilizing the protein backbone and therefore may increase overall efficacy against MDR protease variants. Compound

20 is capable of significantly reducing the RMSD in the protease variants as well as the wild-type compared to the lopinavir control. Stabilizing the protease backbone by increasing the number of contacts between the ligand and the target protein may be an effective strategy to combat multi-drug resistance amongst protease inhibitors.
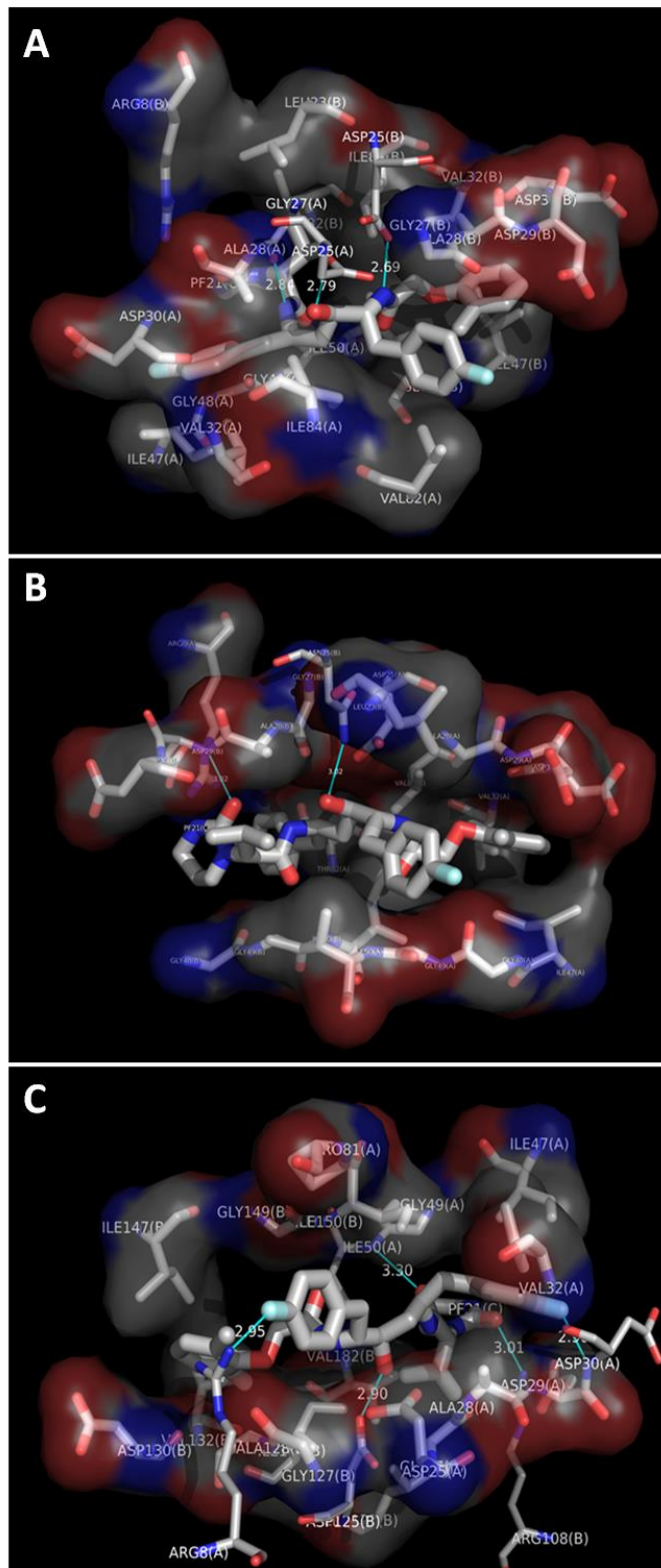
Figure 4.5 Alternative binding pocket induced by p-fluorinated lopinavir in each HIV-1 protease variant
A. Wild type, B. MDR 769, C. I54V

4.4 Author's contribution

The author developed the experimental design, designed the lopinavir analogs, and interpreted the data from the MD simulations. Bradley Keusch performed the docking, the molecular dynamics simulations and the MD data analysis.

Chapter 5: Characterization of multi-drug resistant HIV-1 protease isolates

5.1. Introduction

In the treatment of HIV/AIDS, the HIV-1 protease inhibitors (PIs) represent a key class of drugs [156]. PIs have a higher barrier of resistance relative to other classes of inhibitors [157, 158] in which multiple protease (PR) mutations are needed for developing resistance [157-159]. In spite of an intensive and concerted effort, no straightforward solution exists to the HIV-1 PR drug resistance challenge. The HIV-1 PR is a small aspartyl protease consisting of 99 amino acid residues. It is significantly smaller than mammalian aspartyl proteases and has a dimeric structure of two identical monomers [160, 161]. Two aspartyl residues, one from each monomer, are responsible for catalyzing proteolyses of the HIV-1 polyproteins. The HIV-1 PR active site is located in a cleft that binds the viral polyprotein in which large conformational changes occur upon substrate or inhibitor binding.

While the design of HIV-1 PIs has been a success resulting in the PIs ATV, DRV, FPV, IDV, NFV, LPV, SQV, and TPV, the problem of HIV-1 PR drug resistance remains unsolved. Shown in figure 1 the HIV-1 protease of a patient who currently receives ART with a combination of drugs other than PIs since resistance testing of the patient's HIV-1 has indicated resistance to all licensed PIs. Recently, the patient has developed resistance to her current ART drugs, leaving this patient with challenging future treatment options. In this chapter, a set of Detroit patient isolates has been selected, including this patient's drug resistant HIV-1 PR.
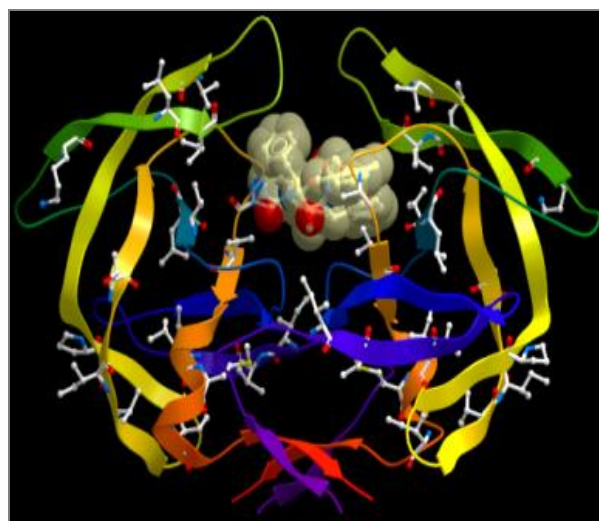
Figure 5.1. HIV-1 protease resistance mutations from a Michigan patient isolate selected for our studies. The resistance mutations are shown by the white side chains. The theoretical model of the complex (PR: rainbow diagram, LPV: space filling model) is based on our crystal structure (1RV7) of another MDR HIV-1 protease bound to LPV [162].

According to the UNAIDS, 70% of treatment failures are caused by drug resistant mutations. This highlights the importance of understanding the molecular mechanisms by which HIV-1 drug targets are able to evade inhibition by potent inhibitors. The Detroit isolates differ from isolates previously studied in our group in that these contain the major drug resistance mutations I47V, I50V, I54M, L76V, V82I/F, and I84F not present in the previous cohort. The Detroit isolates also contain previously identified non-polymorphic accessory mutations L10V/G, V11I, K20T/R, L33F/I/M, K43T, F53L, A71L, T74P, and L89V. Interestingly, all of the Detroit isolates contain the previously unidentified I13V mutation and L33F. The Detroit isolates represent an interesting cluster to study the effect of both major and accessory mutations on protease inhibitor resistance.

Sequence comparisons between the Detroit Isolates highlight the differences as well as the common mutations present in each isolate (figure 5.2). All three isolates contain the 33F, 46I, and 84V major drug resistance mutations. The structural mechanisms leading to differences in predicted vircoTYPE scores between these isolates is unclear from the virtual phenotype predictions alone. Molecular dynamics simulations of the Detroit isolates were performed using NAMD. The results of

these simulations show that (1) V32I and I47V play a structural role in tethering the protease flaps to the active site, (2) I54M and L90M may be responsible for asymmetric movement of the protease flaps, and (3) Alternative hydrogen bonding networks with ligands are important factors contributing to the molecular mechanisms of protease inhibitor resistance.
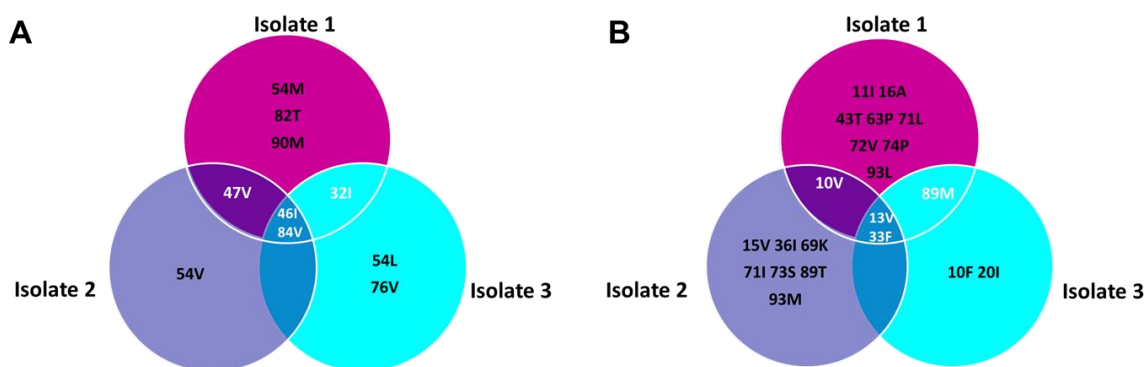
Figure 5.2. Mutations present in the Detroit Isolates. A. Major HIV-1 protease drug resistance mutations, B. Minor/accessory mutations.

5.2. Results

5.2.1 The Detroit isolates display multi-drug resistant virtual phenotype

The protease sequences of the Detroit Isolates were submitted for virtual phenotype predictions with vircoTYPE. This software uses an input sequence, along with known information regarding resistance mutations to calculate quantitative levels of phenotypic susceptibility to the entire class of protease inhibitors. Clinicians use this information as a guide when prescribing personalized therapy for their HIV infected patients. The vircoTYPE predictions of the Detroit Isolates suggest that DetMDR1 is completely resistant to all 9 protease inhibitors currently on the market (Table 1). DetMDR2 may be susceptible to DRV with reduced susceptibility to IDV, SQV, LPV, and ATV. DetMDR3 however may still be susceptible to saquinavir and tipranavir with reduced susceptibility to lopinavir, atazanavir and indinavir. In addition, we performed the same analysis using the a rule based genotypic resistance algorithm provided by the Stanford Database and the virtual phenotypes align nicely in that DetMDR1 is

resistant to everything, DetMDR2 displays low level resistance to darunavir, and DetMDR3 displays low level resistance to tipranavir (Table 5.1).

Table 5.1. Virtual phenotype predictions of the Detroit Isolates with VircoType suggest multidrug resistant phenotype. Red: Minimal Response; Orange: Reduced Response; Green: Maximal Response; X/r = ritonavir boosted

Isolate	IDV	IDV/r	NFV	SQV/r	FPV/r	LPV/r	ATV/r	TPV/r	DRV/r
Isolate 1	87.3	87.3	65.2	49.0	68.5	113.2	79.2	123.2	208.2
Isolate 2	22.5	22.5	34.1	17.1	31.2	27.5	28.9	16.1	9
Isolate 3	8.8	8.8	10.1	0.9	70.0	39.4	17.8	0.7	151.6

Table 5.2. Predicted phenotypes of the Detroit isolates from the Stanford Database rule based algorithm

	Isolate	IDV	IDV/r	NFV	SQV/r	FPV/r	LPV/r	ATV/r	TPV/r	DRV/r
HIGH level resistance / LOW level resistance	1	HIGH	HIGH	HIGH	HIGH	HIGH	HIGH	HIGH	HIGH	HIGH
	2	HIGH	HIGH	HIGH	HIGH	HIGH	HIGH	HIGH	HIGH	LOW
	3	HIGH	HIGH	HIGH	HIGH	HIGH	HIGH	HIGH	LOW	HIGH

5.2.2 Mutations in the Detroit isolates reveal alternative protein dynamics

Molecular dynamics simulations (Chapter 2.5) were performed for 40 ns with the Detroit Isolates. Root mean squared deviation (RMSD) of the PR backbone show increased fluctuation of all 3 isolates compared to the wild-type protease (Figure 3). DetMDR1 showed a jump in flexibility as while DetMDR2 shows are sharp increase in RMSD and sustained deviation for the rest of the trajectory. DetMDR3 displays short bursts of increased flexibility but no sustained changes in RMSD. This data suggest a large conformational change in isolates 1 and 2 but not in DetMDR3 or the WT.
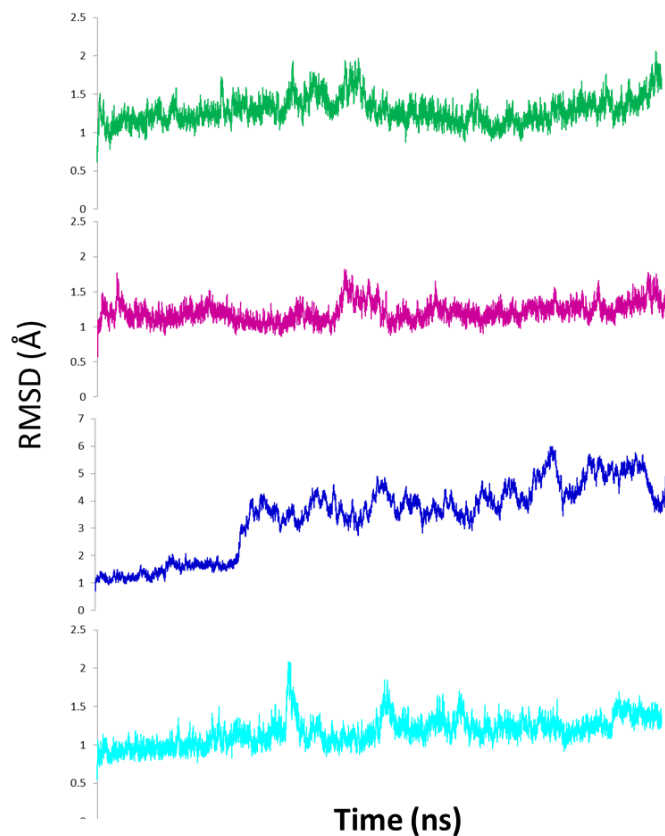
Figure 5.3. Root mean square deviation (RMSD) of Cα positions of the uncomplexed HIV-1 protease isolates. Wild-type is shown in green, DetMDR1 in pink, DetMDR2 in blue and DetMDR3 in cyan.

Analysis of the average RMSD for each residue in the HIV-1 PR simulations compared to the WT highlight the differences in flexibility between these 2 and especially show the increased flexibility of certain regions of the PR. Specifically, the jump in average backbone RMSD of DetMDR1 is caused by asymmetric fluctuation of chain B in the flap regions of the PR corresponding to residues 45-55. Interestingly, the same region of DetMDR2 shows high flexibility variations compared to the WT however in DetMDR1 this sustained increased RMSD is not restricted to one chain rather the flap regions of DetMDR2 show significant deviation in both chains of the PR.

5.2.3 Flap opening may play a role in drug resistance of the Detroit Isolates

Visual analysis of the trajectory shows that these increases in RMSD are due to opening of the flaps in DetMDR1 and DetMDR2. In DetMDR1 the flaps open and then close. In contrast, the flaps of DetMDR2 open and stay open for the remainder of the trajectory. The WT and DetMDR3 flaps do not open during these simulations. These differences in flap movement correspond to the presence or absence of particular mutations. Interactions between the V32I and I47V mutations cause flap closure in HIV-1 protease. I47V is present in both DetMDR1 and 2 where the flaps open, but not in DetMDR3 where the flaps do not open V32I is therefore a compensatory mutation which tethers the flaps to the active site through its vdW interactions with I47V (Figure 5.4). Similarly, the WT and DetMDR3 have V32 and I47 at these loci and therefore the vdW interactions in the WT and DetMDR3 are maintained. The absence of V32I in DetMDR2 disrupts this interaction and therefore the flaps remain open in DetMDR2.
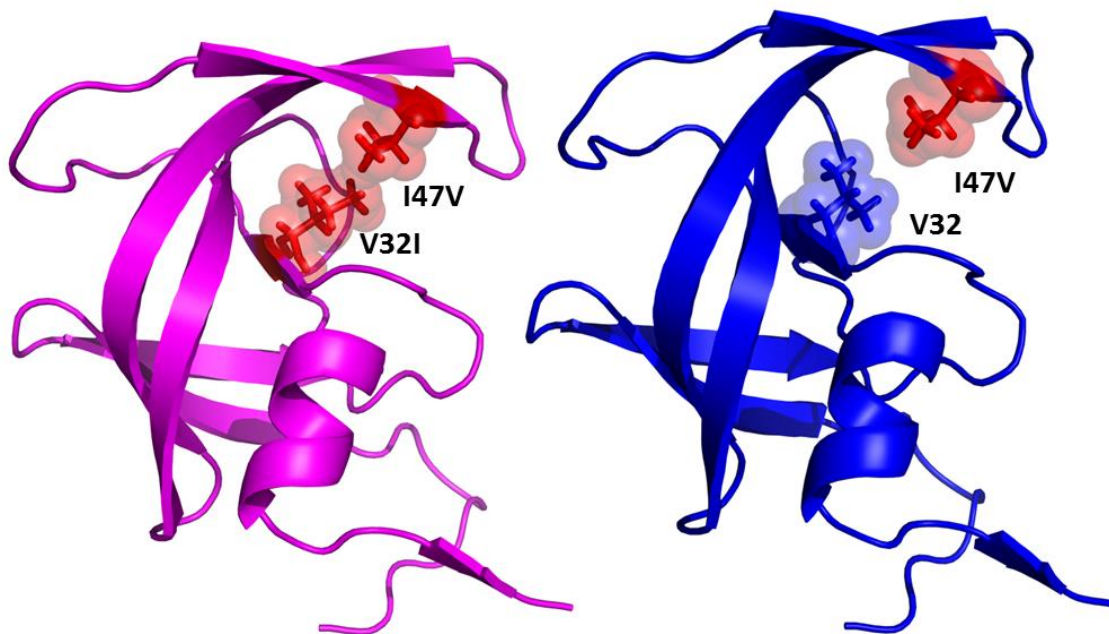
Figure 5.4 Change in the van der Waals volume induced by the drug resistance mutations I47V and V32I. The left panel shows DetMDR1; the right panel shows DetMDR2.
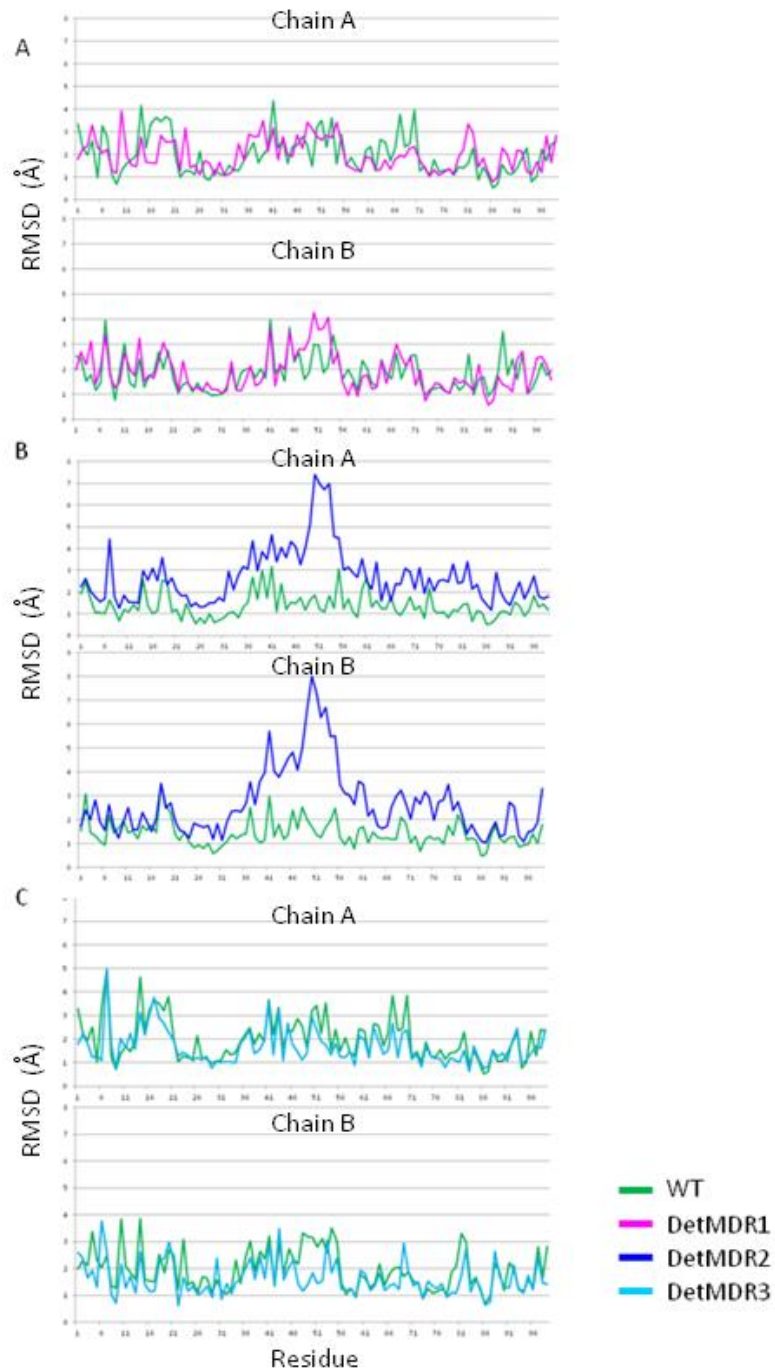
Figure 5.5 RMSD per residue of the uncomplexed HIV-1 protease isolates compared to WT reveal alternate flap dynamics of WT and Detroit MDRs: A. DetMDR1 B. DetMDR2 and C. DetMDR3. The flap regions corresponding to residues 47-54 show increase in RMSD on both protease chains in DetMDR2 and only on chain B of DetMDR1

I54M and L90M are associated with asymmetric movement in DetMDR1 corresponding to opening of the flaps. The RMSD of L90M on chain B is different than that of chain A. The asymmetric movement of the flaps indicated by the differences in RMSD at each residue show a difference in residues 47-54 on chain B compared to chain A (Figure 5.5). Movement of the residues in this region is symmetric in DetMDR2 where the residue fluctuation per residue is conserved between both chains of the PR.

5.2.4 Darunavir, atazanavir and lopinavir binding stabilize the HIV-1 protease flaps

The WT, DetMDR1, DetMDR2, and DetMDR3 in complex with DRV, ATV and LPV were submitted for 40 ns molecular dynamic simulations. The opening of the flaps observed in the uncomplexed simulations of DetMDR1 and DetMDR2 does not occur in the complex simulations. Drug binding maintains a closed flap conformation in DetMDR2 (Figure 5.6).
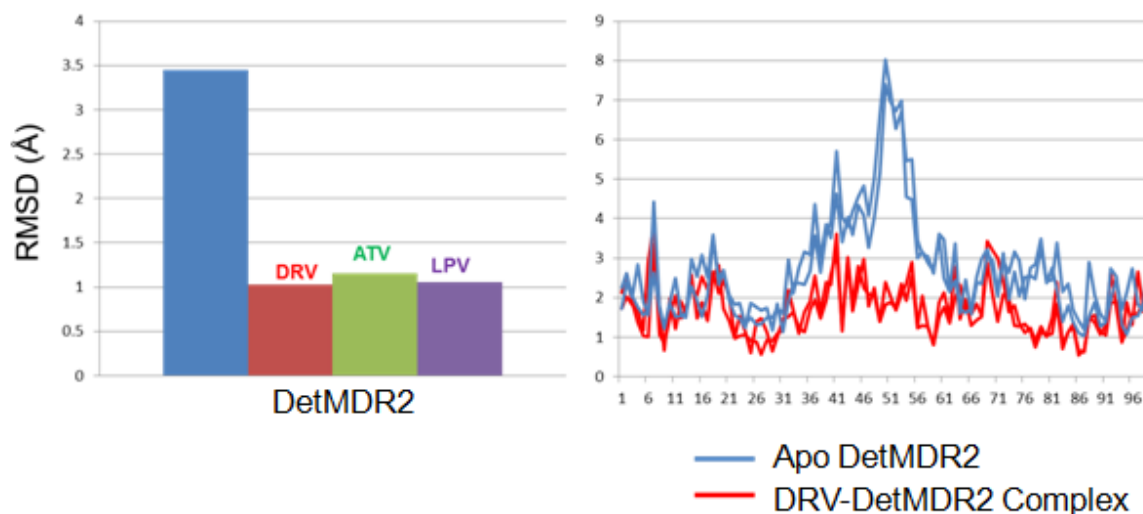
Figure 5.6 Darunavir, atazanavir and lopinavir binding stabilize the HIV-1 protease flaps. The left panel showsn the average RMSD of DetMDR2 either alone (blue) or in complex with DRV (red) ATV (green) and LPV (purple). The RMSD per residue is shown in the right panel.

In addition to the altered protein dynamics, there is a change in the hydrogen bonding interactions in the WT compared the MDR isolate complex (Table 5.2). DetMDR1 has 2.3%, 0.8% and 19.2%

reduced hydrogen bond formation when complexed with darunavir, atazanavir and lopinavir respectively. Interestingly, DetMDR2 and DetMDR3 have increasing hydrogen bond formation when in complex with DRV and ATV; and a 21% and 36% decrease in hydrogen bond formation when in complex with lopinavir. The increase in hydrogen bonds is likely due to an alteration in the residues involved in an interaction with the protease thus, while changing the binding pocket may increase hydrogen bond formation; this also alters the conformation of the inhibitor.

5.3. Discussion

Three multi-drug resistant HIV-1 protease patient clinical isolates were selected from Wayne State University Infectious Disease Clinic failing antiviral treatment therapy using protease inhibitor based regimens. To explore the structural mechanisms resulting in treatment failure, we performed 40ns MD simulations on the Detroit MDR series. Our results indicate a novel structural role for the I47V, V32I, I54M and L90M resistance mutations.

The V32I and I47V mutations play a structural role in tethering the flaps to the active site. Sequence analysis comparisons of the DetMDR protease isolates showed that DetMDR2 does not contain the V32I and I47V mutation combination rather it contains only the I47V mutation. Without the V32I mutation there is a loss in van der Waals contact volume between these two residues. Therefore, we postulate that I47V is responsible for flap opening however V32I is a compensatory mutation that may be responsible for tethering the flaps to the active site through its contacts with I47V.

I54M and L90M may be responsible for asymmetric movement of the protease flaps. This mutation combination is only present in DetMDR1 which is the only protease out of the series in which the flaps asymmetrically open and then close after 4 ns. The mechanism explaining asymmetric flap opening will be explored further in future characterization studies of the HIV-1 protease isolates.

The role of these structural changes in drug resistance was investigated using molecular dynamics simulations with the Detroit isolates in complex with the protease inhibitors atazanavir, darunavir and lopinavir. These MD results suggest that drug resistance occurs through alternate hydrogen bonding

interactions in each of the mutants. The alternate hydrogen bonding networks in addition to the flexibility of the flaps are stabilized with the protease inhibitors bound to the active site. This work highlights the importance of individualized treatment options specific to unique drug resistance variants identified in patients.

Table 5.3 Hydrogen bonding network with darunavir, atazanavir, and lopinavir

	LPV		ATV		DRV	
	Chain A*	Chain B	Chain A*	Chain B	Chain A*	Chain B
WT	L23 D25 A28 D29 D30 V32 I47 G49 I50 P81 V82 I84	R8 L23 A28 D30 V32 I48 G49 I50 I54 V56 L76 P81 V82 I84	R8 D25 D29 G48 I50	R8 D29 D30 G48 G49 I50	D25 D29 D30 I50	D30 G49 I50
DetMDR1	D25 A28 D29 D30 I32 V47 G48 G49 I50 T82	A28 D29 D30 V47 G49 I50 M54 L76 P81 T82 V84	R8 D25 D29 D30 I50 T82	R8 D29 D30 G48 G49 I50 T82	D25 D29 D30 I50	D29 D30 I50 T82
DetMDR2	L23 D25 A28 D29 D30 V32 V47 V49 V81 V82	R8 A28 D29 D30 V32 G49 I50 V82 V84	R8 D25 D29 D30 G48 I50	D29 D30 G49 I50	D29 D30 I50	D30 G49 I50

	V84					
DetMDR3	D25	R8	R8	R8	D25	D29
	D28	A28	D25	D29	D29	D30
	D29	D29	D29	D30	D30	G49
	D30	D30	G48	G48	I50	I50
	V32	I47	I50	G49		
	I47	G49		I50		
	G48	I50				
	G49	P81				
	I50	V82				
	P81	I84				
	I84					

5.4 *Author's contribution*

The author developed the experimental design and interpreted the analysis of the MD trajectories.

Poorvi Chordia performed the MD simulations and the analysis of the MD.

Chapter 6: Reduced flexibility of HIV-1 integrase as a mechanism of raltegravir resistance

6.1. Introduction

HIV-1 integrase (IN) is a 32kDa protein encoded in the pol gene along with protease and reverse transcriptase. IN contains three structural domains; the N-terminal domain (NTD), catalytic core domain (CCD) and C-terminal domain (CTD). In order for HIV-1 viral replication to occur, the viral cDNA must be integrated into the host chromosome. This process, mediated by IN involves two chemical reactions. The first reaction is 3' processing in which a specific dinucleotide sequence of the viral DNA 3' ends are cleaved to generate reactive hydroxyl groups. Next, the IN enzyme facilitates the transesterification reaction known as strand transfer, resulting in the successful integration of the viral DNA into the host chromosome [35].

IN represents an interesting target for therapeutic intervention as it is essential to progression of HIV infection. IN requires divalent metal ions Mn^{2+} or Mg^{2+} for catalytic function [163]. Although reported crystal structures display only one metal ion (1BIU) in the active site coordinated by D64 and D116, crystal structures of the Avian Sarcoma Virus IN (1VSH) a structurally and functionally related enzyme show two metal ions in the active site. Aryl-2,4-diketobutanoic acids (DKAs) were identified as the first compounds to show successful inhibition of HIV IN likely via interactions with the required metal ions [164]. DKAs selectively bind to the IN donor substrate complex and inhibit strand transfer by competing with the target DNA [53]. IN strand transfer inhibitors are believed to bind to the IN-DNA complex post 3' processing and sequester the Mg^{2+} ions coordinated by the catalytic triad residues D64, D116, and E152 [165]. Raltegravir (RAL) (Isentress, Merck & Co., Inc.), the first HIV-1 IN inhibitor to be approved by the FDA in 2007 for antiretroviral treatment, was optimized from the initial DKA pharmacophore and inhibits the strand transfer reaction in a mechanism that is not yet clearly defined [41].

Several mutations leading to resistance to RAL have been observed both clinically and *in vitro*. The Stanford HIV Drug Resistance Database reports mutations at codons 92, 121, 140, 143, 148, and 155 are associated with greater than 5-10 fold decreases in susceptibility to RAL **(Fig.1).** Primary mutations at 143, 148 and 155 along with associated secondary mutations constitute the three main pathways leading to RAL resistance [166]. The Q148HRK/G140SA resistance pathway was observed most frequently in clinical trials and has been shown to be more fit than the RAL resistant single or double mutants in the presence of RAL suggesting that the G140 mutation may serve a compensatory role in rescuing IN activity [166, 167]. While the structural mechanisms explaining RAL resistance in the Y143 integrase mutants has been suggested to be through a loss of aromatic interactions in the 140's loop, the precise mechanism by which the other mutations are RAL resistant remains unclear [168].

Crystal structures of HIV-1 IN CCD have been previously reported, however none of these investigate structural changes, if any, that may occur as a result of these resistance mutations. The structure of the prototype foamy virus (PFV) intasome, a functionally related enzyme, complexed with DNA and RAL has provided some insight into IN structural properties and binding interactions, in the absence of available structural information involving the HIV-1 IN CCD and RAL [169]. Molecular dynamics (MD) simulations in combination with automated docking have been done to gain information regarding these resistance pathways and to identify possible binding modes of RAL in the CCD active site [170, 171].

Using MD, the keto-enol groups of DKA IN inhibitors have been shown to be coordinated with magnesium ions in the active site as well as stabilize the flexible 140's loop (138-149) through hydrophobic contacts [172]. Conformational changes in the 140's loop have been implicated in binding interactions with the strand transfer IN inhibitors [173]. Here, we perform MD simulations concurrently on HIV-1 IN CCD and RAL to analyze protein and inhibitor flexibility as well as binding interactions within the protein inhibitor complex in the context of the 148/140 resistance pathway to investigate the structural changes occurring in the HIV-1 IN CCD as a result of these resistance mutations. The change in

flexibility of the flaps of retroviral protease variants has suggested an important role in protein flexibility on inhibitor binding [174]. The mutant variants display an increased probability of the formation of a transient intraloop structure that causes increased rigidity and impairs the gating function of the catalytic 140's loop resulting in decreased RAL accessibility to the IN active site. In this paper, we explore the reduction in flexibility of HIV-1 IN as a mechanism for raltegravir resistance.

6.2 Results

6.2.1 Reduced flexibility of the HIV-1 integrase catalytic core domain caused by raltegravir induced drug resistant mutations

The interaction between the CCD and the inhibitor RAL is mediated through two Mg^{2+} ions in the active site. These ions coordinate the carboxylate groups of the catalytic residues Asp 64, Asp 116, and Glu 152 such that the DDE motif interacts with the Mg^{2+} ions. The coplanar oxygen atoms on RAL also coordinate to the Mg^{2+} ions thereby inhibiting the movement and function of the catalytic residues. The coordination of the PFV structure shows monodentate interactions with Mg^{2+} for Asp116, and bidentate for Glu 152. Our simulations post equilibration suggests the possibility of bidentate for both Asp 116 and Glu 152.

Figure 6.1a shows the average RMSD of the backbone atoms for each complex over the duration of the MD simulation calculated in reference to the starting structure for each complex. The initial increase in RMSD is due to the energy minimization and equilibration steps. The average RMSD values for the wild-type, 148H, 148H/140S, 148R, 148R/140A complexes are 2.43 Å, 1.92 Å, 1.99 Å, 1.86 Å and 1.63 Å respectively. Mutations as residue 148 and 140 cause reduced flexibility with the most rigidity observed in the 148R/140A mutant.

The residues with the highest RMSD values are shown in **figure 6.1** (b-f). With the exception of the 148H mutant, the α6 helix at the C-terminal end of the CCD contains residues with high RMSD values **(Fig 6.1b).** The high RMSD residues in the 148H mutant are localized to the loop connecting helix α5 and α6. The catalytic residue Glu 152 is located on the N-terminal side of α4. The 148R and

148R/140A mutants shown in **figure 6.1e** and **6.1f** respectively have high RMSD residues in the hinge region between helix α4 and α5. This increased flexibility changes the shape of the active site by causing helix α4 to bend outward. The strain of this helix causes the side chain of Glu152 to move out of range for an ionic interaction coordinating the Mg^{2+} ion between Glu 152 and Asp 64. The chelation of the active site Mg^{2+} ions by raltegravir is required for inhibition of integrase strand transfer [165].
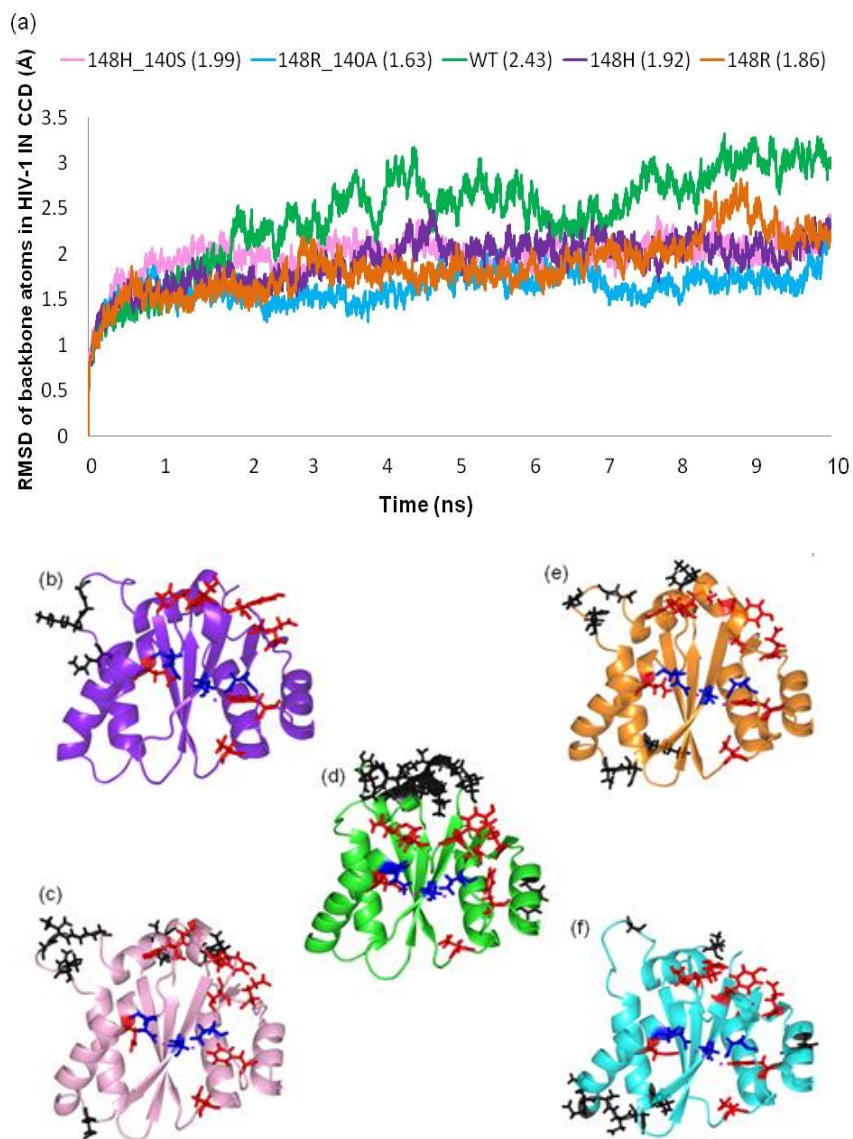
Fig. 6.1 The HIV-1 integrase mutants are less flexible than the wild type. RMSD of backbone atoms for IN during 10 ns MD simulation. High RMSD residues are shown in black, catalytic residues in blue and RAL resistance mutations shown in red. **a** RMSD in Angstroms per frame over the 10 ns

trajectory. Average RMSD values are shown in parenthesis. **b** 148H. **c** 148H/140S. **d** WT. **e** 148R. **f** 148R/140S.
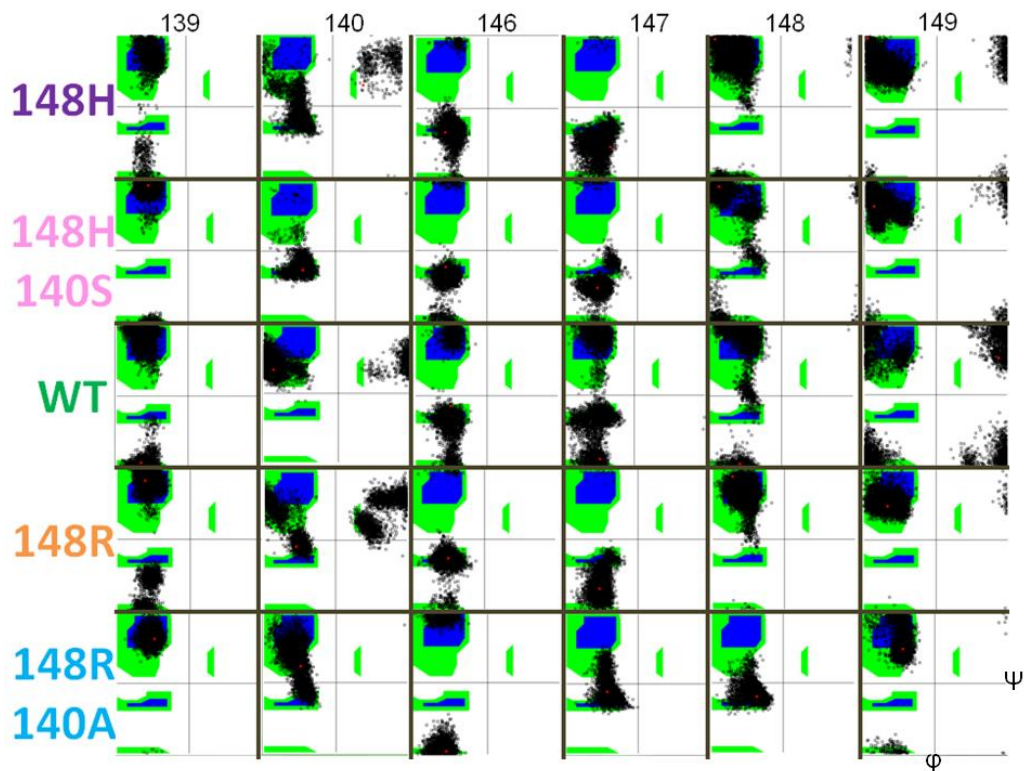
Figure 6.2. Changes in the 140's intraloop region as indicated by variation in φ, ψ angles in the codon 140 and 148 mutants of the HIV-1 integrase. Ramachandran plot of φ, ψ angles in the 140's loop over the 10 ns trajectory.

6.2.2 Transient helix formation and variability in the catalytic 140's loop

The 140's loop (139-150) transiently changes from a random coil to an intraloop helix throughout the 10 ns simulation (**Table 6.1**). In the WT, F139 has average φ, ψ angles of -119.6° and -170.9° respectively corresponding to a β sheet conformation; however values for these angles do occupy the right-handed helix range at times during the trajectory **(Fig. 6.2).** The span of calculated φ, ψ angles is similar to that of WT for the 148H and 148R single mutants however the average φ, ψ angles for residue F139 in 148H are -95.5° and -74.6° respectively, corresponding to a movement towards a more alpha helical structure. G140 residue (WT, 148H, and 148R) experiences changes in its ψ angle spanning values

for β sheets with few frames drifting towards a left-handed helix. In contrast, the double mutants containing G140S and G140A substitutions change values for the φ angle resulting in averages corresponding to α helix and β sheet respectively. While the single mutants also contain a glycine at residue 140 these mutants experience changes in both φ and ψ angles throughout the trajectory.

The φ and ψ angles of residues 141-145 are relatively consistent in each complex; while most of the time this loop is in the form of a random coil, a transient helix is formed in this region as well (Table 6.1. The formation of a 3 residue helix in this loop is a naturally occurring secondary structure element as observed in the wild-type (**Fig 6.3c**). Sample frames were taken post energy minimization and at 1 ns intervals. In the WT a helix is formed in the 140's loop consisting of residues 144-146, 141-143, or 141-146 during the 10 ns sampling. When a helix forms in this loop it likely inhibits binding of RAL to the IN CCD. The 140's loop helix forms in the 148R **(fig. 6.3d)** mutant. Similar to the wild-type, the 144-146 and the 141-146 helix forms. The Q148R mutation induces the formation of a new helix consisting of residues 141-144 and is the only helix formed in the 148R/140A mutant **(fig. 6.3e)**. The 141-144 helix is likely an extension of the 141-143 helix observed in the WT ensemble.

Table 6.1 Intraloop helix formation in the catalytic 140's loop. Composition of the intraloop helices observed during the simulation are indicated with the letter Y.

HIV IN structure	Helix Residues						
	141-143 (3)	141-144 (4)	141-146 (6)	141-147 (7)	143-147 (5)	144-146 (3)	144-147 (4)
WT	Y		Y			Y	
Q148H		Y	Y		Y	Y	Y
Q148H_G140S			Y	Y		Y	y
Q148R		Y	Y			Y	
Q148R_G140A		Y					

The 148H mutant (**Fig.6.3a**) forms a helix with residues 141-144, 144-146, 144-147, 141-146, and 143-147. In the 148H/140S mutant **(Fig 6.3b)**, the 144-147 helix formed with the 148H mutation alone was formed. The 141-146 and the 144-146 helix observed in the WT also occurred in the

148H/140S double mutant. A fourth helix was formed consisting of residues 141-147. The 144-147 helix is an extension of the 144-146 helix observed in the WT. In each of the double mutants the most frequently formed helix represents a shift from a 3-residue helix in the WT to a 4-residue helix in the mutant suggesting that in addition to the frequency of helix formation, the length of the helix is also a contributing factor to RAL resistance. The single mutation of Q148H/R induces the formation of a new 4 residue helix that is advantageous against RAL. The secondary mutation, G140S/A, ensures the formation of an extended helix.
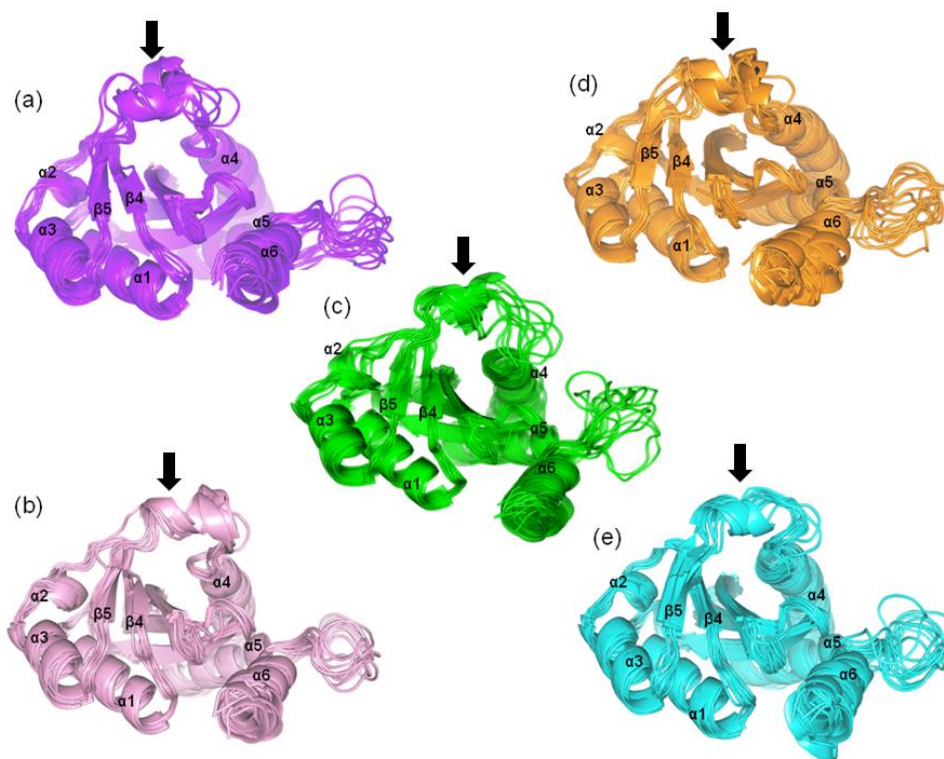
Figure 6.3. Extension of the HIV-1 integrase 140's intraloop helix for the codon 140 and 148 mutants. Structure ensemble composed of frames post energy minimization and 1ns intervals demonstrate transient structural changes occurring during the 10 ns MD simulation. The arrows indicate the position of the 140's loop helix. **a** 148H **b** 148H/140S. **c** WT. **d** 148R. **e** 148R/140A

Variations in the φ, ψ angles begin again at residue 146 which is the end of the observed helices formed in WT IN. Q146 has similar φ ψ angles for the WT, 148H, 148H/140S, and 148R. The 148R mutant however has an average φ angle of 172.3° corresponding to β-sheet structure and none of the

frames during the 10 ns have φ, ψ angles corresponding to α-helix throughout the 10ns simulation. In the presence of the 148H/S mutation S147 is primarily restricted to angles that form helical secondary structure however in the WT this residue can span the entire range of allowed φ angles. Important in catalytic function, this transient intraloop structure is likely responsible for impaired dynamics of the 140's loop gating function in these mutants [175].

Residues 120 to 122 compose a transient helix, α2 that is observed as a random coil in some crystal structures of the IN CCD and an α-helix in others. In the ensemble presented here, α2 is a random coil in the WT ensemble, while the mutants 148R, 148R/140A, 148H and the 148H/140S double mutant remains structured as a helix. F121Y , located in this region, is a resistance mutation that has been observed in patients that leads to cross resistance in clinically tested IN inhibitors including RAL [176]. This mutation does not occur concurrently with mutations at 140 and 148 however the presence or absence of α2 may play an important role in resistance.

In the 148H/140S mutant, β5; which consists of residues 136-139 is missing in the structures at post-equilibrium and 10 ns resulting in an extension of the 140s loop by 6 residues. Helix α2 is also missing in these structures. E138K is a resistance mutation that leads to a 2 fold decrease in susceptibility to RAL and other IN inhibitors compared to the WT [176].

6.3 Discussion

In this study, 10 ns MD simulations were carried out to investigate the structural changes occurring in the HIV IN CCD as a consequence of the RAL resistance mutations Q148H/R and G140S/A. The RMSD data show that the mutants have reduced flexibility. Detailed analysis of the φ, ψ angles using the Ramachandran plots in the 140's loop revealed alternative positions of the transiently formed helix in this region. The transient loss of secondary structure in α2 and β5 suggest a common mechanism for resistance to RAL as 2 of the 3 major pathways to resistance involve residues located in these regions with alternating secondary structure. The ability of this loop to experience these conformational changes in our modeled system supports the requirement for DNA in order for RAL to effectively inhibit strand

transfer**.** The increased rigidity of the 140's loop may impair its gating ability contributing to both a decrease in normal catalytic function as well as a resistance mechanism to RAL [91]. This loss of protein flexibility may serve to decrease the residence time observed in the RAL resistance mutants compared to wild type [52]. These secondary structure elements are not only required for function but play an important role in the development of HIV IN resistance to RAL and other integrase strand transfer inhibitors.

6.4 Author's contribution

The author performed the system setup, energy minimization and molecular dynamics, and data analysis.

Chapter 7: Structure based modeling of the HIV-1 intasome

7.1 Introduction

HIV-1 integrase is a 32kDa protein with 288 amino acid residues comprising three distinct domains; the N-terminal domain (NTD), catalytic core domain (CCD) and the C-terminal domain (CTD). To date, structures of the NTD, CTD, CCD, NTD with CCD and CCD with CTD have been deposited into the Protein Data Bank; however crystallization of the full length HIV-1 integrase remains elusive [177-180]. Structural information on the full length HIV-1 integrase is necessary to more fully understand host-viral interactions, understand antiviral resistance as well as aid in the development of a platform for structure based drug design.

The NTD contains four helices and tetrahedally coordinates His12, His16, Cys40 and Cys43 to a zinc cation as shown in figure 7.1 [181]. This domain is involved in multimerization as well as facilitating the interaction between HIV-1 integrase and the cellular host factor lens epithelium-derived growth factor (LEDGF) [182]. LEDGF-IN binding primarily determines the efficiency and specificity of HIV-1 integration into actively transcribed regions of the host chromosomal DNA [183, 184].
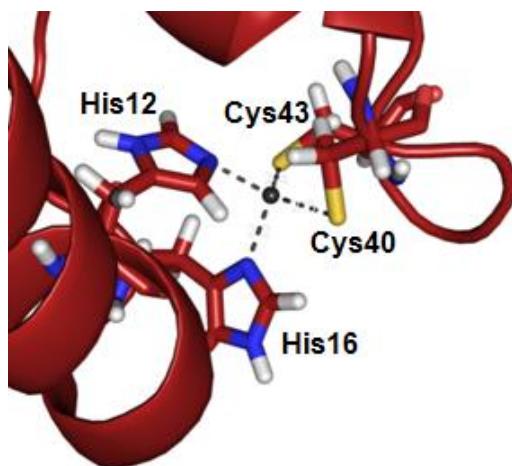
Figure 7.1 The N-terminal domain of HIV-1 integrase is tetrahedrally coordinated to a Zinc cation in an HHCC motif. Zn^{2+} is shown as a black sphere, the dashed lines represent coordination to the HHCC motif.

The CCD is responsible for chelation of divalent metal ions magnesium and/or manganese in the active site, is involved in DNA binding and has a highly conserved D,DX35E motif consisting of Asp64, Asp116, and Glu152 serving as the catalytic triad [185]. The catalytic core domain performs 3'processing and strand transfer via in-line bimolecular nucleophilic substitution (S_N2) reaction [186]. In addition to catalytic function the CCD contains residues 186-188, involved in multimerization and may be important for cellular localization [187].

The CTD is involved in nonspecific DNA binding. It contains an 18-residue C-terminal tail which has not been solved structurally but may play an important role in mediating the interaction between integrase and reverse transcriptase; as mutant integrase virions display a reverse transcription defect [188]. The CTD has also been reported to interact with several host integration factors including importin alpha3, transportin 3 and transportin-SR2 to assist in reverse transcription, nuclear import, or integration [189-192].
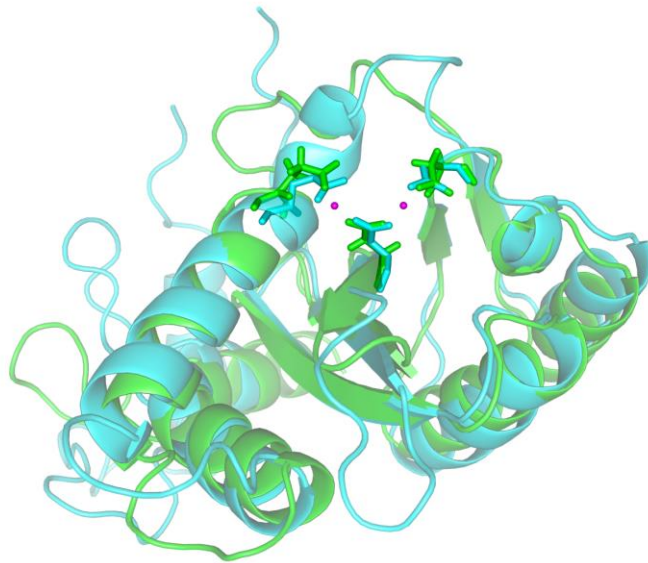
Figure 7.2 structural similarities between HIV-1 integrase and PFV integrase catalytic core domains. Superposition of the catalytic domain of the PFV intasome (cyan) and HIV-1 CCD (green). Magnesium ions (magenta) from the starting HIV-1 crystal structure 1BL3. Catalytic residues are shown in stick model.

The full length structure of the prototype foamy virus (PFV) integrase, a structurally related retrovirus, was solved in the presence of its cognate DNA, divalent metal ions, and a number of strand transfer inhibitors, including RAL, EVG and DTG [169]. Figure 7.2 shows the superposition the HIV-1 catalytic core domain with the PFV structure. These structures have provided insights into the mechanism of action of integrase inhibitors by serving as a model for HIV-1 intasome [193]. Using the PFV structure we have developed a model of the full length HIV-1 intasome shown in figure 7.3. Here, we perform 15 ns molecular dynamics simulations of the full length HIV-1 integrase in complex with the viral DNA ends and raltegravir to investigate the structural interactions in this ternary complex leading to reduced efficacy of raltegravir against resistant HIV-1 integrase mutants.
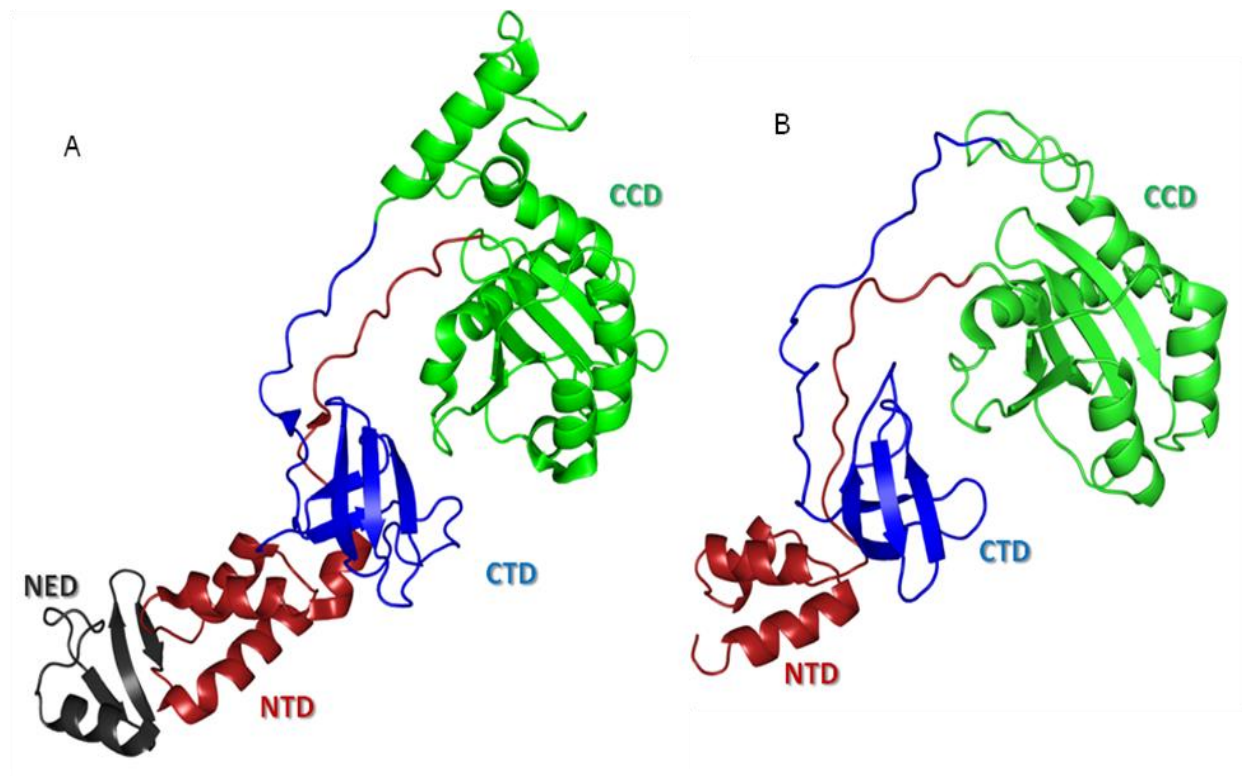
Figure 7.3 Full length HIV-1 integrase modeled from PFV integrase. (A) Prototype foamy virus integrase from PDB 3OYA with the CCD shown in green, CTD shown in blue, NTD shown in red and NED shown in dark grey. (B) Full length model of HIV-1 integrase with same color scheme for each domain. The HIV-1 IN model was built from the CCD structure (1BL3), NTD and CCD structure 1K6Y, and the CTD and CCD structure (1EX4).

7.2 Results

7.2.1 Reduced flexibility of raltegravir resistant Q148H, G140S and N155H, E92Q double mutants

The full length model of HIV-1 integrase was built by combining the CCD structure (1BL3), NTD and CCD structure 1K6Y, and the CTD and CCD structure (1EX4). Therefore, initial increase in RMSD (Figure 7.4 A) is due to energy minimization of the modeled HIV-1 integrase. The average RMSD of backbone atoms for the entire 15 ns trajectory was 6.22 Å, 4.89 Å and 4.61 Å in the WT, HS and HQ simulations respectively (Figure 7.4 B). Consistent with the findings from modeling the CCD with RAL (Chapter 6), the double mutants Q148H, G140S (HS) and N155H, E92Q (HQ) have reduced flexibility compared to the wild-type(WT) integrase in the RAL, DNA, integrase complex.
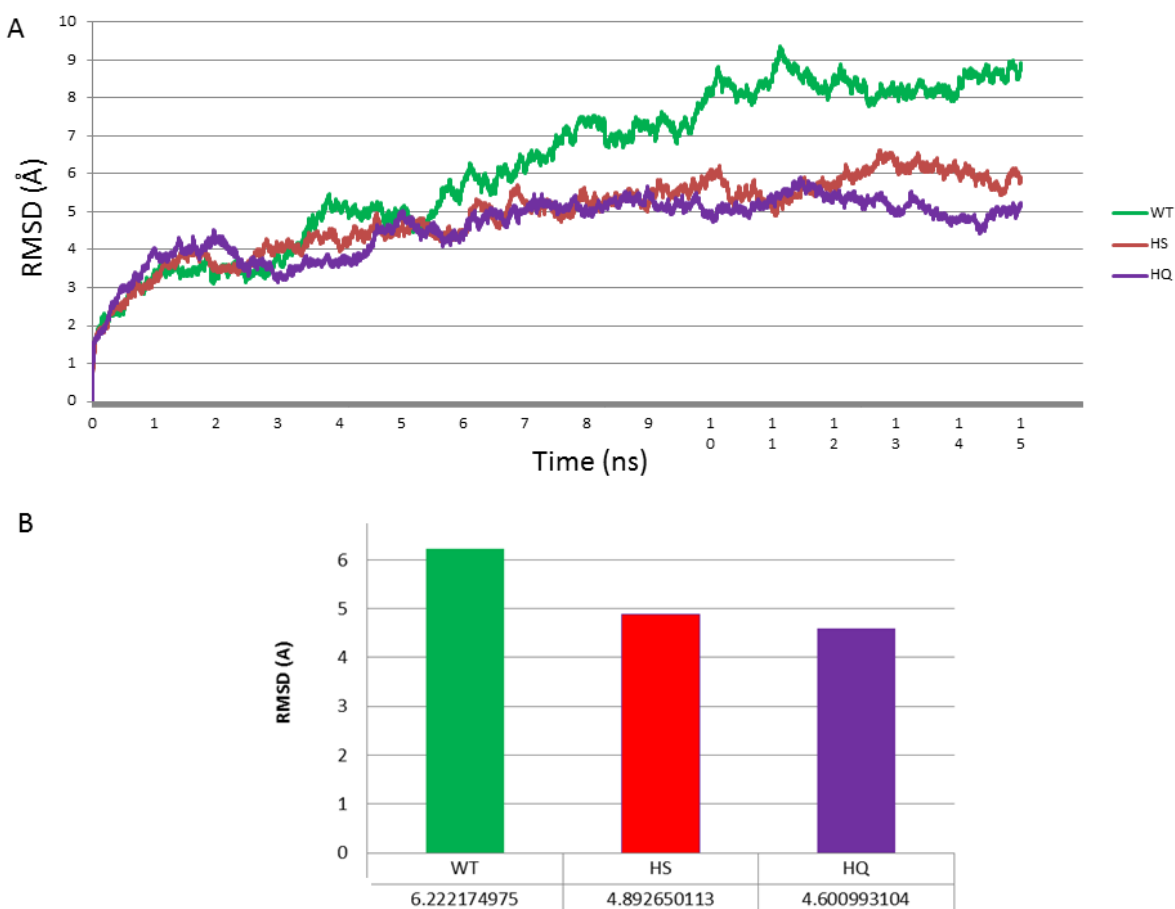
Figure 7.4. Root mean square deviation (RMSD) for backbone Cα calculated (A) as a function of time and (B) the average RMSD over the 15 ns trajectory.

7.2.2 Changes in the hydrogen bonding network alter the binding mode of raltegravir

In the WT integrase complex hydrogen bonding interactions occur between RAL and the main chain atoms of residues Y143 and S119 as well as with the side chains of residues T66, S119, and Q146. In addition, RAL makes hydrogen bonding contacts with the conserved viral DNA ends; cytosine 16 and adenine 17 in the IN active site (Table 7.1). In the HS mutant the interactions with S119 are maintained however the Y143 main chain interaction is lost and contact is only made with the Y143 side chain. Interestingly, the C-terminal residue R231 makes contacts with RAL and the contacts with the viral DNA are completely lost.

Table 7.1. Hydrogen bonding interactions with raltegravir.

	Residues involved in H-bond		
	Main chain	Side chain	DNA
Wild Type	Y143 S119	T66 Q146 S119	Ade 17 Cyt 16
Q148H_G140S		S119 Y143 R231	
N155H_E92Q	Y143	S119	Ade 17 Cyt 16

Like the WT, the HQ mutant makes main chain contacts with residue Y143, side chain of S119 and with the viral DNA cytosine 16 and adenine 17 however the main chain S119 interaction as well as the side chain Q146 and T66 interactions is lost. The total number of hydrogen bonds is reduced to 36% of the WT in the HQ mutant and only 4% of the WT in the HS mutant. These changes in total hydrogen bonding interactions as well as specific contacts alter the shape of the RAL binding pocket and therefore change the binding mode of RAL in the mutants compared to the WT (Figure 7.5). The differences in

hydrogen bonding contacts between the HS and HQ mutants highlight the importance of the viral DNA ends in RAL binding.
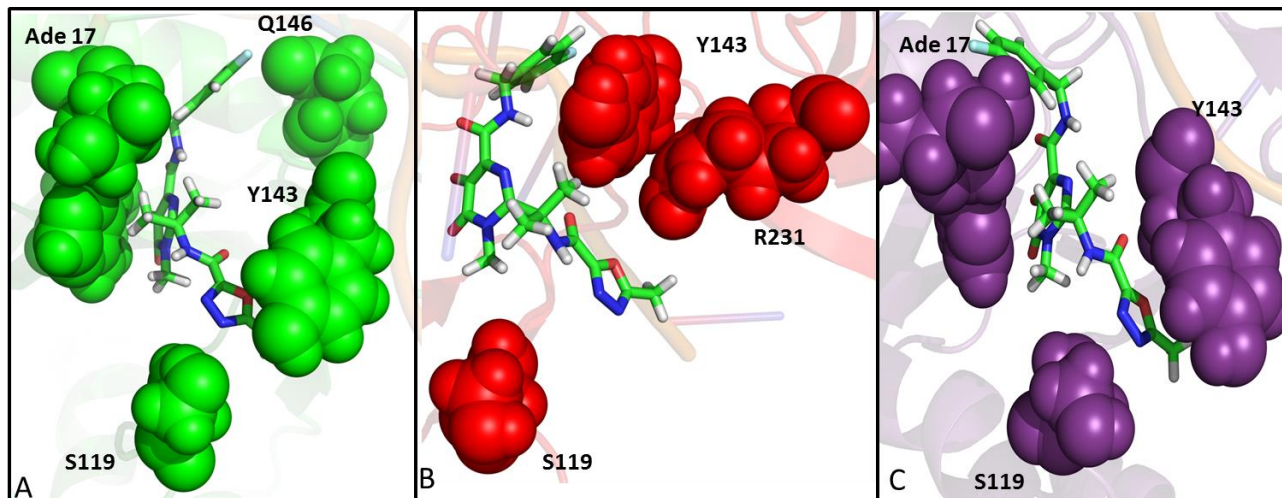
Figure 7.5 Hydrogen bonding interactions between HIV-1 IN and RAL (A) WT Complex (B) Q148H_G140S Complex (C) N155H_E92Q Complex. Residues involved in hydrogen bond with RAL are shown in sphere representation to demonstrate their van der Waals volume.

7.2.3 Changes in viral DNA interactions cause conformational changes of the integrase active site

Main chain hydrogen bonding contacts with residues D207, I141, Q146, R263, S147, S153 and V150 observed in the WT complex are lost in the HS complex while hydrogen bonding interactions are gained with residues C65, G189, G190, G247, I208, P145, R262 and interestingly the G140S mutation (Figure 7.6). The hydrogen bonding interactions in the WT complex with residues H67, D139, I141, Q146, S153, V150, D207, and E246 are lost in the HQ mutant while interactions with glycine residues G189, G190, G192 and G247 are gained. These changes in the hydrogen bonding network between IN and the viral DNA correspond to a 30% increase in the HS mutant and a 12% decrease in the HQ mutant. These changes in non-covalent interactions result in a conformational change of the viral DNA in the IN active site (Figure 7.6). This therefore alters the conformation of the RAL binding pocket and thus these alterations may be responsible for reduced susceptibility of RAL in the HS and HQ mutants compared to WT.
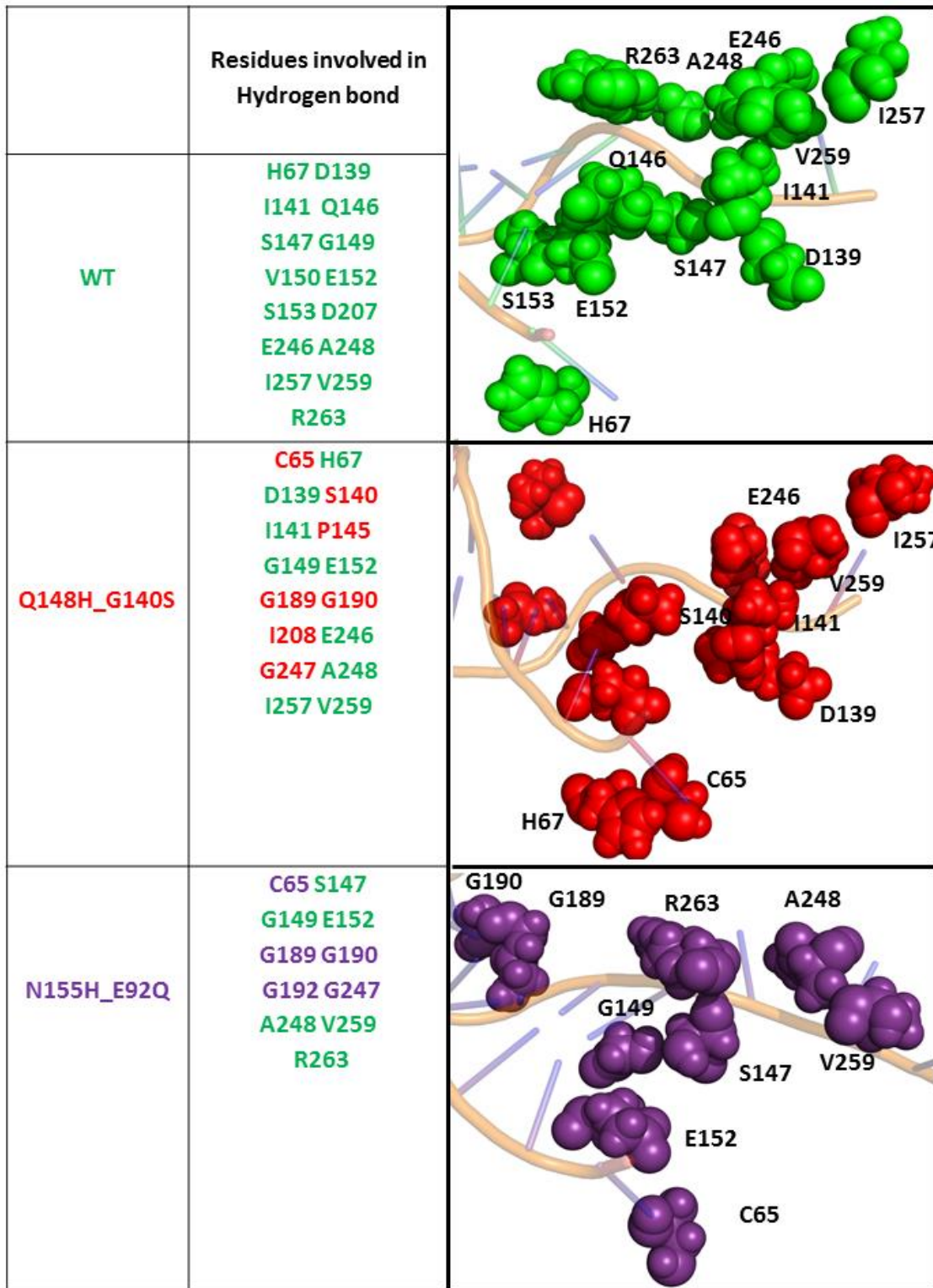
Figure 7.6 Alternative DNA binding pocket caused by RAL resistant mutations Q148H, G140S, N155H and E92Q. Residues involved in hydrogen bonding networks with the viral DNA are shown in sphere representation. Viral DNA is shown in cartoon model.

7.3 Discussion

Treatment of HIV-1 infection with the integrase strand transfer inhibitor RAL has been shown to lead to the development of RAL resistant HIV-1 IN variants. The double mutations Q148H, G140S (HS) or N155H, E92Q (HQ) cause a 100-fold decrease in susceptibility to RAL and other integrase strand transfer inhibitors (Table 7.2). To understand the structural mechanisms of RAL resistance in these two mutation pathways, we generated a model of the full length HIV-1 integrase and performed 15 ns molecular dynamics simulations on the mutants as well as the WT in complex with the conserved viral DNA template and RAL.

Table 7.2 Published *in vitro* susceptibility data of HS and HQ raltegravir resistance integrase mutants

	Fold change compared to wild type susceptibility[¥]		
	Raltegravir	Elvitegravir	Dolutegravir
148H + 140S	>150	>150	3
155H + 92Q	80-150	125-150	3

¥ Data were combined from six references in the Stanford HIV Drug Resistance Database and compiled by Blanco et al., 2011 [49, 89, 194-198].

Our results suggest that the mutations cause a reduction in protein flexibility as indicated by the decrease in RMSD and changes in the hydrogen bonding network between IN and RAL. In addition, changes in the hydrogen bonding network between IN and the viral DNA cause conformational changes in the active site. These differences in conformational flexibility compared to the WT therefore alter the binding pocket of RAL.

This change in the RAL binding pocket subsequently causes a change in the binding mode of RAL therefore pushing the metal chelating oxygen atoms out of range to interact with the Mg2+ cofactors in the active site. This effectively reduces the efficacy of RAL inhibition in the mutant integrase complexes. Understanding the mutation induced conformational changes can lead to the design of

modified strand transfer inhibitors which help to stabilize RAL in the active site by making additional contacts to the mutated residues.

7.4 Author's contribution

The author developed the full length HIV-1 integrase model, performed the molecular dynamics simulations and did the analysis of the MD trajectories.

Chapter 8: Future Directions

Treatment options for the treatment of multi-drug resistant HIV-1 infection are severely limited. The goal of this work was to elucidate the structural mechanisms of drug resistance and furthermore to use that information to design modified compounds to target drug resistant variants.

8.1. HIV-1 Protease

We plan to perform molecular dynamics on the top scoring lopinivir analogs, identified in Chapter 4, in complex with the Detroit isolates characterized in Chapter 5. We have expressed and purified MDR 769 with the L33F mutation common to all of the Detroit isolates. We will explore the structural implications on drug resistance as a result of this novel mutation with X-ray crystallography and molecular dynamics studies. In addition we will synthesize P1/P1' di-fluorinated lopinavir and test it's inhibitory efficacy *in vitro*.

8.2. HIV-1 Integrase

We are planning to express and purify the full length Q148H, G140S HIV-1 integrase in complex with a viral DNA template and the HIV-1 integrase inhibitors raltegravir, elvitegravir and dolutegravir. In addition we will perform molecular dynamics, using the biologically active dimer of the full length model developed here, in complex with the integrase inhibitors and the viral DNA template.

8.3. Human cancer and Charcot-Marie-Tooth Disease Type 1 B

Structure based drug design could aid in making synthetic decisions on not only modified compounds for the treatment of HIV-1 but has applications in any target system. We are currently using the concepts we have gained from this work in understanding the molecular pathology of Charcot-Marie – Tooth disease Type 1B, a genetic neurological disorder and designing peptides to target mutant K-RAS, an important oncogene implicated in various cancers.

REFERENCES

1. Blattner, W.A., et al., *HTLV: epidemiology and relationship to disease.* Princess Takamatsu Symp, 1984. **15**: p. 93-108.

2. Sarngadharan, M.G., et al., *HTLV-III: the etiologic agent of AIDS.* Princess Takamatsu Symp, 1984. **15**: p. 301-8.

3. Gallo, R.C., *Kaplan memorial lecture. The family of human lymphotropic retroviruses called HTLV: HTLV-I in adult T-cell leukemia (ATL), HTLV-II in hairy cell leukemias, and HTLV-III in AIDS.* Princess Takamatsu Symp, 1984. **15**: p. 13-38.

4. Schupbach, J., M.G. Sarngadharan, and R.C. Gallo, *Antigens on HTLV-infected cells recognized by leukemia and AIDS sera are related to HTLV viral glycoprotein.* Science, 1984. **224**(4649): p. 607-10.

5. Sarngadharan, M.G., et al., *Antibodies reactive with human T-lymphotropic retroviruses (HTLV-III) in the serum of patients with AIDS.* Science, 1984. **224**(4648): p. 506-8.

6. Schupbach, J., et al., *Serological analysis of a subgroup of human T-lymphotropic retroviruses (HTLV-III) associated with AIDS.* Science, 1984. **224**(4648): p. 503-5.

7.   Gallo, R.C., et al., *Frequent detection and isolation of cytopathic retroviruses (HTLV-III) from patients with AIDS and at risk for AIDS.* Science, 1984. **224**(4648): p. 500-3.

8.   Popovic, M., et al., *Detection, isolation, and continuous production of cytopathic retroviruses (HTLV-III) from patients with AIDS and pre-AIDS.* Science, 1984. **224**(4648): p. 497-500.

9.   (UNAIDS), J.U.N.P.o.H.A. *UNAIDS Report on the Global AIDS epidemic*. 2012 06/25/13; Available from: http://www.unaids.org/en/.

10.   Martoglio, B., R. Graf, and B. Dobberstein, *Signal peptide fragments of preprolactin and HIV-1 p-gp160 interact with calmodulin.* EMBO J, 1997. **16**(22): p. 6636-45.

11.   Information, N.C.f.B. 2013   [cited 2013 06/26/13]; Available from: http://www.ncbi.nlm.nih.gov/.

12.   Pancera, M., et al., *Structure of HIV-1 gp120 with gp41-interactive region reveals layered envelope architecture and basis of conformational mobility.* Proc Natl Acad Sci U S A, 2010. **107**(3): p. 1166-71.

13.   Fletcher, T.M., 3rd, et al., *Nuclear import and cell cycle arrest functions of the HIV-1 Vpr protein are encoded by two separate genes in HIV-2/SIV(SM).* EMBO J, 1996. **15**(22): p. 6155-65.

14. Landi, A., et al., *One protein to rule them all: modulation of cell surface receptors and molecules by HIV Nef.* Curr HIV Res, 2011. **9**(7): p. 496-504.

15. Munk, C., et al., *Running loose or getting lost: how HIV-1 counters and capitalizes on APOBEC3-induced mutagenesis through its Vif protein.* Viruses, 2012. **4**(11): p. 3132-61.

16. Flint, S.J., *Principles of virology : molecular biology, pathogenesis, and control of animal viruses.* 2nd ed. 2004, Washington, D.C.: ASM Press. xxvi, 918 p.

17. Navia, M.A. and B.M. McKeever, *A role for the aspartyl protease from the human immunodeficiency virus type 1 (HIV-1) in the orchestration of virus assembly.* Ann N Y Acad Sci, 1990. **616**: p. 73-85.

18. Szecsi, P.B., *The aspartic proteases.* Scand J Clin Lab Invest Suppl, 1992. **210**: p. 5-22.

19. Bott, R., E. Subramanian, and D.R. Davies, *Three-dimensional structure of the complex of the Rhizopus chinensis carboxyl proteinase and pepstatin at 2.5-A resolution.* Biochemistry, 1982. **21**(26): p. 6956-62.

20.   James, M.N. and A.R. Sielecki, *Stereochemical analysis of peptide bond hydrolysis catalyzed by the aspartic proteinase penicillopepsin.* Biochemistry, 1985. **24**(14): p. 3701-13.

21.   Oh, S., W. Chang, and J. Suh, *An aspartic protease analogue: intermolecular catalysis of peptide hydrolysis by carboxyl groups.* Bioorg Med Chem Lett, 2001. **11**(11): p. 1469-72.

22.   Choi, G., et al., *Asp-99 donates a hydrogen bond not to Tyr-14 but to the steroid directly in the catalytic mechanism of Delta 5-3-ketosteroid isomerase from Pseudomonas putida biotype B.* Biochemistry, 2000. **39**(5): p. 903-9.

23.   Palmeira, V.F., et al., *Secretory aspartyl peptidase activity from mycelia of the human fungal pathogen Fonsecaea pedrosoi: effect of HIV aspartyl proteolytic inhibitors.* Res Microbiol, 2006. **157**(9): p. 819-26.

24.   Suguna, K., et al., *Binding of a reduced peptide inhibitor to the aspartic proteinase from Rhizopus chinensis: implications for a mechanism of action.* Proc Natl Acad Sci U S A, 1987. **84**(20): p. 7009-13.

25.   Tang, J., et al., *Structural evidence for gene duplication in the evolution of the acid proteases.* Nature, 1978. **271**(5646): p. 618-21.

26. Swanstrom, R. and J. Erona, *Human immunodeficiency virus type-1 protease inhibitors: therapeutic successes and failures, suppression and resistance.* Pharmacol Ther, 2000. **86**(2): p. 145-70.

27. de Vera, I.M., et al., *Elucidating a Relationship between Conformational Sampling and Drug Resistance in HIV-1 Protease.* Biochemistry, 2013.

28. Lam, P.Y., et al., *Rational design of potent, bioavailable, nonpeptide cyclic ureas as HIV protease inhibitors.* Science, 1994. **263**(5145): p. 380-4.

29. Leach, A.R., *Molecular modelling : principles and applications*. 2nd ed. 2001, Harlow, England ; New York: Prentice Hall. xxiv, 744 p., 16 p. of plates.

30. Hyland, L.J., et al., *Human immunodeficiency virus-1 protease. 1. Initial velocity studies and kinetic characterization of reaction intermediates by 18O isotope exchange.* Biochemistry, 1991. **30**(34): p. 8441-53.

31. Liu, Z., et al., *Nine crystal structures determine the substrate envelope of the MDR HIV-1 protease.* Protein J, 2011. **30**(3): p. 173-83.

32. Liu, Z., et al., *Conserved hydrogen bonds and water molecules in MDR HIV-1 protease substrate complexes.* Biochem Biophys Res Commun, 2013. **430**(3): p. 1022-7.

33. Yedidi, R.S., et al., *Crystal structures of multidrug-resistant HIV-1 protease in complex with two potent anti-malarial compounds.* Biochem Biophys Res Commun, 2012. **421**(3): p. 413-7.

34. Lu, R., et al., *Genetic analyses of DNA-binding mutants in the catalytic core domain of human immunodeficiency virus type 1 integrase.* J Virol, 2005. **79**(4): p. 2493-505.

35. Pommier, Y., A.A. Johnson, and C. Marchand, *Integrase inhibitors to treat HIV/AIDS.* Nat Rev Drug Discov, 2005. **4**(3): p. 236-48.

36. Levin, A., et al., *Transportin 3 and importin alpha are required for effective nuclear import of HIV-1 integrase in virus-infected cells.* Nucleus, 2010. **1**(5): p. 422-31.

37. Pandey, K.K., S. Bera, and D.P. Grandgenett, *The HIV-1 integrase monomer induces a specific interaction with LTR DNA for concerted integration.* Biochemistry, 2011. **50**(45): p. 9788-96.

38. Gijsbers, R., et al., *Role of the PWWP domain of lens epithelium-derived growth factor (LEDGF)/p75 cofactor in lentiviral integration targeting.* J Biol Chem, 2011. **286**(48): p. 41812-25.

39. Rom, I., et al., *Activation of HIV-1 LTR by Rad51 in microglial cells.* Cell Cycle, 2010. **9**(18): p. 3715-22.

40. Eron, J.J., Jr., et al., *Raltegravir once daily or twice daily in previously untreated patients with HIV-1: a randomised, active-controlled, phase 3 non-inferiority trial.* Lancet Infect Dis, 2011. **11**(12): p. 907-15.

41. Summa, V., et al., *Discovery of raltegravir, a potent, selective orally bioavailable HIV-integrase inhibitor for the treatment of HIV-AIDS infection.* J Med Chem, 2008. **51**(18): p. 5843-55.

42. Brainard, D.M., et al., *Clinical pharmacology profile of raltegravir, an HIV-1 integrase strand transfer inhibitor.* J Clin Pharmacol, 2011. **51**(10): p. 1376-402.

43. Fayet Mello, A., et al., *Cell disposition of raltegravir and newer antiretrovirals in HIV-infected patients: high inter-individual variability in raltegravir cellular penetration.* J Antimicrob Chemother, 2011. **66**(7): p. 1573-81.

44. Lampiris, H.W., *Elvitegravir: a once-daily, boosted, HIV-1 integrase inhibitor.* Expert Rev Anti Infect Ther, 2012. **10**(1): p. 13-20.

45. DeJesus, E., et al., *Antiviral activity, pharmacokinetics, and dose response of the HIV-1 integrase inhibitor GS-9137 (JTK-303) in treatment-naive and treatment-experienced patients.* J Acquir Immune Defic Syndr, 2006. **43**(1): p. 1-5.

46. Sato, M., et al., *Novel HIV-1 integrase inhibitors derived from quinolone antibiotics.* J Med Chem, 2006. **49**(5): p. 1506-8.

47. Koh, Y., H. Haim, and A. Engelman, *Identification and characterization of persistent intracellular human immunodeficiency virus type 1 integrase strand transfer inhibitor activity.* Antimicrob Agents Chemother, 2011. **55**(1): p. 42-9.

48. Zembruski, N.C., et al., *Potential of novel antiretrovirals to modulate expression and function of drug transporters in vitro.* J Antimicrob Chemother, 2011. **66**(4): p. 802-12.

49. Kobayashi, M., et al., *In Vitro antiretroviral properties of S/GSK1349572, a next-generation HIV integrase inhibitor.* Antimicrob Agents Chemother, 2011. **55**(2): p. 813-21.

50. Min, S., et al., *Antiviral activity, safety, and pharmacokinetics/pharmacodynamics of dolutegravir as 10-day monotherapy in HIV-1-infected adults.* AIDS, 2011. **25**(14): p. 1737-45.

51. Hare, S., et al., *Structural and functional analyses of the second-generation integrase strand transfer inhibitor dolutegravir (S/GSK1349572).* Mol Pharmacol, 2011. **80**(4): p. 565-72.

52. Hightower, K.E., et al., *Dolutegravir (S/GSK1349572) exhibits significantly slower dissociation than raltegravir and elvitegravir from wild-type and integrase inhibitor-resistant HIV-1 integrase-DNA complexes.* Antimicrob Agents Chemother, 2011. **55**(10): p. 4552-9.

53. Espeseth, A.S., et al., *HIV-1 integrase inhibitors that compete with the target DNA substrate define a unique strand transfer conformation for integrase.* Proc Natl Acad Sci U S A, 2000. **97**(21): p. 11244-9.

54. Pandey, K.K., et al., *Physical trapping of HIV-1 synaptic complex by different structural classes of integrase strand transfer inhibitors.* Biochemistry, 2010. **49**(38): p. 8376-87.

55. Li, X., et al., *Structural biology of retroviral DNA integration.* Virology, 2011. **411**(2): p. 194-205.

56. Bacchi, A., et al., *Investigating the Role of Metal Chelation in HIV-1 Integrase Strand Transfer Inhibitors.* J Med Chem, 2011. **54**(24): p. 8407-20.

57. Barreca, M.L., et al., *Induced-fit docking approach provides insight into the binding mode and mechanism of action of HIV-1 integrase inhibitors.* ChemMedChem, 2009. **4**(9): p. 1446-56.

58. Garvey, E.P., et al., *Potent inhibitors of HIV-1 integrase display a two-step, slow-binding inhibition mechanism which is absent in a drug-resistant T66I/M154I mutant.* Biochemistry, 2009. **48**(7): p. 1644-53.

59. Al-Mawsawi, L.Q. and N. Neamati, *Allosteric inhibitor development targeting HIV-1 integrase.* ChemMedChem, 2011. **6**(2): p. 228-41.

60. Zheng, R., T.M. Jenkins, and R. Craigie, *Zinc folds the N-terminal domain of HIV-1 integrase, promotes multimerization, and enhances catalytic activity.* Proc Natl Acad Sci U S A, 1996. **93**(24): p. 13659-64.

61. Carayon, K., et al., *A cooperative and specific DNA-binding mode of HIV-1 integrase depends on the nature of the metallic cofactor and involves the zinc-containing N-terminal domain.* Nucleic Acids Res, 2010. **38**(11): p. 3692-708.

62. Masuda, T., et al., *Genetic analysis of human immunodeficiency virus type 1 integrase and the U3 att site: unusual phenotype of mutants in the zinc finger-like domain.* J Virol, 1995. **69**(11): p. 6687-96.

63. Engelman, A. and R. Craigie, *Identification of conserved amino acid residues critical for human immunodeficiency virus type 1 integrase function in vitro.* J Virol, 1992. **66**(11): p. 6361-9.

64. Wu, X., et al., *Human immunodeficiency virus type 1 integrase protein promotes reverse transcription through specific interactions with the nucleoprotein reverse transcription complex.* J Virol, 1999. **73**(3): p. 2126-35.

65. Rhodes, D.I., et al., *Crystal Structures of Novel Allosteric Peptide Inhibitors of HIV Integrase Identify New Interactions at the LEDGF Binding Site.* Chembiochem, 2011.

66. Williams, K.L., et al., *Mass spectrometric analysis of the HIV-1 integrase-pyridoxal 5'-phosphate complex reveals a new binding site for a nucleotide inhibitor.* J Biol Chem, 2005. **280**(9): p. 7949-55.

67. Rhee, S.Y., et al., *Human immunodeficiency virus reverse transcriptase and protease sequence database.* Nucleic Acids Res, 2003. **31**(1): p. 298-303.

68. Shafer, R.W., *Rationale and uses of a public HIV drug-resistance database.* J Infect Dis, 2006. **194 Suppl 1**: p. S51-8.

69. Wang, Y., et al., *The higher barrier of darunavir and tipranavir resistance for HIV-1 protease.* Biochem Biophys Res Commun, 2011. **412**(4): p. 737-42.

70. Adolescents, P.o.A.G.f.A.a. *Guidelines for the use of antiretroviral agents in HIV-1 infected adults and adolescents.* 2013 02/12/2013 [cited 2013 7/2/2013]; Available from: http://aidsinfo.nih.gov/ContentFiles/AdultandAdolescentGL.pdf

71. Kempf, D.J., et al., *Identification of genotypic changes in human immunodeficiency virus protease that correlate with reduced susceptibility to the protease inhibitor lopinavir among viral isolates from protease inhibitor-experienced patients.* J Virol, 2001. **75**(16): p. 7462-9.

72. Vermeiren, H., et al., *Prediction of HIV-1 drug susceptibility phenotype from the viral genotype using linear regression modeling.* J Virol Methods, 2007. **145**(1): p. 47-55.

73. Colonno, R., et al., *Identification of I50L as the signature atazanavir (ATV)-resistance mutation in treatment-naive HIV-1-infected patients receiving ATV-containing regimens.* J Infect Dis, 2004. **189**(10): p. 1802-10.

74. Clemente, J.C., et al., *Analysis of HIV-1 CRF_01 A/E protease inhibitor resistance: structural determinants for maintaining sensitivity and developing resistance to atazanavir.* Biochemistry, 2006. **45**(17): p. 5468-77.

75. Mitsuya, Y., et al., *N88D facilitates the co-occurrence of D30N and L90M and the development of multidrug resistance in HIV type 1 protease following nelfinavir treatment failure.* AIDS Res Hum Retroviruses, 2006. **22**(12): p. 1300-5.

76. Garriga, C., et al., *Mutational patterns and correlated amino acid substitutions in the HIV-1 protease after virological failure to nelfinavir- and lopinavir/ritonavir-based treatments.* J Med Virol, 2007. **79**(11): p. 1617-28.

77. De Meyer, S., et al., *Characterization of virologic failure patients on darunavir/ritonavir in treatment-experienced patients.* AIDS, 2009. **23**(14): p. 1829-40.

78. Vierling, P. and J. Greiner, *Prodrugs of HIV protease inhibitors.* Curr Pharm Des, 2003. **9**(22): p. 1755-70.

79. Rusconi, S., et al., *Efficacy and safety of a dual boosted protease inhibitor- based regimen, atazanavir and fosamprenavir/ritonavir, against HIV: experience in a pediatric population.* BMC Infect Dis, 2012. **12**: p. 179.

80. Condra, J.H., et al., *Genetic correlates of in vivo viral resistance to indinavir, a human immunodeficiency virus type 1 protease inhibitor.* J Virol, 1996. **70**(12): p. 8270-6.

81.	Eira, M., M. Araujo, and A.C. Seguro, *Urinary NO3 excretion and renal failure in indinavir-treated patients.* Braz J Med Biol Res, 2006. **39**(8): p. 1065-70.

82.	Barber, T.J., et al., *Frequency and patterns of protease gene resistance mutations in HIV-infected patients treated with lopinavir/ritonavir as their first protease inhibitor.* J Antimicrob Chemother, 2012. **67**(4): p. 995-1000.

83.	Soares, R.O., et al., *Understanding the HIV-1 protease nelfinavir resistance mutation D30N in subtypes B and C through molecular dynamics simulations.* J Mol Graph Model, 2010. **29**(2): p. 137-47.

84.	van Westen, G.J.P., et al., *Significantly Improved HIV Inhibitor Efficacy Prediction Employing Proteochemometric Models Generated From Antivirogram Data.* Plos Computational Biology, 2013. **9**(2).

85.	Kagan, R.M., et al., *Structural analysis of an HIV-1 protease I47A mutant resistant to the protease inhibitor lopinavir.* Protein Science, 2005. **14**(7): p. 1870-1878.

86.	Chan-Tack, K.M., K.A. Struble, and D.B. Birnkrant, *Intracranial hemorrhage and liver-associated deaths associated with*

tipranavir/ritonavir: review of cases from the FDA's Adverse Event Reporting System. AIDS Patient Care STDS, 2008. **22**(11): p. 843-50.

87. Chan-Tack, K.M., et al., *HIV clinical trial design for antiretroviral development: moving forward.* AIDS, 2008. **22**(18): p. 2419-27.

88. Chan-Tack, K.M. and J.S. Murray, *Antiviral therapy and outcomes in hospitalized patients with influenza.* Clin Infect Dis, 2008. **46**(10): p. 1628-9; author reply 1629-30.

89. da Silva, D., et al., *HIV-1 resistance patterns to integrase inhibitors in antiretroviral-experienced patients with virological failure on raltegravir-containing regimens.* J Antimicrob Chemother, 2010. **65**(6): p. 1262-9.

90. Delelis, O., et al., *The G140S mutation in HIV integrases from raltegravir-resistant patients rescues catalytic defect due to the resistance Q148H mutation.* Nucleic Acids Res, 2009. **37**(4): p. 1193-201.

91. Pommier, Y., et al., *Biochemical and Pharmacological Analyses of HIV-1 Integrase Flexible Loop Mutants Resistant to Raltegravir.* Biochemistry, 2010. **49**(17): p. 3715-3722.

92. Hare, S., et al., *Molecular mechanisms of retroviral integrase inhibition and the evolution of viral resistance.* Proc Natl Acad Sci U S A, 2010. **107**(46): p. 20057-62.

93. Young, B., et al., *Transmission of integrase strand-transfer inhibitor multidrug-resistant HIV-1: case report and response to raltegravir-containing antiretroviral therapy.* Antiviral Therapy, 2011. **16**(2): p. 253-6.

94. Goethals, O., et al., *Resistance to raltegravir highlights integrase mutations at codon 148 in conferring cross-resistance to a second-generation HIV-1 integrase inhibitor.* Antiviral Res, 2011. **91**(2): p. 167-76.

95. Reigadas, S., et al., *Structure-analysis of the HIV-1 integrase Y143C/R raltegravir resistance mutation in association with the secondary mutation T97A.* Antimicrob Agents Chemother, 2011. **55**(7): p. 3187-94.

96. Metifiot, M., et al., *MK-0536 inhibits HIV-1 integrases resistant to raltegravir.* Antimicrob Agents Chemother, 2011. **55**(11): p. 5127-33.

97. Shimura, K., et al., *Broad antiretroviral activity and resistance profile of the novel human immunodeficiency virus integrase inhibitor elvitegravir (JTK-303/GS-9137).* J Virol, 2008. **82**(2): p. 764-74.

98. Molina, J.M., et al., *Efficacy and safety of once daily elvitegravir versus twice daily raltegravir in treatment-experienced patients with HIV-1 receiving a ritonavir-boosted protease inhibitor: randomised, double-*

blind, phase 3, non-inferiority study. Lancet Infect Dis, 2012. **12**(1): p. 27-35.

99. Margot, N.A., et al., *In vitro resistance selections using elvitegravir, raltegravir, and two metabolites of elvitegravir M1 and M4.* Antiviral Res, 2011.

100. Goethals, O., et al., *Resistance mutations in human immunodeficiency virus type 1 integrase selected with elvitegravir confer reduced susceptibility to a wide range of integrase inhibitors.* J Virol, 2008. **82**(21): p. 10366-74.

101. Hombrouck, A., et al., *Mutations in human immunodeficiency virus type 1 integrase confer resistance to the naphthyridine L-870,810 and cross-resistance to the clinical trial drug GS-9137.* Antimicrob Agents Chemother, 2008. **52**(6): p. 2069-78.

102. Metifiot, M., et al., *Elvitegravir overcomes resistance to raltegravir induced by integrase mutation Y143.* AIDS, 2011. **25**(9): p. 1175-8.

103. Quashie, P.K., et al., *Characterization of the R263K mutation in HIV-1 integrase that confers low-level resistance to the second-generation integrase strand transfer inhibitor Dolutegravir.* J Virol, 2011.

104. Canducci, F., et al., *Cross-resistance profile of the novel integrase inhibitor Dolutegravir (S/GSK1349572) using clonal viral variants selected in patients failing raltegravir.* J Infect Dis, 2011. **204**(11): p. 1811-5.

105. Garrido, C., et al., *Resistance associated mutations to dolutegravir (S/GSK1349572) in HIV-infected patients--impact of HIV subtypes and prior raltegravir experience.* Antiviral Res, 2011. **90**(3): p. 164-7.

106. Silverman, R.B., *The organic chemistry of drug design and drug action*. 2nd ed. 2004, Amsterdam ; Boston: Elsevier Academic Press. xix, 617 p., 12 p. of plates.

107. Hansch, C., E. Kutter, and A. Leo, *Homolytic constants in the correlation of chloramphenicol structure with activity.* J Med Chem, 1969. **12**(5): p. 746-9.

108. Penniston, J.T., et al., *Passive permeation of organic compounds through biological tissue: a non-steady-state theory.* Mol Pharmacol, 1969. **5**(4): p. 333-41.

109. Kutter, E. and C. Hansch, *Steric parameters in drug design. Monoamine oxidase inhibitors and antihistamines.* J Med Chem, 1969. **12**(4): p. 647-52.

110. Rhyu, K.B., H.C. Patel, and A.J. Hopfinger, *A 3D-QSAR study of anticoccidial triazines using molecular shape analysis.* J Chem Inf Comput Sci, 1995. **35**(4): p. 771-8.

111. Welch, M., et al., *Design parameters to control synthetic gene expression in Escherichia coli.* PLoS One, 2009. **4**(9): p. e7002.

112. Otwinowski, Z. and W. Minor, *Processing of X-ray diffraction data collected in oscillation mode*, in *Methods in Enzymology*, C.W. Carter and R.M. Sweet, Editors. 1997, Academic Press, Inc.: New York, NY. p. 307-326.

113. COLLABORATIVE COMPUTATIONAL PROJECT NUMBER 4, *The CCP4 suite: programs for protein crystallography.* Acta Crystallogr D Biol Crystallogr, 1994. **50**(Pt 5): p. 760-3.

114. Emsley, P. and K. Cowtan, *Coot: model-building tools for molecular graphics.* Acta Crystallogr D Biol Crystallogr, 2004. **60**(Pt 12 Pt 1): p. 2126-32.

115. Laskowski, R.A., et al., *PROCHECK: a program to check the stereochemical quality of protein structures.* J Appl Cryst, 1993. **26**: p. 283-291.

116. Karplus, M. and J.A. McCammon, *Molecular dynamics simulations of biomolecules.* Nat Struct Biol, 2002. **9**(9): p. 646-52.

117. Levitt, D.G., *Kinetics of diffusion and convection in 3.2-A pores. Exact solution by computer simulation.* Biopolymers, 1973. **13**(2): p. 186-206.

118. Karplus, M., B.R. Gelin, and J.A. McCammon, *Internal dynamics of proteins. Short time and long time motions of aromatic sidechains in PTI.* Biophys J, 1980. **32**(1): p. 603-18.

119. McCammon, J.A. and M. Karplus, *Internal motions of antibody molecules.* Nature, 1977. **268**(5622): p. 765-6.

120. McCammon, J.A., B.R. Gelin, and M. Karplus, *Dynamics of folded proteins.* Nature, 1977. **267**(5612): p. 585-90.

121. Brooks, B.R., et al., *CHARMM: A Program for Macromolecular Energy, Minimization, and Dynamics Calculations.* J. Comp. Chem, 1983. **4**: p. 187-217.

122. Brooks, B.R., et al., *CHARMM: the biomolecular simulation program.* J Comput Chem, 2009. **30**(10): p. 1545-614.

123. Phillips, J.C., et al., *Scalable molecular dynamics with NAMD.* J Comput Chem, 2005. **26**(16): p. 1781-802.

124. Darden, T., D. York, and L. Pedersen, *Particle Mesh Ewald - an N.Log(N) Method for Ewald Sums in Large Systems.* J Chem Phys, 1993. **98**(12): p. 10089-10092.

125. Sotomayor, M. and K. Schulten, *Molecular dynamics study of gating in the mechanosensitive channel of small conductance MscS.* Biophys J, 2004. **87**(5): p. 3050-65.

126. Hsu, C.K. and S. Park, *Computational and mutagenesis studies of the streptavidin native dimer interface.* J Mol Graph Model, 2010. **29**(3): p. 295-308.

127. Arnold, K., et al., *The SWISS-MODEL workspace: a web-based environment for protein structure homology modelling.* Bioinformatics, 2006. **22**(2): p. 195-201.

128. Berman, H.M., et al., *The Protein Data Bank.* Nucleic Acids Res, 2000. **28**(1): p. 235-42.

129. Maignan, S., et al., *Crystal structures of the catalytic domain of HIV-1 integrase free and complexed with its metal cofactor: high level of similarity of the active site with other viral integrases.* J Mol Biol, 1998. **282**(2): p. 359-68.

130. Kawasuji, T., et al., *A platform for designing HIV integrase inhibitors. Part 1: 2-hydroxy-3-heteroaryl acrylic acid derivatives as novel HIV integrase inhibitor and modeling of hydrophilic and hydrophobic pharmacophores.* Bioorg Med Chem, 2006. **14**(24): p. 8430-45.

131. DeLano, W., *The PyMol Molecular Graphics System, Version 1.3.* Shrödinger, LLC.

132. Krishnan, L., et al., *Structure-based modeling of the functional HIV-1 intasome and its inhibition.* Proc Natl Acad Sci U S A, 2010. **107**(36): p. 15910-5.

133. Humphrey, W., A. Dalke, and K. Schulten, *VMD: visual molecular dynamics.* J Mol Graph, 1996. **14**(1): p. 33-8, 27-8.

134. Hazuda, D.J., et al., *Inhibitors of strand transfer that prevent integration and inhibit HIV-1 replication in cells.* Science, 2000. **287**(5453): p. 646-650.

135. Foye, W.O., T.L. Lemke, and D.A. Williams, *Foye's principles of medicinal chemistry*. 6th ed. 2008, Philadelphia: Lippincott Williams & Wilkins. xiv, 1377 p., 8 p. of plates.

136. Grosdidier, A., V. Zoete, and O. Michielin, *SwissDock, a protein-small molecule docking web service based on EADock DSS.* Nucleic Acids Res, 2011. **39**(Web Server issue): p. W270-7.

137. Grosdidier, A., V. Zoete, and O. Michielin, *Fast docking using the CHARMM force field with EADock DSS.* J Comput Chem, 2011.

138. Halgren, T.A., *Merck molecular force field .1. Basis, form, scope, parameterization, and performance of MMFF94.* Journal of Computational Chemistry, 1996. **17**(5-6): p. 490-519.

139. Halgren, T.A., *Merck molecular force field .2. MMFF94 van der Waals and electrostatic parameters for intermolecular interactions.* Journal of Computational Chemistry, 1996. **17**(5-6): p. 520-552.

140. Halgren, T.A. and R.B. Nachbar, *Merck molecular force field .4. Conformational energies and geometries for MMFF94.* Journal of Computational Chemistry, 1996. **17**(5-6): p. 587-615.

141. Halgren, T.A., *Merck molecular force field .5. Extension of MMFF94 using experimental data, additional computational data, and empirical rules.* Journal of Computational Chemistry, 1996. **17**(5-6): p. 616-641.

142. Halgren, T.A., *Merck molecular force field .3. Molecular geometries and vibrational frequencies for MMFF94.* Journal of Computational Chemistry, 1996. **17**(5-6): p. 553-586.

143. Halgren, T.A. and R.B. Nachbar, *MMF94: The Merck molecular force field. Bridging the gap - From small organics to proteins.* Abstracts of Papers of the American Chemical Society, 1996. **211**: p. 70-Comp.

144. Haberthur, U. and A. Caflisch, *FACTS: Fast analytical continuum treatment of solvation.* J Comput Chem, 2008. **29**(5): p. 701-15.

145. Pettersen, E.F., et al., *UCSF chimera - A visualization system for exploratory research and analysis.* Journal of Computational Chemistry, 2004. **25**(13): p. 1605-1612.

146. Prasad, J.V., et al., *Nonpeptidic potent HIV-1 protease inhibitors.* Drug Des Discov, 1996. **13**(3-4): p. 15-28.

147. Kempf, D.J., et al., *Design of orally bioavailable, symmetry-based inhibitors of HIV protease.* Bioorg Med Chem, 1994. **2**(9): p. 847-58.

148. Wang, Y., et al., *X-Ray Crystal Structure and Dynamics Reveal Hiv-1 Protease Drug Interactions.* Studia Universitatis Babes-Bolyai Chemia, 2011. **56**(3): p. 221-230.

149. Sham, H.L., et al., *ABT-378, a highly potent inhibitor of the human immunodeficiency virus protease.* Antimicrob Agents Chemother, 1998. **42**(12): p. 3218-24.

150. Vickrey, J.F., et al., *HIV-1 protease variants from 100-fold drug resistant clinical isolates: expression, purification, and crystallization.* Protein Expr Purif, 2003. **28**(1): p. 165-72.

151. Panel on Antiretroviral Guidelines for Adults and Adolescents, *Guidelines for the use of antiretroviral agents in HIV-1-infected adults and adolescents*, Department of Health and Human Services, Editor. 2011. p. 41.

152. Yedidi, R.S., et al., *Contribution of the 80s loop of HIV-1 protease to the multidrug-resistance mechanism: crystallographic study of MDR769 HIV-1 protease variants.* Acta Crystallogr D Biol Crystallogr, 2011. **67**(Pt 6): p. 524-32.

153. Reddy, G.S., et al., *Design and synthesis of HIV-1 protease inhibitors incorporating oxazolidinones as P2/P2' ligands in pseudosymmetric dipeptide isosteres.* J Med Chem, 2007. **50**(18): p. 4316-28.

154. Rhee, S.Y., et al., *HIV-1 Protease Mutations and Protease Inhibitor Cross Resistance.* Antimicrob Agents Chemother, 2010. **54**(10): p. 4253-4261.

155. Beck, Z.Q., et al., *Identification of efficiently cleaved substrates for HIV-1 protease using a phage display library and use in inhibitor development.* Virology, 2000. **274**(2): p. 391-401.

156. *Guidelines for the Use of Antiretroviral Agents in HIV-1-Infected Adults and Adolescents.* http://aidsinfo.nih.gov/guidelines 2013.

157. Maarseveen, N.V.a.B., C. , *Antiretroviral Resistance in Clinical Practice.* 2008, London: Mediscript Ltd.

158. Johnson, V.B.-V., F; Clotet, B; Gunthard, HF; Kuritzkes, DR; Pillay, D; Schapiro, JM; Richman, DD, *Update of the drug resistance mutations in HIV-1.* Topics in HIV medicine 2009. **17**(5): p. 138–45.

159. McCoy, C., *Darunavir: A nonpeptidic antiretroviral protease inhibitor.* Clinical Therapeutics, 2007. **29**(8): p. 1559-1576.

160. Dunn, B.M., *Proteases of infectious agents.* 1999, San Diego, Calif.: Academic. xvii, 282 , [15] of col. plates.

161. Dunn, B.M., *Structure and Function of Aspartic Proteinases: Genetics, Structures and Mechanisms.* 1992, New York: Plenum Press.

162. Logsdon, B.C., et al., *Crystal structure of a Multidrug-Resistant Human Immunodeficiency Virus Type 1 Protease Reveals an Expanded Active-Site Cavity.* J Virol, 2004. **78**(6): p. 3123-3132.

163. Engelman, A. and R. Craigie, *Efficient magnesium-dependent human immunodeficiency virus type 1 integrase activity.* J Virol, 1995. **69**(9): p. 5908-11.

164. Grobler, J.A., et al., *Diketo acid inhibitor mechanism and HIV-1 integrase: implications for metal binding in the active site of phosphotransferase enzymes.* Proc Natl Acad Sci U S A, 2002. **99**(10): p. 6661-6.

165. Kawasuji, T., et al., *A platform for designing HIV integrase inhibitors. Part 2: a two-metal binding model as a potential mechanism of HIV integrase inhibitors.* Bioorg Med Chem, 2006. **14**(24): p. 8420-9.

166. Hu, Z. and D.R. Kuritzkes, *Effect of raltegravir resistance mutations in HIV-1 integrase on viral fitness.* J Acquir Immune Defic Syndr, 2010. **55**(2): p. 148-55.

167. Cooper, D.A., et al., *Subgroup and resistance analyses of raltegravir for resistant HIV-1 infection.* N Engl J Med, 2008. **359**(4): p. 355-65.

168. Balaraju, T., et al., *Aromatic interaction profile to understand the molecular basis of raltegravir resistance.* Structural Chemistry, 2012: p. 1-14.

169. Hare, S., et al., *Retroviral intasome assembly and inhibition of DNA strand transfer.* Nature, 2010. **464**(7286): p. 232-6.

170. Perryman, A.L., et al., *A dynamic model of HIV integrase inhibition and drug resistance.* J Mol Biol, 2010. **397**(2): p. 600-15.

171. Xue, W., et al., *Understanding the structural and energetic basis of inhibitor and substrate bound to the full-length NS3/4A: insights from molecular dynamics simulation, binding free energy calculation and network analysis.* Mol Biosyst, 2012. **8**(10): p. 2753-65.

172. Huang, M., G.H. Grant, and W.G. Richards, *Binding modes of diketo-acid inhibitors of HIV-1 integrase: A comparative molecular dynamics simulation study.* J Mol Graph Model, 2011. **29**(7): p. 956-64.

173. Xue, W., et al., *Exploring the molecular mechanism of cross-resistance to HIV-1 integrase strand transfer inhibitors by molecular dynamics simulation and residue interaction network analysis.* J Chem Inf Model, 2013. **53**(1): p. 210-22.

174. Rose, R.B., C.S. Craik, and R.M. Stroud, *Domain flexibility in retroviral proteases: structural implications for drug resistant mutations.* Biochemistry, 1998. **37**(8): p. 2607-21.

175. Lee, M.C., et al., *Large-scale conformational dynamics of the HIV-1 integrase core domain and its catalytic loop mutants.* Biophys J, 2005. **88**(5): p. 3133-46.

176. Serrao, E., et al., *Raltegravir, elvitegravir, and metoogravir: the birth of "me-too" HIV-1 integrase inhibitors.* Retrovirology, 2009. **6**: p. 25.

177. Wang, J.Y., et al., *Structure of a two-domain fragment of HIV-1 integrase: implications for domain organization in the intact protein.* EMBO J, 2001. **20**(24): p. 7333-43.

178. Cai, M., et al., *Solution structure of the N-terminal zinc binding domain of HIV-1 integrase.* Nat Struct Biol, 1997. **4**(7): p. 567-77.

179. Dyda, F., et al., *Crystal structure of the catalytic domain of HIV-1 integrase: similarity to other polynucleotidyl transferases.* Science, 1994. **266**(5193): p. 1981-6.

180. Eijkelenboom, A.P.A.M., et al., *The DNA-Binding Domain of Hiv-1 Integrase Has an Sh3-Like Fold.* Nature Structural Biology, 1995. **2**(9): p. 807-810.

181. Jaskolski, M., et al., *Piecing together the structure of retroviral integrase, an important target in AIDS therapy.* FEBS J, 2009. **276**(11): p. 2926-46.

182. Hare, S., et al., *A novel co-crystal structure affords the design of gain-of-function lentiviral integrase mutants in the presence of modified PSIP1/LEDGF/p75.* PLoS Pathog, 2009. **5**(1): p. e1000259.

183. Ferris, A.L., et al., *Lens epithelium-derived growth factor fusion proteins redirect HIV-1 DNA integration.* Proc Natl Acad Sci U S A, 2010. **107**(7): p. 3135-40.

184. Wang, H., et al., *HRP2 determines the efficiency and specificity of HIV-1 integration in LEDGF/p75 knockout cells but does not contribute to the antiviral activity of a potent LEDGF/p75-binding site integrase inhibitor.* Nucleic Acids Res, 2012. **40**(22): p. 11518-30.

185. Wlodawer, A., *Crystal structures of catalytic core domains of retroviral integrases and role of divalent cations in enzymatic activity.* Adv Virus Res, 1999. **52**: p. 335-50.

186. Engelman, A., K. Mizuuchi, and R. Craigie, *HIV-1 DNA integration: mechanism of viral DNA cleavage and DNA strand transfer.* Cell, 1991. **67**(6): p. 1211-21.

187. Berthoux, L., et al., *The role of lysine 186 in HIV-1 integrase multimerization.* Virology, 2007. **364**(1): p. 227-36.

188. Dar, M.J., et al., *Biochemical and virological analysis of the 18-residue C-terminal tail of HIV-1 integrase.* Retrovirology, 2009. **6**: p. 94.

189. Larue, R., et al., *Interaction of the HIV-1 intasome with transportin 3 protein (TNPO3 or TRN-SR2).* J Biol Chem, 2012. **287**(41): p. 34044-58.

190. De Houwer, S., et al., *Identification of residues in the C-terminal domain of HIV-1 integrase that mediate binding to the transportin-SR2 protein.* J Biol Chem, 2012. **287**(41): p. 34059-68.

191. Jayappa, K.D., et al., *Identification of critical motifs within HIV-1 integrase required for importin alpha3 interaction and viral cDNA nuclear import.* J Mol Biol, 2011. **410**(5): p. 847-62.

192. Ao, Z., et al., *Importin alpha3 interacts with HIV-1 integrase and contributes to HIV-1 nuclear import and replication.* J Virol, 2010. **84**(17): p. 8650-63.

193. Yin, Z. and R. Craigie, *Modeling the HIV-1 Intasome: A Prototype View of the Target of Integrase Inhibitors.* Viruses, 2010. **2**(12): p. 2777-81.

194. Blanco, J.L., et al., *HIV-1 integrase inhibitor resistance and its clinical implications.* J Infect Dis, 2011. **203**(9): p. 1204-14.

195. McColl, D.J. and X. Chen, *Strand transfer inhibitors of HIV-1 integrase: bringing IN a new era of antiretroviral therapy.* Antiviral Res, 2010. **85**(1): p. 101-18.

196. Kobayashi, M., et al., *Selection of diverse and clinically relevant integrase inhibitor-resistant human immunodeficiency virus type 1 mutants.* Antiviral Res, 2008. **80**(2): p. 213-22.

197. Fransen, S., et al., *Loss of raltegravir susceptibility by human immunodeficiency virus type 1 is conferred via multiple nonoverlapping genetic pathways.* J Virol, 2009. **83**(22): p. 11440-6.

198. Jones, G.S., et al., *Preclinical evaluation of GS-9160, a novel inhibitor of human immunodeficiency virus type 1 integrase.* Antimicrob Agents Chemother, 2009. **53**(3): p. 1194-203.

ABSTRACT

BIOCHEMICAL, STRUCTURAL, AND DRUG DESIGN STUDIES OF MULTI-DRUG RESISTANT HIV-1 THERAPEUTIC TARGETS

TAMARIA GRACE DEWDNEY

December 2013

Advisor: Dr. Ladislau C. Kovari

Major: Biochemistry and Molecular Biology

Degree: Doctor of Philosophy

Protein point mutations acquired as a mechanism of survival against therapeutics cause structural changes that effect protein function and inhibitor binding. This work investigates the structural mechanisms that lead to multi-drug resistance to HIV-1 protease and integrase inhibitors.

Proper proteolytic processing of the HIV-1 Gag/Pol polyprotein is required for HIV infection and viral replication. This feature has made HIV-1 protease an attractive target for antiretroviral drug design for the treatment of HIV-1 infected patients, thus the development of drug resistance has arisen as a major therapeutic and drug design challenge. To understand the molecular mechanisms leading to drug resistance we selected and characterized three multi-drug resistant HIV-1 protease patient isolates, identifying a previously unreported structural role for V32I, I47V, I54M and L90M in protease dynamics. To examine the role of the P1 and P1' positions of the substrate in inhibitory efficacy of multi-drug resistant HIV-1 protease 769 (MDR 769), we performed a structure-function studies. We designed a series of ligands and evaluated them using a combination of computational and experimental methods. Our results suggest two important strategies for rational drug design of protease inhibitors: (1) the presence of fluorinated P1 or P1' groups enhance the binding affinities in both wild-type and MDR PR variants and (2) non-identical P1/P1' residues play an important role in binding to multi-drug resistant HIV-1 protease.

HIV-1 integrase is an essential enzyme necessary for the replication of the HIV virus as it catalyzes the insertion of the viral genome into the host chromosome. Raltegravir was the first integrase inhibitor approved by the FDA for treatment of HIV-1 infection. HIV patients on raltegravir containing regimens may develop drug resistance mutations at residue 140 and 148 in the catalytic 140's loop resulting in a 5-10 fold decrease in susceptibility to raltegravir. To understand the molecular mechanisms of drug resistance in HIV-1 integrase we performed molecular dynamics studies on the catalytic core domain of raltegravir resistant HIV-1 protease in complex with raltegravir. These experiments suggest a gating function of the catalytic 140's loop in active site accessibility as well as reduced flexibility as a mechanism of raltegravir resistance. In addition, we developed a model for the full length HIV-1 integrase and performed molecular dynamics of our model in complex with raltegravir and the viral DNA ends, identifying unique alterations in non-bonded interactions between the protein, DNA, and raltegravir as a result of the drug resistant mutations.

The results of this work provide detailed structural information on HIV-1 protease and integrase in order to aid in the development of new therapeutics against these targets. Our work has implications not only on HIV-1 therapy but the techniques described here can be used to study other proteins, design new compounds, and help aid in our understanding of protein structure.

AUTOBIOGRAPHICAL STATEMENT

Education
09/2009-12/2013   Ph.D. in Biochemistry and Molecular Biology
Department of Biochemistry and Molecular Biology
Wayne State University School of Medicine

09/2004- 08/2009   B.S. in Biological Sciences
Department of Biological Sciences
Wayne State University

Publications
Dewdney, T.G., Wang, Y., Reiter, S.J., Brunzelle, J., Kovari, I.A., Kovari L.C. 2013 Ligand Modifications to reduce the relative resistance of multidrug resistance HIV-1 protease. *Biorg Med Chem* 21(23): 7430-7434

Dewdney, T.G., Wang, Y., Reiter, S.J., Kovari, I.A., Kovari L.C. 2013. Reduced HIV-1 integrase flexibility as a mechanism for raltegravir resistance. *J Struct Biol* S1047-8477(13)00188-3. 10.1016/j.jsb.2013.07.008

Liu, Z., Yedidi, R.., Wang, Y., **Dewdney, T.G**., Reiter, S.J., Brunzelle, J.S., Kovari, I.A., Kovari, L.C. 2013. Crystallographic study of multi-drug resistant HIV-1 protease lopinavir complex: Mechanism of drug recognition and resistance. *Biochem Biophys Res Commun* 437(2):199-204

Liu, Z., Yedidi, R.., Wang, Y., **Dewdney, T.G**., Reiter, S.J., Brunzelle, J.S., Kovari, I.A., Kovari, L.C. 2013. Insights into the mechanism of drug resistance: X-ray structure analysis of multi-drug resistant HIV-1 protease Ritonavir complex. *Biochem Biophys Res Commun* 431(2): 232-8

Liu, Z., Wang, Y., Yedidi, R., **Dewdney, T.G**., Reiter, S.J., Brunzelle, J.S., Kovari, I.A., Kovari, L.C. 2013. Conserved hydrogen bonds and water molecules in MDR HIV-1 protease substrate complexes. *Biochem Biophys Res Commun* 430 (3): 1022-7

Wang, Y., **Dewdney, T.G**., Liu, Z., Reiter, S.J., Brunzelle, J., Kovari, I.A., Kovari L.C. 2012. Higher desolvation energy reduces molecular recognition in multi-drug resistant HIV-1 protease. Biology *1*(1), 81-93

Wang, Y., **Dewdney, T.G**., Liu, Z., Reiter S.J., Brunzelle, J.S., Kovari, I.A., Kovari L.C. 2011 X-ray crystal structure and dynamics reveal HIV-1 protease drug interactions. *Studia UBB Chemia*

Wang, Y., Liu, Z., Brunzelle, J.S., Kovari, I.A., **Dewdney, T.G**. Reiter S.J., Kovari L.C. 2011 The higher barrier of darunavir and tipranavir resistance for HIV-1 protease. *Biochem Biophys Res Commun.* 412(4): 737-42